Natural Resources Canada | Ressources naturelles Canada

GEOLOGICAL SURVEY OF CANADA
OPEN FILE 8982

Sandstone composition and diagenesis of the Paskapoo Formation and their significance for a shallow groundwater aquifer in the Fox Creek area, west-central Alberta

D. Lavoie, V. Tremblay, and C. Rivard

2023

Canada

GEOLOGICAL SURVEY OF CANADA
OPEN FILE 8982

Sandstone composition and diagenesis of the Paskapoo Formation and their significance for shallow groundwater aquifer in the Fox Creek area, west-central Alberta

D. Lavoie, V. Tremblay, and C. Rivard

2023

Permanent link: https://doi.org/10.4095/331923

This publication is available for free download through GEOSCAN (https://geoscan.nrcan.gc.ca/).

Recommended citation
Lavoie, D., Tremblay, V., and Rivard, C., 2023. Sandstone composition and diagenesis of the Paskapoo Formation and their significance for shallow groundwater aquifer in the Fox Creek area, west-central Alberta; Geological Survey of Canada, Open File 8982, 92 p. https://doi.org/10.4095/331923

Publications in this series have not been edited; they are released as submitted by the authors.

ISSN 2816-7155
ISBN 978-0-660-48962-9
Catalogue No. M183-2/8982E-PDF

TABLE OF CONTENTS

Page

LIST OF FIGURES

LIST OF TABLES

List of Annexes

Abstract

The shallow aquifer in the Fox Creek area is hosted by the Paleocene Paskapoo Formation. The formation consists of fluvial deposits with channel-filled high-energy sandstone cutting through fine-grained, low energy overbank sediments. Three internal members are recognized, these members define three hydrostratigraphic units (two aquifers and one aquitard).

In fall 2022, three boreholes were drilled and cored. The succession is slightly dominated by sandstone with subordinate fine-grained sediments and thin coal intervals. The calcareous to non-calcareous sandstone is either tight and well compacted or porous, friable to unconsolidated. The litharenite is composed of quartz, various types of rock fragments, chert, and feldspars. Detrital carbonates can be abundant.

The post-sedimentation history of the sandstone recorded cementation and dissolution events from near surface, through shallow burial and late tectonic exhumation. The events include early clay coatings on grains, dissolution of metastable minerals, calcite cementation, kaolinite and minor chlorite and late near surface fault-controlled freshwater circulation and dissolution. The late event resulted in friable to unconsolidated sandstone intervals.

Résumé

L'aquifère peu profond de la région de Fox Creek est formé par la Formation de Paskapoo du Paléocène. La formation se compose de dépôts fluviaux avec des grès de haute énergie en remplissage de chenaux recoupant des sédiments sub-aériens à grain fin et de faible énergie. Trois membres internes sont reconnus, ces membres définissent trois unités hydrostratigraphiques (deux aquifères et un aquitard).

À l'automne 2022, trois puits ont été forés et carottés. La succession est légèrement dominée par le grès avec quantités moindres de sédiments à grain fin et de minces intervalles de charbon. Le grès calcareux à non calcareux est soit bien compacté ou poreux, friable à non consolidé. La litharénite est composé de quartz, de divers types de fragments de roche, de chert et de feldspaths. Les carbonates détritiques peuvent être abondants.

L'histoire post-sédimentation du grès a enregistré des événements de cimentation et de dissolution de la surface, jusqu'à l'enfouissement peu profond et l'exhumation tectonique tardive. Les événements comprennent de minces couvertures précoces d'argile sur les grains, la dissolution de minéraux métastables, la cimentation de calcite, de kaolinite et de chlorite mineure et des dissolutions locales tardives contrôlées par l’infiltration d’eau météorique le long de failles près de la surface. L'événement tardif a produit des intervalles de grès friables à non consolidés.

Introduction

A multidisciplinary and multi-institutional project was initiated in the Fox Creek area (west-central Alberta) in April 2019 to study environmental impacts of hydrocarbon development activities. The initial objective was to specifically study their potential impacts on water resources. In this region, water resources come from both surface water and shallow groundwater.

Different sectors within NRCan rapidly (fall 2019) identified the Fox Creek area as a region of interest for developing regional cumulative effects evaluation methods in support of the new impact assessment legislation. As a result, the scope of the project is now much broader and the project includes studies of vegetation, forest, snow cover, landscape evolution over time, and contributes to a woodland caribou habitat study. The project involves many collaborators from the federal and provincial governments, as well as the academic community. The present study is focussed on the main shallow groundwater aquifer unit in the Fox Creek area, the fluvial sandstones of the Paleocene (Lower Cenozoic) Paskapoo Formation.

Regional hydrogeological context

The Western Canada Sedimentary Basin (WCSB) is the geological domain that underlies most of Alberta. The regional-scale shallow groundwater system is dominated by various permeable clastic units, either continuous or irregularly interconnected (Lennox, 1993). Overall, the regional groundwater flow in the WCSB is from the Cordillera Foothills towards the Precambrian basement to the east (Lennox, 1993). The shallow bedrock geology hosting the aquifers of a large part of the WCSB, especially in central and western Alberta, consists primarily of coarse-grained clastic dominated units which range in age from Jurassic (Mesozoic) to Paleocene (Cenozoic) (Lennox, 1993).

Study area and purpose of the study

This project, evaluating the cumulative environmental effects of hydrocarbon development on water resources, takes place in the area of the small Town of Fox Creek (260 km northwest of Edmonton), where significant oil production started in the late 1940's and is still ongoing today with hundreds of oil and gas wells drilled, fractured, and put into production. The current study focuses on a 700 km^2 watershed just southwest of Fox Creek (Fig. 1). It aims, among other things, at better documenting the overall hydrogeological context of the shallow groundwater aquifer, as well as characterizing the quality of groundwater including potential contamination from deep (>1.5 km) hydrocarbon exploration and production. This area is more or less heavily forested and largely unpopulated; no agricultural activities are taking place and water is only used for the oil and gas industry development.

The shallow bedrock geology of the study area consists of clastic units of the Paleocene Paskapoo Formation (Prior et al., 2013). This formation consists of a complex succession of mudstone and siltstone with sandstone channels (see below). Within the Paskapoo Formation, the various fluvial sandstone channels make an effective aquifer, although lateral continuity and yield can vary significantly over short distances. In 2020, nine shallow monitoring wells (35-90 m) were drilled with a percussion drill rig for the project, and in October 2022, three boreholes (32-100 m) were core drilled (Fig. 1), then all converted into 32 m monitoring wells, in which some anomalous friable to unconsolidated sandstone intervals are present within an otherwise well compacted sandstone, siltstone and mudstone

succession. These friable and unconsolidated sandstone intervals could not be recognized from the previous percussion drilling program, for which only drill cuttings were available.

The goal of this study is to understand the cause of these anomalous loose sandstone intervals through detailed petrographic examination of samples. Sandstones of the Paskapoo Formation have been the subject of two significant but limited recent petrographic studies, by Grasby et al. (2007) and Hughes et al. (2017a). The study of Grasby et al. (53 samples) focused on the Paskapoo Formation in southern Alberta, in the area between Calgary and Edmonton, whereas the work of Hughes et al. (20 samples) covered an area south of the current study area. The presence of unconsolidated sandstone intervals is not mentioned in neither one of these petrographic studies.

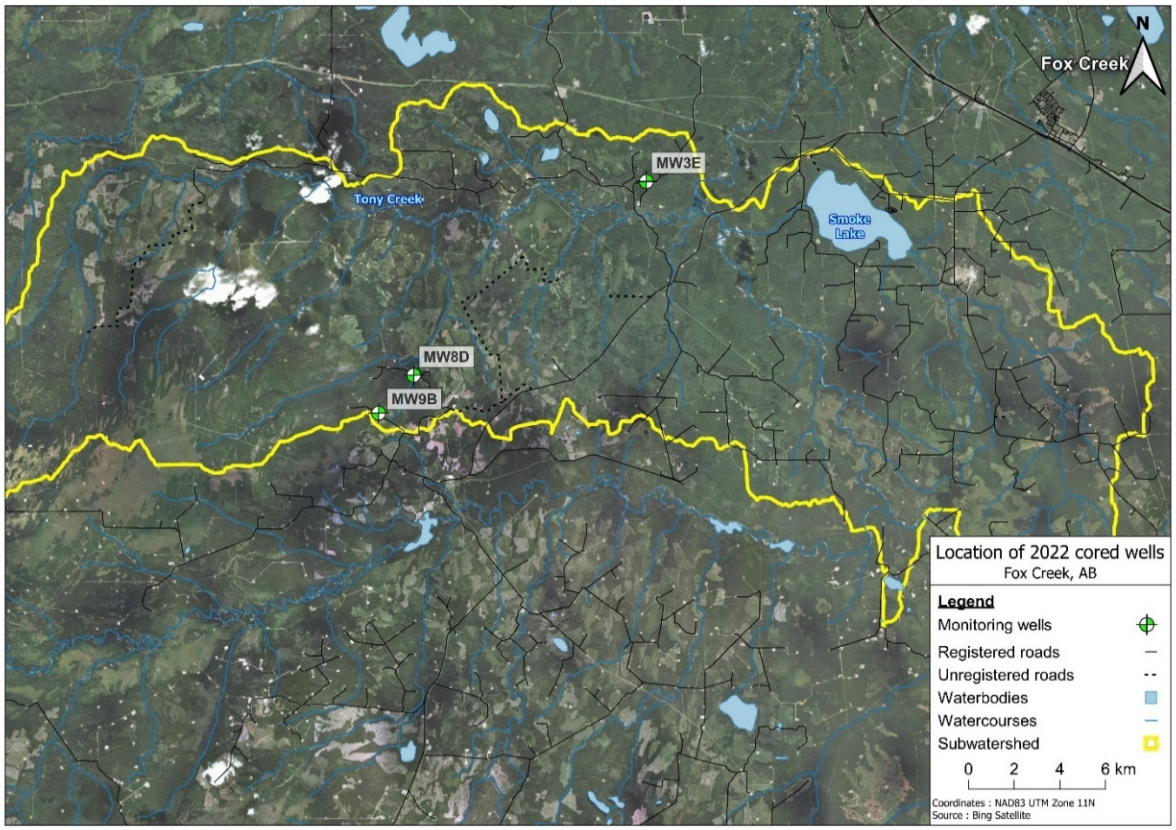

Figure 1. Localization map of the study area and the location of the three monitoring wells under study. Modified from Google Earth Satellite Image.

Geological setting

Stratigraphy of the Fox Creek area of WCSB

In the WCSB, overlying the Precambrian basement up to modern erosional surface, the succession consists of sediments that range in age from the Middle Cambrian to the Paleocene (Fig. 2). The Fox Creek area is in the West-Central Plains domain in Alberta (AGS, 2019).

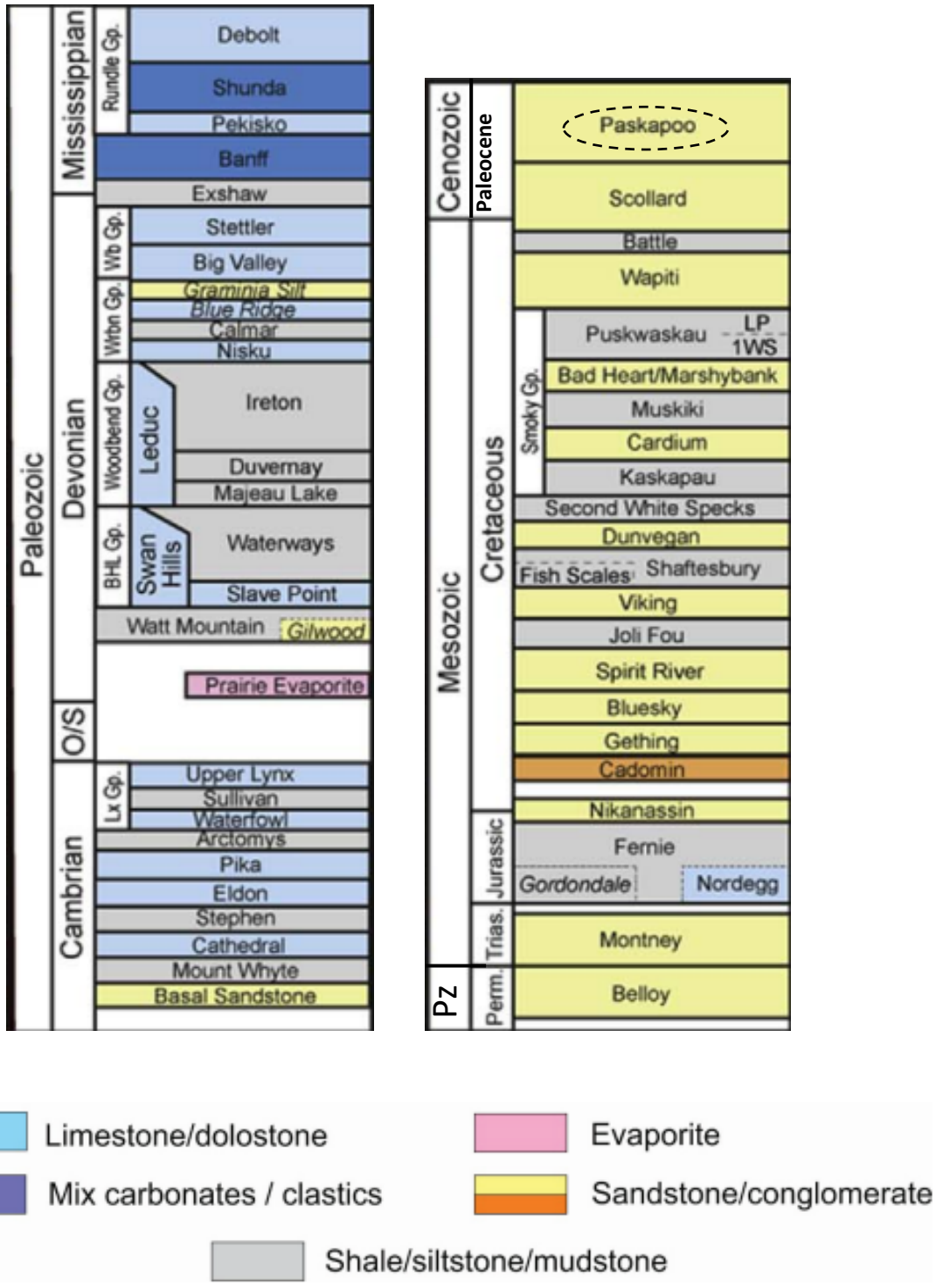

Figure 2. Stratigraphic summary of the Fox Creek area, the Lower Cenozoic Paskapoo Formation is encircled. Gp. is for Group; O/S is for Ordovician / Silurian; Perm. is for Permian; Pz is for Paleozoic; 1WS is for First White Specks shale (informal), BHL is for Beaverlake Hill Group, LP is for Lea Park Formation, Lx is for Lynx Group, WB is for Wabamun Group, WBN is for Winterburn Group. Modified from Corlett et al. (2018) and AGS (2019).

In the Fox Creek area, the Phanerozoic sedimentary package over the Precambrian basement is around 4 to 4.5 km thick, and the succession thickens westward. The base of the preserved succession is progressively younger easterly with the youngest basal sediments over the Precambrian basement being Early Devonian in the area northeast of the Fox Creek area (Corlett et al., 2018; AGS, 2019), this results from an easterly-directed, Paleozoic marine onlapping over an irregular topography on top of the Precambrian basement. The succession in the Fox Creek area can be divided into two broad stratigraphic assemblages.

The first assemblage (1.5 to 2 km thick) is Middle Cambrian to Mississippian in age and is primarily made up of shallow marine carbonates (limestone and dolostone) with major Devonian reef complexes interbedded with and/or laterally equivalent to fine-grained clastic sediments (shale, mudstone, and siltstone). Some thick evaporite (halite and anhydrite) intervals are present in the Devonian section. The second younger assemblage (2.5 to 3 km thick) ranges from the Permian to the Paleocene; the succession is strongly dominated by clastics with fluvial-deltaic-nearshore coarse-grained units (sandstone and conglomerate) being interbedded with finer-grained intervals (shale, mudstone, and siltstone). The shallow aquifers of the Fox Creek area are hosted by sandstones of the Paleocene Paskapoo Formation (Figs. 2 and 3).

Paskapoo Formation

The Paskapoo Formation forms the shallow bedrock unit over more than 65,000 km^2 in southern and central Alberta (Prior et al., 2013). The Paskapoo Formation represents a vast eastward thinning wedge of non-marine sediments deposited in a tectonically collapsing foreland basin created in response to the rising of Paleozoic to Mesozoic units in the Cordillera Foothills (Price, 1994). The Paskapoo Formation attains a maximum thickness of 800 m near the Foothills margin and represents the youngest preserved bedrock deposits in the WCSB (Hamblin, 2004; AGS, 2019). The Paskapoo Formation strata range in age from lower to upper Paleocene (Fig. 3) (Demchuk and Hills, 1991). A lower Paleocene basin wide, erosional unconformity marks the base of the Paskapoo Formation (Lerbekmo and Sweet, 2000) and separates it from the Cretaceous to lower Paleocene Scollard Formation (Fig. 3). The Paskapoo Formation comprises thin to thick-bedded sandstone with various amounts of shale, siltstone, sandy mudstone, and coal seams that were deposited in a non-marine environment (Hamblin, 2004).

The sandstone of the Paskapoo Formation is interpreted to represent diverse fluvial deposits with a dominant proximal alluvial fan assemblage to the west, near the Cordilleran thrust front, to a more distal fluvial plain channel assemblage to the east (Jerzykiewicz, 1977; Hamblin, 2004). The abundant associated fine-grained muddy sediments are the expression of diverse overbank and ephemeral flood plain sediments. The thicker and most significant coals of the Paskapoo Formation are almost entirely restricted to the northwestern domain of the WCSB, this situation reflects a more humid climatic setting northward compared to sub-tropical and semi-arid conditions to the south (Jerzykiewicz and Sweet, 1988; Carmichael et al., 2017).

In central Alberta, the Paskapoo Formation is divided into three members: (1) the lower Haynes Member, (2) the upper Lacombe Member and, (3) the Dalehurst Member, a laterally equivalent unit to part of the Lacombe Member, only present near the Foothills (Demchuk and Hills, 1991) (Fig. 3).

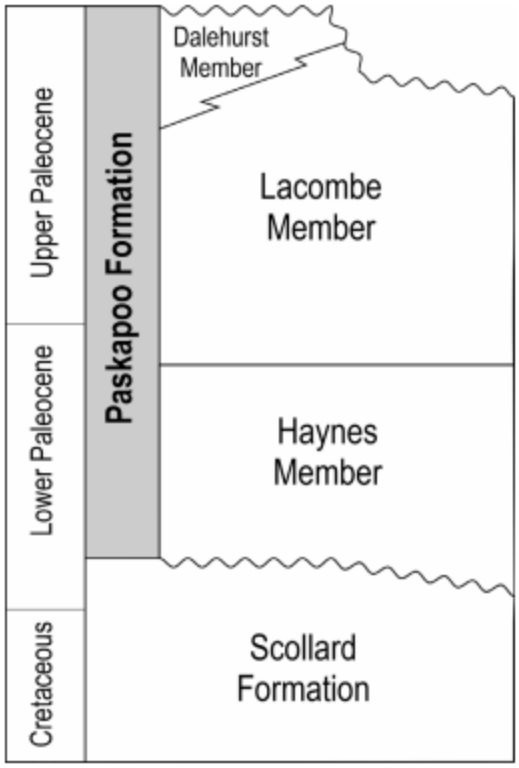

Figure 3. Internal stratigraphy of the Paskapoo Formation (modified from Demchuk and Hills, 1991).

Haynes Member

The Haynes Member overlies an erosional contact with the Scollard Formation and is comprised of dominant, thick-bedded, medium- to coarse-grained sandstone and conglomerate, minor and subordinate siltstone, mudstone, shale, and coal beds (Demchuk and Hills, 1991). Paleontological studies of the Haynes Member confirm the Paleocene age for this member of the Paskapoo Formation (Demchuk and Hills, 1991).

Lacombe Member

The Lacombe Member consists of a dominant succession of interbedded siltstone, mudstone, shale, and thin coal with subordinate fine- to medium-grained sandstone. Plant fragments and pedogenic structures including rooting and soil slickensides are abundant (Demchuk and Hills, 1991). Paleontological studies indicate a Paleocene age (Demchuk and Hills, 1991).

Dalehurst Member

The Dalehurst Member is comprised of massive to planar, fine to coarse-grained sandstone, siltstone, mudstone, shale, and abundant m-thick coal seams. This unit is largely restricted to the northwestern part of the WCSB. Pedogenic structures are also abundant in the fine-grained facies. The only paleontological investigation of the upper Paskapoo Formation indicates that it covers the uppermost part of the Paleocene (Demchuk and Hills, 1991).

Paskapoo Formation cores

In October 2022, as part of the Fox Creek project, three boreholes were drilled and cored in the Paskapoo Formation (Table 1, Fig. 1). These boreholes were the first ones to be cored from top to bottom in this area. They are located at contrasting elevations (799, 934 and 1047 m asl) and given their short lengths, the local horizontal bedding and the absence of any reported significant fault displacement, there is likely no overlap of the stratigraphy intercepted by the three boreholes. All three boreholes were converted into 32 m wells as the walls of the 100 m borehole collapsed. Wells MW9B and MW8D were drilled near the southern limit of the watershed, whereas well MW3E is located at the northern limit of the watershed (Fig. 1). The detailed lithologic description of each well is provided in the Annexes 1 to 3, as well as the position of the sandstone sampled for this study. Sandstone samples are also located alongside the schematic stratigraphic logs for each borehole presented in Figures 4, 5 and 6.

The following description succinctly presents the successions as a suite of lithofacies assemblages of a fine-grained association (shale, mudstone and siltstone dominated) and a coarse-grained one (sandstone dominated) with significant intervals of friable to unconsolidated sandstone. Sandstone mineralogical composition details and trends are discussed in the petrographic section. Coal beds and laminae can be found in both lithofacies assemblages even if they are more common in the mudstone – siltstone association. Rare (<1%) cm-thick layers of very soft green bentonite clays are found in MW3E well. The limit between fine (0.06 – 0.25 mm), medium (0.25 – 0.5 mm) and coarse (0.5 – 2 mm) grained sandstone is based on the average grain size of a specific bed / interval. For the sandstone, the stratigraphic position of very poorly to unconsolidated intervals are listed. Tables 2a and 2b offer a summary of the megascopic observations for the diverse lithologies present in the wells; representative core photographs are presented in Annexes 4 to 6. In the description below, interval numbers are included on the well stratigraphic log figures.

Table 1. Location and total drilled depth of the 3 studied cored wells.

Well Name	Longitude	Latitude	Z (m asl)	Total Drilled Depth (m)
MW3E	-117.0795	54.3769	799	100.4
MW8D	-117.2357	54.3005	934	32
MW9B	-117.2593	54.2856	1047	32

Table 2a. Summary of megascopic observations for the lithologies present in the three cored boreholes. Average abundance is for the total 3 wells. For sandstone, the grain size range is: fine (0.06 – 0.25 mm), medium (0.25 – 0.5 mm) and coarse (0.5 – 2 mm).

Lithology	Average abundance	Bed thickness	Visual porosity	Color	Carbonate abundance
Coal	5%	1 mm to 15 cm	0%	Black	None
Shale	5%	5 mm to 20 cm	0%	Green	Very rare

Mudstone	20%	5 mm to 25 cm	0%	Grey to green	Rare
Siltstone	15%	5 cm to 25 cm	0%	Grey	Rare
Fine-grained sandstone	20%	12 cm to 30 cm	<5%	Grey	Rare to common
Medium-grained sandstone	25%	10 cm to 35 cm	0% - 10%	Grey and brown	Common
Coarse-grained sandstone	10%	5 cm to 50 cm	0% - 20%	Grey and brown	Common

Table 2b. Summary of the lithology main characteristics, sedimentary and pedogenic features and fauna. For sandstone, the grain size range is: fine (0.06 – 0.25 mm), medium (0.25 – 0.5 mm) and coarse (0.5 – 2 mm).

Lithology	**Description**	**Sedimentary, pedogenic and/or other features**	**Fossils**
Coal	Dark, lustrous	Fractures	None
Shale	Well compacted, locally burrowed	Clay shrinkage	None
Mudstone	Usually well compacted. Burrows are locally abundant	Soil slickensides and vertisols	Locally, some bioclastic material
Siltstone	Quartz-rich	Faint laminations	Rare plant fragments
Fine-grained sandstone	Rarely friable and quartz-rich. Local internal fine coal laminations	Laminations	Shell fragments
Medium-grained sandstone	Locally friable. Quartz-rich and dark rock fragments	Cross-laminations	Bivalves and gastropods
Coarse-grained sandstone	Locally friable. Quartz-rich, common dark rock fragments, rare feldspars. Some intervals with well rounded, cm-sized mudstone clasts	Parallel- and cross-laminations, channels, injection, gravel lags	Bivalves, shell fragments

MW9B well

This well is in the southern domain of the study area (Table 1; Figs. 1, 4; Annexes 1 and 4).

1. Unconsolidated till and sand are present from 0 to 13.7 m.

2. The first rock association consists of siltstone, mudstone and shale present from 13.7 to 21.3 m. Soil slickensides are visible at 15.8 m and a 20 cm-thick vertisol profile is developed at 19.8 m.
3. An interval dominated by fine- to coarse-grained sandstone is found from 21.3 to 30.5 m. These brownish oxidized sandstones are very poorly consolidated to unconsolidated, they are largely non-calcareous.
4. Bottom of the core (30.5 – 32 m) consists of well consolidated grey siltstone.

MW8D well

This well is also in the southern domain of the study area (Table 1; Figs. 1, 5; Annexes 2 and 5).

1. Unconsolidated mixed material of till, clay, silt, and sand occurs at the top of the well from 0 to 9.5 m.
2. A siltstone, mudstone and shale interval with minor (1%) fine-grained sandstone is present between 9.5 and 13.7 m.
3. A well to poorly consolidated calcareous medium- to coarse-grained sandstone occurs between 13.7 and 19.4 m. From 14.9 to 18.3 m, the sandstone is friable.
4. A fractured mudstone dominated interval is observed between 19.4 to 21.8 m.
5. Fine-grained slightly calcareous sandstone with 10% interbedded mudstone is present between 21.8 and 24.7 m.
6. Mudstone and shale with 5% of cm-thick coal beds are seen between 24.7 and 31.5 m, the mudstone is locally heavily burrowed.
7. The bottom of the well, from 31.5 to 32 m, is made up of slightly calcareous fine-grained sandstone, the sandstone is friable at places.

MW3E well

This well is in the northern part of the study area (Table 1; Figs. 1, 6; Annexes 3 and 6).

1. Unconsolidated till material occurs at the top of the well from 0 to 8.8 m.
2. The first lithofacies assemblage consists of shale, mudstone and siltstone present between 8.8 and 12.7 m.
3. The next assemblage from 12.7 to 25.9 m is dominated by fine- to medium-grained sandstone with about 10% of interbedded mudstone and siltstone. The fine-grained sandstone is slightly to non-calcareous, whereas medium- to rare coarse-grained sandstones are strongly calcareous; bivalves are locally abundant in the interval.
4. From 25.9 to 38.4 m, the succession is dominated by shale, mudstone and siltstone, locally slightly calcareous, in this interval 5% of mm-laminae of coal and 5% of cm-thick beds of fine-grained sandstone are present. A bentonite interval from 26.3 to 26.5 m. Locally abundant bivalves and gastropods, one prominent 20 cm-thick soil profile with shrinkage cracks at 26.52 m.
5. A thick package of fine to coarse-grained sandstone is developed between 38.4 to 76.9 m, rare (2%) mudstone and siltstone are present. This interval is characterized by irregularly alternating well-consolidated and friable / unconsolidated sandstone. The most prominent unconsolidated intervals are from 44.2 to 53.3 m, 59.4 to 59.6 m, 62.5 to 63.6 m and from 67.5 to 68.6 m. Almost invariably, more or less calcareous fine-grained sandstone is well compacted, whereas almost all uncemented intervals are made up of medium- to coarse-grained, calcareous

sandstone. From 64.3 to 65.8 m, well rounded to elongated mudstone fragments are set as a gravel lag in a fine-grained sandstone.

6. From 76.9 to 100.4 m, the succession is dominated by mudstone and siltstone, this interval offers abundant (20%) cm- to dm-thick coal beds which can be highly fractured. Green bentonite from 86.1 to 86.2 m. A 2.8 m-thick zone of fine-grained calcareous cross-laminated sandstone is developed from 96 to 98.8 m.

It is noteworthy that, for the three boreholes, the unconsolidated sandstone intervals are almost invariably in physical association with surrounding zones of friable sandstone. There is only one interval in MW3E (56.4 to 63.6 m) where some unconsolidated sandstone intervals are surrounded immediately by well compacted sandstone without the presence of a friable zone.

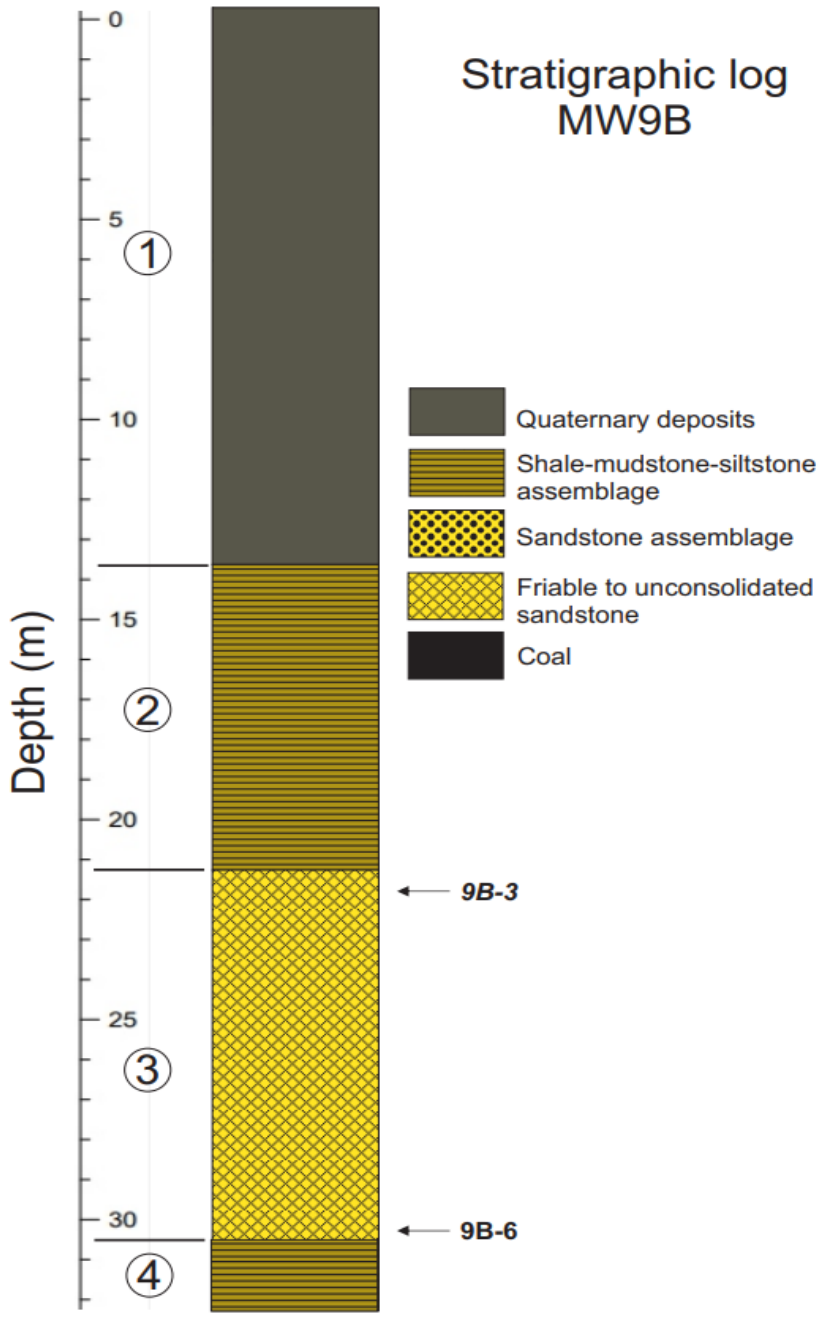

Figure 4. Internal lithofacies associations for MW9B borehole described in the text and position of the samples to the right (e.g. "9B-3"). In bold: thin section; in bold and italic: thin section and carbonate stable isotopes. See Annex 1 for detailed descriptions and Annex 4 for selected core photographs.

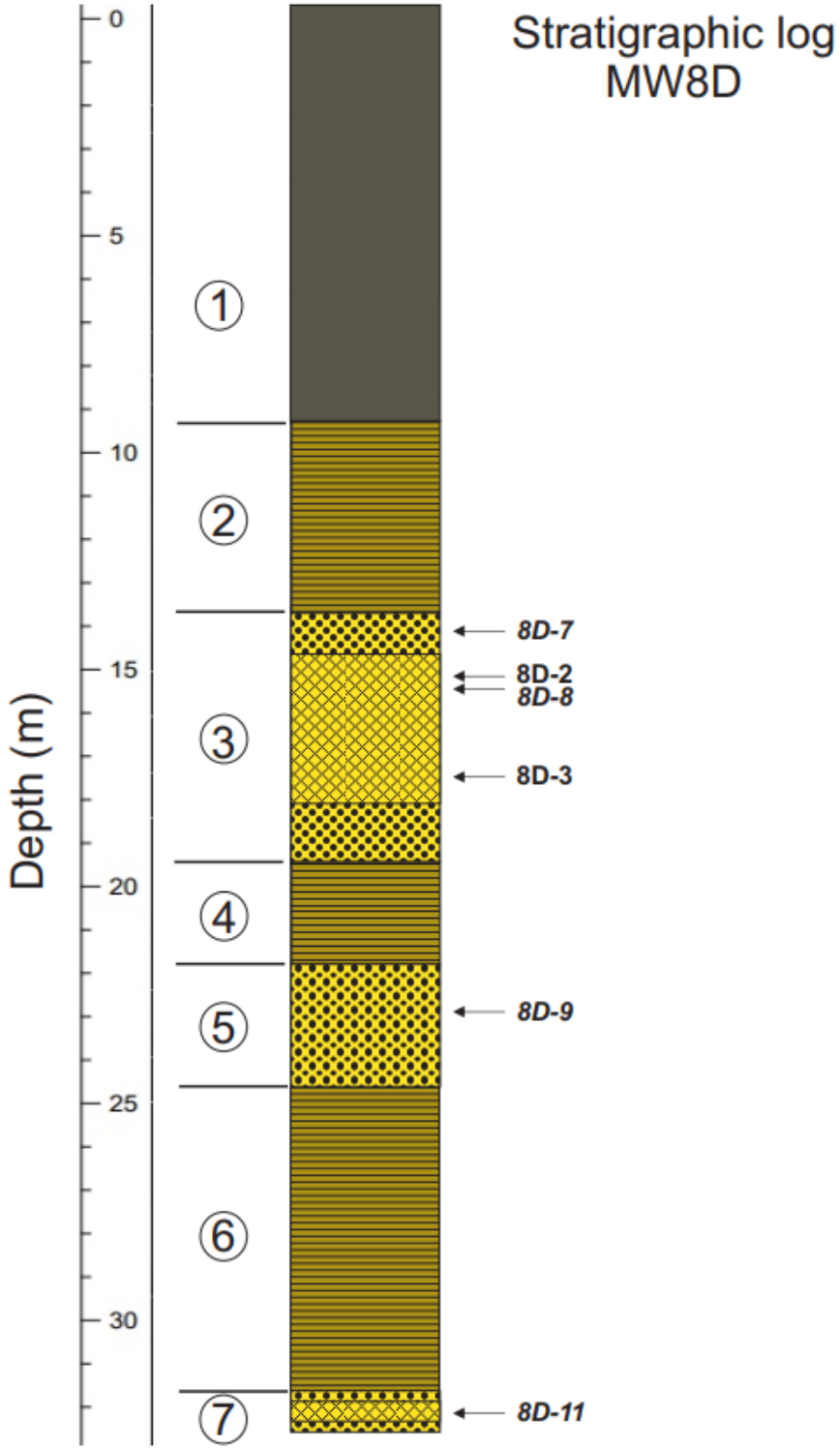

Figure 5. Internal lithofacies associations for MW8D borehole described in text and position of the samples to the right (e.g. "8D-7"). In bold: thin section; in bold and italic: thin section and carbonate stable isotopes. See Figure 4 for legend, Annex 2 for detailed descriptions and Annex 5 for selected core photographs.

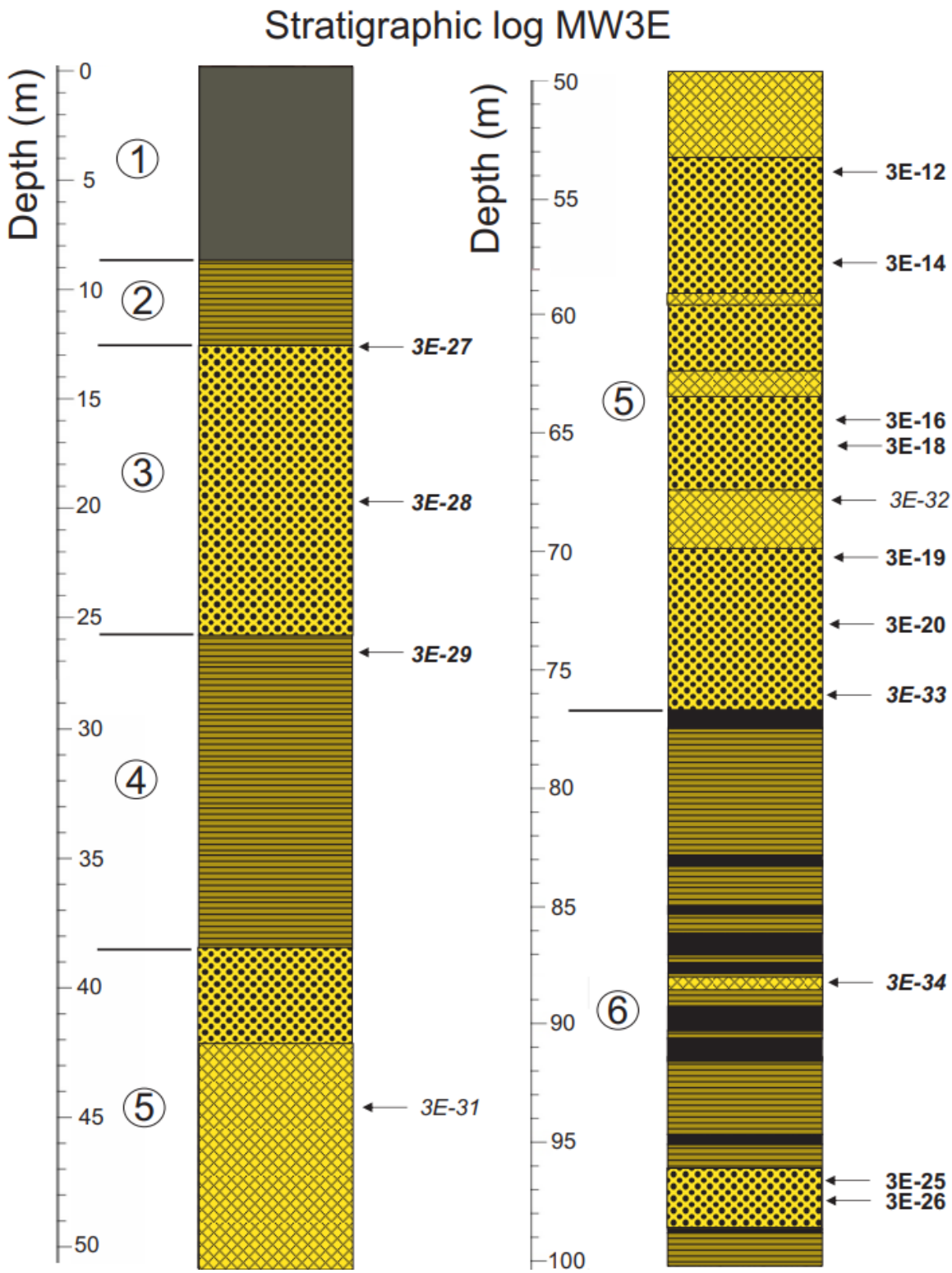

Figure 6. Internal lithofacies associations for MW3E borehole described in text and position of the samples to the right (e.g. "9E-27"). In bold: thin section; in bold and italic: thin section and carbonate stable isotopes; in italic: carbonate stable isotopes only. See Figure 4 for legend, Annex 3 for detailed descriptions and Annex 6 for selected core photographs.

Interpreted stratigraphic assignment of the cored intervals

The succession consists of slightly dominant (around 55% average in the three wells) more-or-less calcareous, fine- to coarse-grained sandstone and subordinate shale-mudstone-siltstone; coals are locally present but in minor percentage and in thin intervals except in well MW3E where they are more abundant in the interval between 76.9 to 100.4 m (Tables 2a and 2b, Figures 4 to 6). This overall specific assemblage could be correlated with either the Lacombe or Dalehurst members of the Paskapoo Formation, as the successions present in cores are at the limit between truly sandstone-dominated and mudstone-dominated assemblages and both members are known to carry coal intervals.

In their synthesis regional geological map of the area, Hughes et al. (2017a, b) have suggested the presence of both the Lacombe Aquitard and Sunchild Aquifer (i.e., Dalehurst Member) as shallow bedrock / hydrostratigraphic units.

Regional hydrostratigraphic units

The Paskapoo Formation belongs to the basin-wide Jurassic to Cenozoic, first-order "upper clastic" hydrostratigraphic unit of Lennox (1993). However, the formation does not correspond to a single homogeneous unit from a hydrogeology perspective and the need to have significant lateral connectivity of sandstone units for efficient groundwater flow makes the definition of aquifers and aquitards a challenging task when dealing with complex array of channel-fill deposits in an overall muddy succession. As with the lithostratigraphic division of the formation into three members, the Paskapoo Formation internally encompasses three hydrostratigraphic units, from base to top: the Haynes Aquifer, the Lacombe Aquitard and the Sunchild Aquifer (Lyster and Andriashek, 2012). The threshold for distinction of aquifers from aquitards is the presence of >55% sandstone in a 25 m thick interval which leads to efficient connectivity of the sandstone bodies; conversely, where sandstones represent less than <35%, the succession is considered an aquitard (Lyster and Andriashek, 2012).

The internal lithofacies association for the Haynes Member is strongly dominated by thick beds of coarse-grained sandstone with conglomerate. These sandstone bodies are filling major channels that are cutting through finer-grained deposits or previous channel-fill sandstones. The Haynes Aquifer is porous with high hydraulic conductivity (Grasby et al., 2007, 2008), it is widely distributed in the subsurface of southwestern Alberta and can locally reach over 100 m in thickness near the Cordillera deformation front.

The Lacombe Member is characterized by a dominant lithofacies association of shale-mudstone-siltstone, channel-filled sandstone is usually fine-grained and of limited lateral extension. Based on the cut-off values of Lyster and Andriashek (2012), the Lacombe Aquitard thins to the northeast, being over 500 m thick at the Cordilleran deformation front to less than 50 m near the eastern margin of the WCSB.

The Dalehurst Member is dominated by sandstone with secondary siltstone-mudstone and thick coal seams in the type location of Obed-Marsh (Demchuk and Hills, 1991). The term "Sunchild Aquifer" was introduced by Lyster and Andriashek (2012) to designate the upper hydrostratigraphic unit of the Paskapoo Formation, because of the local presence of thick coals in the original description of the Dalehurst Member and the difficulty of correlating regionally with this unit (Demchuk and Hills, 1991). Like the underlying hydrostratigraphic units, the Sunchild Aquifer is also thicker near the Cordillera deformation front, locally reaching close to 750 m. Based on the definition and work of Lyster and

Andriashek (2012) and Hughes et al. (2017a), both the Sunchild Aquifer and Lacombe Aquitard are present in the subsurface of the study area.

Petrography of sandstones

The purpose of the current study is to understand the cause for the presence of anomalous unconsolidated sand and crumbly sandstone intervals frequently present between cemented and compacted sandstones. These unconsolidated / friable intervals have significant implications for water transmissivity of the groundwater aquifer of the area.

Previous sandstone petrographic studies

Early petrographic studies of Cretaceous – Paleocene sandstones were focussing on regional and time evolution in the nature and percentage of the embedded rock fragments (volcanic, sedimentary, metamorphic) and heavy minerals to provide information about source areas for the detrital material (Allan and Sanderson, 1945; Meyboom, 1961; Mack and Jerzykiewicz, 1989).

A first regional detailed petrographic study of diverse Cretaceous – Paleocene sandstone-dominated units, including the Paskapoo Formation, is provided by Carrigy (1971). However, as discussed in Hamblin (2004), the erroneous inclusion of sandstone samples likely from the Scollard and lower Ravenscrag formations in the Paskapoo Formation in Carrigy (1970, 1971) casts doubt on some of the proposed compositional differences and source evolution. Nevertheless, thorough framework grains, cements and visible porosity estimates are presented. For the Paskapoo Formation, quartz and rock fragments dominate the detrital assemblage and pore-filling cements consist of grain-coating chlorite and/or montmorillonite followed by time-overlapping precipitation of kaolinite and calcite.

Grasby et al. (2007) carried out a detailed petrographic study of sandstone in the Paskapoo Formation in central western Alberta. Fifty-three (53), very fine- to coarse-grained sandstone samples were collected from five shallow wells located between Edmonton and Calgary. No detailed description of the cores is provided. These sandstones belong to the Haynes Member/Aquifer.

The sandstone is commonly well sorted (the fine-grained samples) to moderately and/or poorly sorted (the coarse-grained samples). The sandstone classifies as litharenite (Folk, 1980). Quartz (10-80%, average 60%) and rock fragments (10-75%, average 40%) dominate the detrital assemblage, feldspars are rare. The rock fragments component is dominated by volcanic rock fragments and chert, carbonate (primarily dolomite and rare limestone) and clastic (mudstone and siltstone) sedimentary rock fragments are subordinate. Small-sized particles and rock fragments usually show better rounding than coarser particles (e.g., quartz and chert). Minor to strong compaction features are visible although no major sutured contact indicative of deep burial is described. Visible porosity under the microscope ranges between $<$1% to 35% (average around 15%), coarse-grained samples are commonly more porous than fine-grained samples. No trend between porosity with either depth or hydraulic conductivity is present (Grasby et al., 2007, 2008) and there is no mention of unconsolidated sandstone intervals in the cores.

Three types of porosity have been proposed by Grasby et al., (2007): intergranular porosity, secondary porosity and microporosity. Intergranular porosity strongly dominates, secondary porosity is related to dissolution of feldspars and microporosity is associated with leaching of chert and volcanic

rock fragments. The primary intergranular porosity is almost entirely devoid of pore-filling clay matrix. Authigenic pore-filling material is composed of trace to <5% of chlorite and kaolinite, calcite cement is absent from most samples. However, when present, it can form 3-15% of total rock volume. Chlorite occurs as a thin coating around particles and on pore walls and as a more or less developed pore-filling phase. Kaolinite occurs as a pore-filling cement.

The proposed paragenetic interpretation suggests early chlorite coatings as micrometric rims on detrital quartz and rock fragments. This is followed by significant overlapping precipitation of pore-filling chlorite, kaolinite and calcite after some burial of the studied unit and early alteration/dissolution of feldspars and some rock fragments.

Hughes et al. (2017a) presented qualitative petrographic descriptions of 20 sandstone samples from three wells drilled and cored southwest of the Fox Creek area. The geological map indicates that the wells were drilled at the map transition between the Lacombe Member (Lacombe Aquitard) and the Dalehurst Member (Sunchild Aquifer) of the Paskapoo Formation.

The sandstone samples are classified as litharenite (Folk, 1980) with, however, no details on precise mineralogical composition. The sandstone is very fine- to coarse-grained with particle sorting ranging from good for fine-grained sandstone to poor for coarse-grained samples. The porosity, directly measured on parent rock samples with air permeameter, ranges from 0.01 to 15.3% (average 5.8%).

The three types of porosity presented by Grasby et al. (2007) are used in Hughes et al. (2017) with suggested similar origins. Pore-filling cement consists of kaolinite and calcite, although their respective abundance is unknown. Chlorite is described as relatively common (even if in small amount) in the petrographic observation for the Haynes Aquifer sandstone, but is not reported for the Sunchild Aquifer sandstone. No detail on the paragenetic succession of events is provided and no mention of unconsolidated intervals is stated.

Reports of friable to unconsolidated intervals in the Paskapoo sandstone

We have found a limited number of mentions of highly friable to unconsolidated sandstone intervals in cores of the Paskapoo Formation. For all theses cases, no discussion or interpretation for the anomalous friable and unconsolidated material is presented. These mentions are:

- Carrigy (1971) identified numerous intervals of friable and highly friable sandstone occurring between well cemented sandstone beds in shallow cores at the McCleod River dam site (around 100 km south of Fox Creek), this locality is underlain by shallow bedrock of the Lacombe and Dalehurst members (Hughes et al, 2107a).
- Hamblin (2007c) identified a 12 m interval with the presence of some friable sandstone zones in a well drilled in the Haynes Member northeast of Red Deer (ARC Corehole 4-82 Clive).
- Riddle et al. (2009) provided core description of shallow wells drilled between Calgary and Edmonton. From the thick bedded sandstone character and contact with the Scollard Formation, coring of the Paskapoo Formation took place in the Haynes Member. Two wells (75 and 100 km south of Edmonton) have mentions of intervals (1.2 and 0.8 m) consisting of unconsolidated sandstones.

- Smerdon et al. (2016) suggested the presence of a 4.5 m interval of poorly lithified sandstone in cuttings from one borehole located about 7 km SE of our well MW9B. The borehole was drilled in the Dalehurst Member / Sunchild Aquifer.

Petrography of Paskapoo Formation sandstones – Fox Creek area

A total of 20 sandstone (and one mudstone) samples were selected for the current study for conventional petrographic study. The sandstone samples are varied: they are fine-grained to coarse-grained, non-calcareous to strongly calcareous, and have a well-compacted to friable texture. The position of the samples is shown on the three stratigraphic logs of the wells (Figs. 4 to 6) with megascopic details in Annexes 1 to 3. The petrographic observations are summarized in Table 3 with selected photomicrographs presented in Annexes 7 to 9. Table 4 presents the average composition of the sandstones based on granulometry (fine, medium, coarse).

Table 3. Summary of petrographic observations for the three wells.

Sample	Depth	Gr. size	Sort.	Comp.	Q (%)	R (%)	F (%)	ϕ (%)	Chl (%)	Kao (%)	Calc (%)	Remarks
MW9B-3	21.79	F	F	S	60	35	5	<1	0	0	0	Matrix 35%
MW9B-6	30.43	F	G	S	65	30	5	1	0	0	0	Matrix 35%
MW8D-7	14.45	M	G	F	30	70	Tr	15	5	0	5	SRF>VRF>MRF, Dc, Cc
MW8D-2	15.06	C	F	F	35	40	Tr	<1	0	0	25	VRF>SRF, Dc, Cc, Pp+Sp
MW8D-8	15.24	M	G	F	30	70	Tr	25	1	5	5	SRF>VRF>MRF, Dc, Cc, Pp
MW8D-3	17.4	C	P	F	55	35	5	15	3	0	0	Chl coating, SRF>VRF, Dc, Pp
MW8D-9	23.01	F	F	F	70	25	5	5	0	0	0	Matrix 35%
MW8D-11	31.55	F	G	F	75	25	Tr	1	0	0	1	Matrix 45%, Burrows
MW3E-27	12.55	M	G	F	35	60	5	20	1	1	0	Chl coating, SRF>VRF, Dc, Pp+Sp
MW3E-28	19.86	F	G	S	65	35	Tr	5	0	0	1	Matrix 30%
MW3E-29	26.52	F	G	S	2	0	0	15%	0	0	0	Soil mud with shrinkage fractures
MW3E-12	53.34	M	F	S	60	30	5	5	2	3	0	Chl coating, VRF>SRF, Dc, Pp+Sp
MW3E-14	57.81	M	G	S	50	45	5	2	2	3	0	Chl coating, VRF=SRF, Dc, Pp+Sp
MW3E-16	64.77	M	F	S	35	55	10	<1	0	0	0	SRF>VRF>MRF, Matrix 2%
MW3E-18	65.99	M	P	F	35	60	1	5	1	2	1	Chl coating, VRF>SRF>MRF, Dc, Cc, Pp
MW3E-19	70.1	M	G	S	35	50	5	2	1	0	10	Chl coating, SRF>VRF, Dc, Cc, Pp+Sp
MW3E-20	73.28	M	G	F	50	48	2	20	2	2	0	Chl coating, VRF>SRF, Pp+Sp, Coal
MW3E-33	76.15	M	P	S	45	50	2	5	1	3	0	MRF>VRF>SRF, Dc, Pp+Sp, Matrix 10%
MW3E-34	88.34	F	G	S	75	20	5	5	0	0	0	SRF, fractures, coaly laminations
MW3E-25	96.8	F	P	S	65	25	Tr	2	Tr	0	0	Matrix 10%, VRF>SRF
MWE3-26	97.84	F	G	S	80	3	2	0	0	0	0	Matrix 15%, biotite

Notes: Gr. is grain size: F (Fine is 0.06 to 0.25 mm), M (medium is 0.25 to 0.5 mm), C (coarse is 0.5 to 2 mm). Sort. is sorting, P (poor), F (fair), G (good), Comp. is compaction, M (minor), F (fair), S (strong). Q is quartz, R is total rock fragments (including chert), F is total feldspars, ϕ is visual porosity (total primary and secondary), Chl is chlorite, Kao is kaolinite, Calc is calcite. VRF is Volcanic Rock Fragment, SRF is Sedimentary Rock Fragment (includes chert), MRF is Metamorphic Rock Fragment. Dc is Detrital calcite, Cc is Calcite cement. Pp is Primary porosity, Sp is Secondary porosity. Selected photomicrographs are presented in Annexes 7 to 9.

Table 4. Average composition summary based on sandstone grain size from Table 3. Abbreviations are as in Table 3.

Grain size	Number	Sort.	Q (%)	R (%)	F (%)	ϕ (%)	Chl (%)	Kao (%)	Calc (%)	Matrix (%)
Fine-grained	8	G	69.5	26	3	2.5	0	0	0	10
Medium-grained	10	G	40.5	53.8	3.5	10	1.6	1.9	2.1	0
Coarse-grained	2	F	45	50	2.5	7.5	1.5	0	13	0

Detrital components

From the relative abundance of the diverse detrital components in the sandstone, it is classified as litharenite, rare fine-grained quartz-rich sandstones are sub-litharenite (Fig. 7). The description of the detrital components and the textural properties of the sediment follow, authigenic cements are described afterwards.

Quartz particles consist of both monocrystalline (average 65% of total quartz) and polycrystalline (average 35% of total quartz) types. Both types can carry a significant number of inclusions either dispersed or in trails. Quartz particles are usually subrounded (coarse grains) to subangular (fine grains). Overall, quartz is more abundant in fine-grained sandstone (Table 4).

Total rock fragments include volcanic, sedimentary (carbonate, shale, and siltstone), metamorphic rock fragments and chert. Volcanic rock fragments (VRF) are of mafic type with dark colored, aphanitic matrix containing various percentages of small feldspars laths, the VRF are locally partly dissolved (Annex 9, MW3E-20). Sedimentary rock fragments include locally abundant shale and detrital carbonates (both limestone and rare dolostone) and rare siltstone – sandstone. Carbonate fragments are made up of commonly well-rounded clasts of dominant finely crystalline lime mudstone and subordinate clasts of medium- to coarse-grained dolomite rhombs. Shale fragments are present in most samples. Rare metamorphic rock fragments are made up of mica-rich phyllites, the metamorphic rock fragments are only seen in the coarser-grained samples. Like quartz, the rock fragments are either sub-rounded for the coarse particles and sub-angular for the fine-grained cases. Chert fragments are present in all samples, they are microcrystalline some with sweeping extinction. Chert particles are sub-rounded, commonly altered and partially leached (Annex 8, MW8D-2, MW8D-3).

Feldspars are relatively unabundant (10% at the most) and represented by plagioclases. The grains are usually angular and significantly altered (sericite) and leached (Annex 9, MW3E-12). Trace amounts of pyrite, zircons and apatite are rarely present in the sandstones, pyrite is very angular and occurs as replacement, whereas zircon and apatite are sub-rounded to sub-angular. Angular coal fragments are present in about 10% of the sandstone samples and some coaly laminations are present in fine-grained sandstone (Annex 9, MW3E-34). Amorphous detrital more-or-less calcareous matrix is seen in pore space of some fine-and medium-grained sandstone. Sample MW3E-29 (Annex 9) consists of compacted limy mud with abundant open shrinkage fissures with some minor kaolinite cement, representing a soil profile.

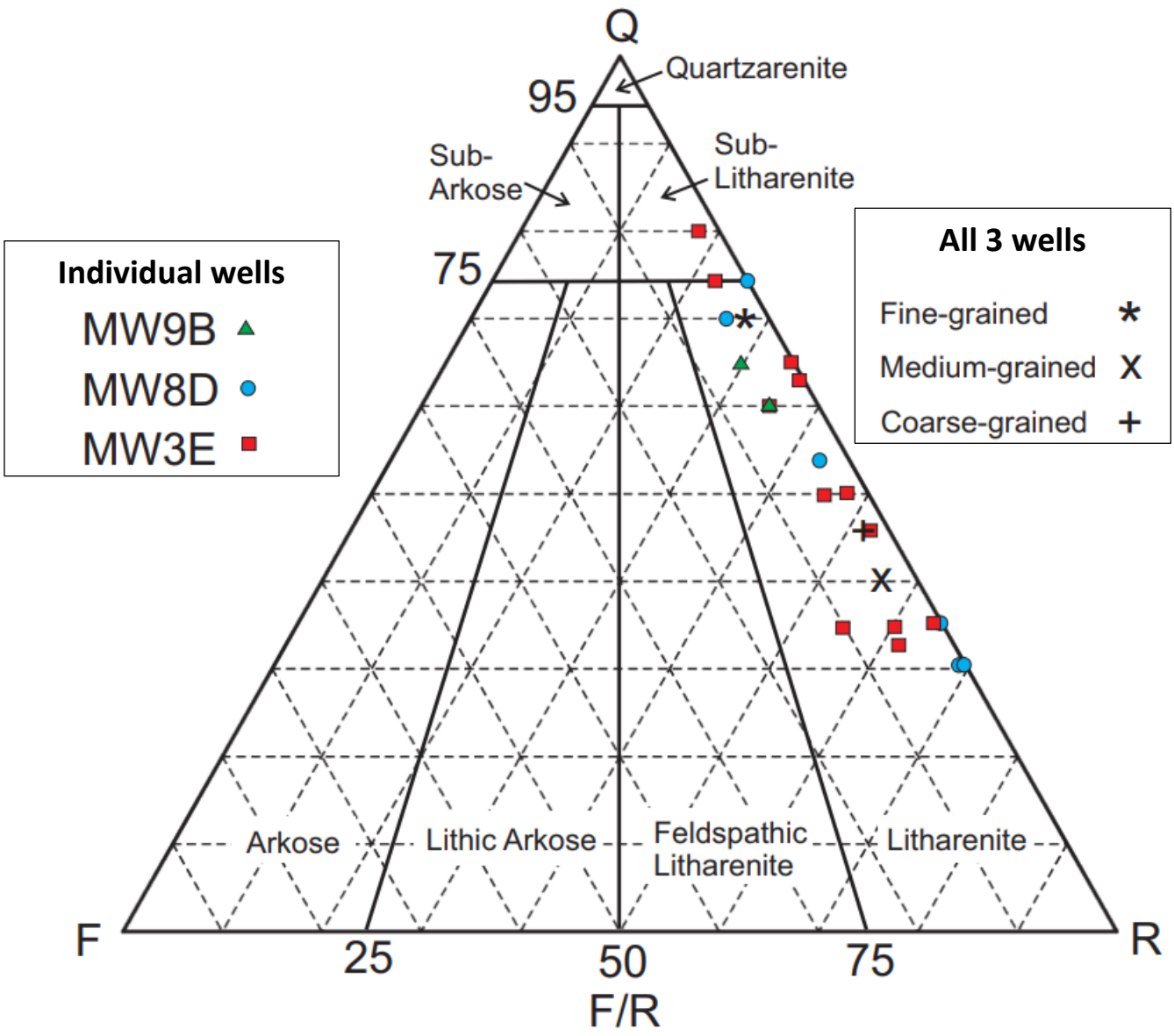

Figure 7. Classification of the sandstone based on Folk (1980). Q is for quartz, F is for feldspars and R is for total rock fragments (chert, sedimentary, volcanic and metamorphic). Average composition of fine, medium and coarse-grained samples is also shown (data in Tables 3 and 4)

Textural properties

The roundness of particles is partly controlled by grain size, with finer-grained samples having dominant sub-angular particles whereas coarser-grained material being characterized by more sub-rounded grains. Grain sorting ranges from good to fair in fine-grained samples whereas coarser-grained samples are mostly characterized by fair to poor sorting (Table 3). Some of the Paskapoo fine-grained sandstones have amorphous intergranular clay matrix. However, almost all medium- and coarse-grained samples present a grain-supported fabric and have no detrital clay matrix. Grains have commonly more or less extensive point-contact, it is noteworthy that the intensity of point contact is lower when grains have full coatings or only partial outer rims of clay material.

Pore-filling authigenic minerals

The pore-filling authigenic minerals fill either totally or partially the post-depositional pore space. Time relationships between these diagenetic phases are ambiguous at places but very clear in other cases (see **paragenesis** below). Overall, total cement is relatively unabundant in the studied samples as it rarely exceeds 5%, kaolinite being the most common cement type. Calcite cement is rarely seen, although when present, it can be abundant (up to 25% of single thin section).

The first element in the intergranular primary pore space consists of rims of clays coating diverse detrital particles. The rims are isopachous layers of 2 to 10 microns thick and the clay material is largely amorphous, although some neomorphism to chlorite is locally visible (Annex 8, MW8D-3). The coatings can be entirely developed over all visible faces of a crystal (Annex 8, MW8D-3) or only on some grain boundaries (Annex 9, MW3E-18). Coatings can also cover multiple contiguous grains lining entire pore walls (Annex 8, MW8D-3), this particularity helps to identify areas where coatings seem to float in pore space, suggesting post-coating dissolution of a precursor chemically unstable mineral (Annex 8, MW8D-3). In places, the coating follows some initial compaction of the sediment as is not present at grains point-contact (Annex 8, MW8D-3). The precise mineralogical nature of the amorphous clay coating is uncertain. A detailed discussion on this topic is presented below (see **Clay coatings on grains** below).

Chlorite cement uses amorphous clay rims to expand into the pore space (Annex 8, MW8D-3). However, pore-coating greenish chlorite is also locally visible (Annex 9, MW3E-19). Overall, the volume of the chlorite cement is very minor in the pore-filling components.

Calcite cement is either totally absent from some samples or can be very important and fills most of the primary pore space in other samples (Annex 9, MW3E-19). The calcite cement is primarily made up of small equigranular pore-filling crystals (Annex 8, MW8D-2). It rarely presents itself as a large poikilotopic single crystal in pore space (Annex 8, MW8D-7; Annex 9, MW3E-18) or as resedimented broken poikilotopic fragment (Annex 8, MW8D-7). No typical cement features (meniscus, pendant or pore floor vadose silts), as reported by Longman (1980), associated with precipitation in water-undersaturated vadose meteoric environment could be identified in the cores of the three available wells.

A relatively common type of authigenic cement is kaolinite, although it rarely represents more than 3% of total components. Nonetheless, microcrystalline kaolinite cement can fill entirely some intergranular pore space (Annex 9, MW3E-20) and commonly engulfs heavily dissolved and broken feldspar crystals (Annex 9, MW3E-12). Kaolinite is definitively formed after clay rims, but the exact physical/time relationships with chlorite and calcite cements is ambiguous.

Porosity

Grasby et al. (2007) have identified three types of porosity in the sandstone of the Haynes Aquifer: 1) intergranular, 2) secondary and 3) microporosity; the same classification of porosity has been used by Hughes et al (2017a) for the Sunchild Aquifer. The intergranular porosity dominates. However, it was not clear from the publication of Grasby et al. (2007) whether their intergranular porosity is only of preserved primary origin or whether it also includes intergranular pore space after some dissolution of early pore-filling cement(s) or detrital minerals. In the current work, we propose that primary porosity consists of preserved initial intergranular porosity, while secondary porosity comprises all small and

large pore spaces generated from early and/or late alteration and dissolution of mineral phases in the presence of chemically aggressive freshwater. There are likely multiple episodes of secondary porosity generation.

Our petrographic thin sections were prepared with blue epoxy allowing to better identify porosity. From our petrographic observations, total porosity visual estimates range between less than 1% up to 25% (Table 3) with medium- and coarser-grained sandstone being more porous (Table 4). Initial intergranular primary porosity is the dominant type of pore space (Annex 9, MW3E-20), constituting over 80% of the overall porosity. The interpretation of initial porosity relies on the absence of preserved evidence of dissolved precursor minerals in the pore space. Where such evidence is visible, this specific pore space is qualified as secondary. The size of the intergranular primary pore space is controlled by the grain size of the sediments, with the interstitial space being up to 0.5 mm wide being seen in little compacted coarse-grained sediment.

Secondary pore space is either minor or significant and originates from partial leaching of either detrital minerals or intergranular primary pore filling cement. Feldspar leaching is the dominant type of secondary porosity with dissolution being commonly initiated along twinning planes (Annex 9, MW3E-12). This type of secondary porosity can be locally connected with intergranular primary pore space making it a potentially significant component of the permeability system. Some volcanic rock fragments offer evidence of leaching (Annex 9, MW3E-20) that could create small secondary pore space as wells as chert (Annex 8, MW8D-2, MW8D-3). Partial leaching of kaolinite cement can be observed; however, this secondary pore space is very small (a few microns) and is not unequivocally connected to the dominant intergranular pore space.

Some detrital carbonate fragments and cements show the effects of multiple events of dissolution and precipitation. One example consists of a calcite clast showing localized dissolution with the resulting pore space being filled by the same small equigranular calcite cement present in the adjacent pore space (Annex 8, MW8D-2). This specific pore-filling calcite cement is also locally dissolved (Annex 8, MW8D-2).

Primary porosity is a post-sedimentary feature controlled by grain size, the presence or absence of a detrital matrix and compaction. While secondary porosity is clearly associated with dissolution of metastable particles or cements, the precise number and timing of such dissolution events (e.g., early *versus* late) are, however, difficult to evaluate.

Carbon and Oxygen stable isotopes of calcites

Shallow and local groundwater in the Fox Creek area is of the Ca-HCO_3 type, suggestive of carbonate contribution to the chemical load, while groundwater slightly deeper and more regional is of the $NaHCO_3$ type, indicating a more chemically evolved water (Rivard, 2022). The Paskapoo Formation aquifer is hosted by more-or-less calcareous sandstone. Twelve sandstone samples were selected for conventional $\delta^{18}O_{VPDB}$ and $\delta^{13}C_{VPDB}$ ratios of their carbonates (Table 5, Fig. 8). The analyses were carried out to identify: (1) the HCO_3^- source involved in the precipitation of calcite cement and (2) the nature of the fluid at the time of cement precipitation. The stable carbon isotope data will also be used in future publications to assess the source of dissolved inorganic carbon in modern groundwater.

Due to the small size of the calcite elements (detrital particles and small pore-filling crystals), it is impossible to sub-sample the various types. Consequently, the results presented come from bulk analyses of a sample. However, 10 of the isotopic analyses were performed on samples from which thin sections were prepared. As such, an estimate of the relative abundance of detrital (fragments, limy matrix) and cement calcite in these individual samples is available (Table 5).

Powdered samples were acidified at 90°C and purified using the Franken-Kiel carbonate preparation device hyphenated to a MAT253 plus isotope ratio mass spectrometer in the Delta-Lab of the Geological Survey of Canada. Isotopic ratios are measured on the derived CO_2 using the long integration dual inlet procedure allowing to maximize ion counting time on samples. The standardisation scheme is based on interlaboratory characterized ETH standards (Bernasconi et al., 2021) with standard deviation below 0.1‰ and 0.3‰ for $\delta^{13}C$ and $\delta^{18}O$ respectively, both reported under the Vienna Pee Dee Belemnite (VPDB) standard.

Table 5. Summary of oxygen and carbon stable isotope values for calcites in the sandstone samples; data are reported on Figure 8.

	Depth	**$\delta^{18}O$**	**$\delta^{13}C$**	**Remarks**
Sample (calcite)	**(m)**	**‰ (VPDB)**	**‰ (VPDB)**	**%Dc (total % CaCO3 on thin section)**
MW9B-3	21.7	N/R	N/R	-------
MW8D-7	14.45	-10.5	0.1	50 (5%)
MW8D-8	15.24	-10.5	-0.2	75 (5%)
MW8D-9	23.01	-11	-0.3	0 (2%)
MW8D-11	31.93	-10.9	-1.6	0 (5%)
MW3E-27	12.55	N/R	N/R	-------
MW3E-28	19.86	-11.5	-0.2	0 (5%)
MW3E-29	26.52	-11.9	1.3	0 (85%)
MW3E-31	46	-12.3	-0.7	No thin section
MW3E-32	66.75	-15.8	-0.8	No thin section
MW3E-33	76.15	-10.6	-0.1	95 (1%)
MW3E-34	88.34	-10.2	-0.1	90 (5%)
Average		-11.5	-0.3	
σ		1.6	0.7	

Notes: %Dc is the relative abundance of detrital calcite over total calcite from thin sections petrographic observation. $\delta^{13}C_{VPDB}$ versus %Dc are plotted on Figure 9. N/R is for no result from insufficient CO_2 gas derived from sample digestion at the laboratory.

The $\delta^{18}O_{VPDB}$ values range from −15.8 to −10.2‰ (average of −11.5 ±1.6‰) and the $\delta^{13}C_{VPDB}$ values range from −1.6 to 1.3‰ (average −0.3 ±0.7‰) (Table 5, Fig. 8). The $\delta^{18}O_{VPDB}$ values are slightly more dispersed than the $\delta^{13}C_{VPDB}$ values. The $\delta^{18}O_{VPDB}$ values of samples from MW3E well are slightly more negative compared to those of MW8D well. There are no obvious significant differences in $\delta^{13}C_{VPDB}$ values between the two wells.

The range of isotopic data for both $\delta^{18}O_{VPDB}$ and $\delta^{13}C_{VPDB}$ for wells MW8D and MW3E is less dispersed than that of the results of Khidir and Catuneanu (2010) from one field section of the lower part of the

slightly older (Maastrichtian; latest Cretaceous) fluvial sandstone of the Willow Creek Formation of southern Alberta (Fig. 8). The samples from the Willow Creek Formation were from calcite cement only (Khidir and Catuneanu, 2010). There is, however, some overlap in values for $\delta^{18}O_{VPDB}$ for the two datasets, but the $\delta^{13}C_{VPDB}$ values are more negative in the Willow Creek Formation samples compared to the results from the Paskapoo Formation (Fig. 8). Detrital calcite fragments are abundant (between 1.3 and 9.2% of total detrital components) in the Willow Creek Formation, although no details on the nature of the detrital calcite is provided (Khidir and Catuneanu, 2010). Calcite cement is common in the Willow Creek Formation (average of 15% of total cement) and is described as either large poikilotopic calcite crystals or detrital micrite. According to Khidir and Catuneanu (2010), calcite cement fills primary and secondary porosity and is interpreted as originating from the vadose zone based on negative $\delta^{18}O_{VPDB}$ values and petrographic observations of vadose soil features (rhizocretions and glaebules) in the samples studied. Our interpretations of both $\delta^{18}O_{VPDB}$ and $\delta^{13}C_{VPDB}$ values for the Paskapoo Formation is presented below (*see* **Type of interstitial fluid and potential source of HCO_3^- for calcite cement**).

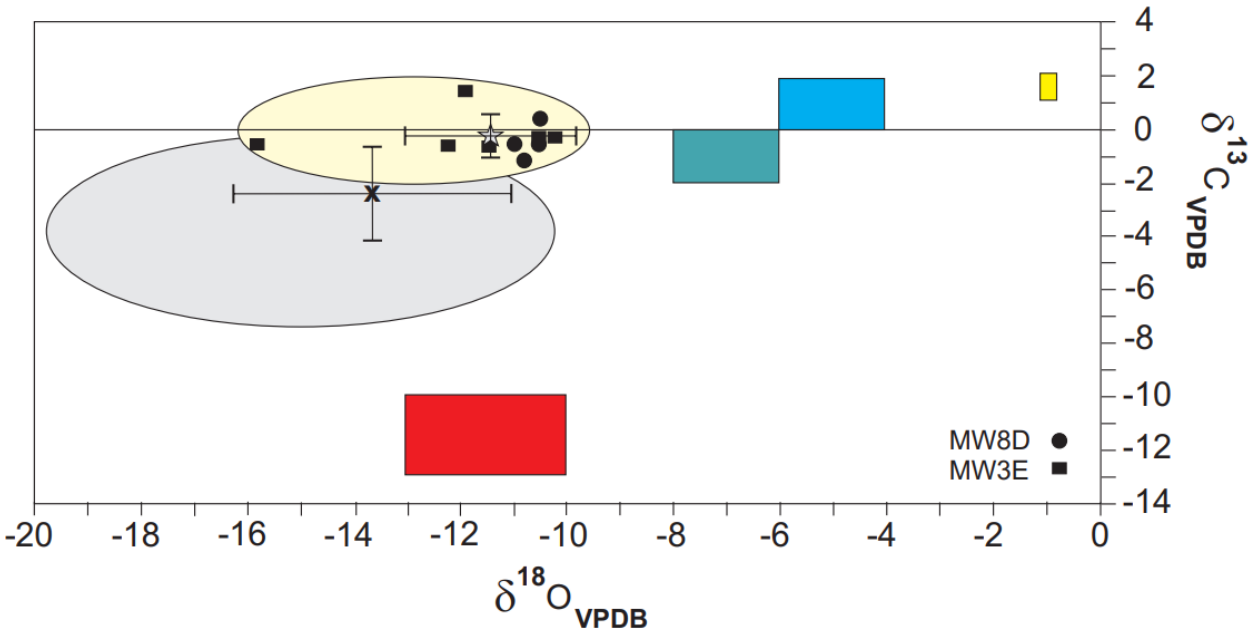

Figure 8. $\delta^{18}O_{VPDB}$ versus $\delta^{13}C_{VPDB}$ values for the carbonate particles and cements from the Paskapoo Formation (pale yellow ellipse; data in Table 5), the grey star (–11.5 ±1.6‰ and –0.3 ±0.7‰) is the average value of $\delta^{18}O_{VPDB}$ and $\delta^{13}C_{VPDB}$, respectively. The grey ellipse illustrates the extent of the field of data (N=18) for the slightly older Willow Creek Formation in southern Alberta (Khidir and Catuneanu, 2010) and the symbol ***x*** *(–13.5 ±2.6‰ and –2.5 ±1.6‰) corresponds to the average value of $\delta^{18}O_{VPDB}$ and $\delta^{13}C_{VPDB}$, respectively. The $\delta^{18}O_{VPDB}$ versus $\delta^{13}C_{VPDB}$ values for seawater calcites (Veizer et al., 1999) are represented by the yellow box (Paleocene), blue box (Devonian-Mississippian), and green box (Cambrian). The red box is the hypothetical $\delta^{18}O_{VPDB}$ versus $\delta^{13}C_{VPDB}$ range of a Paleocene-aged freshwater calcite cement from pool of soil-derived HCO_3^- in the Fox Creek area (see* ***Type of interstitial fluid and potential source of HCO_3^- for calcite cement****).*

Discussion

Burial and temperature history for the Paskapoo Formation in the Fox Creek area

Ardakani (2022) from a detailed organic matter petrographic study of 12 well cutting samples of the shallow Paskapoo Formation in the study area, concluded that the *in-situ* Type III (terrestrial) organic matter is immature with vitrinite reflectance ranging from 0.39 to 0.49% (average of 0.42%). These values are indicative of maximum burial temperatures lower than 60°C. On a more global perspective, the sedimentation of the Paskapoo Formation during the Paleocene took place in the final stages of the Cordillera foreland basin (Hamblin, 2004) near the peak of the Laramide orogeny (Late Cretaceous to Middle Eocene; Lawton, 2019). Based on apatite fission tracks, Issler et al. (1990) suggested that 1.1 to 1.5 km of strata have been eroded post-Laramide orogeny in the western area of the Peace River Arch, a few kilometers to the north of the study area. Issler et al. (1990) proposed that the area closer to the Cordilleran deformation front had a Cenozoic paleogeothermal gradient ranging between 22 to 28°C/km. From a large well database from the Peace River Arch, Bachu and Cao (1992) suggested that the paleogeothermal gradient in Cenozoic times was between 25 to 35°C/km. With an average gradient value of 28°C/km, the top of the Paskapoo Formation in the Fox Creek area was likely buried under less than 2 km of strata. The assumed maximum burial temperature (<60°C) recorded in the organic matter of the Paskapoo Formation in the studied area is a critical element to consider for the interpretation of diagenetic products and history.

Clay coating on grains

It has long been known that early clay coating on depositional particles, in particular quartz, is an efficient porosity and permeability preservation mechanism for sandstone hydrocarbon reservoirs (Heald and Anderegg, 1960; Heald and Larese, 1974). Significant early clay coating can: 1) strengthen the original porous depositional framework, 2) prevent significant quartz grain contacts, thereby reducing silica solution-pressure and early quartz overgrowth and 3) inhibit later pore-filling silica cementation by limiting the available quartz surface as substrate for precipitation (Worden et al., 2020; Griffiths et al., 2021; Charlaftis et al., 2021). In their petrographic studies of the Paskapoo Formation sandstones, Carrigy (1971) and Grasby et al. (2007) interpreted micrometer-thick rims of clay minerals locally coating various detrital grains as being composed of chlorite. These grain coatings are either preserving open pore space or are followed by diverse authigenic minerals (calcite, kaolinite, chlorite) in pore space. No clay coatings have been reported in the petrographic study of Hughes et al. (2017a). In the Late Maastrichtian - Early Paleocene fluvial sandstones from the Willow Creek Formation (slightly older than the Paskapoo Formation) of southern Alberta, smectite early grain coatings, later partially recrystallized into chlorite, have been identified under scanning electron microscopy (SEM) petrography and associated with preservation of the pore network and thus favorable reservoir characteristics (Khidir and Catuneanu, 2010).

For the present study, SEM images or XRD analyses are not available to precise the mineralogical composition of the amorphous clay coating. Based on limited conventional petrographic observations, we assume, like Carrigy (1971) and Grasby et al. (2007), that some chlorite is present. Sandstones with chlorite grain coatings occur in all depositional environments from estuarine to deltaic and fluvial sandstones (Dowey et al., 2012). Chlorite presence as a primary mineral in a detrital clay fraction is common (Griffiths et al., 2018; Worden et al, 2020) and grain coating develops rapidly after

sedimentation. Chlorite does not easily precipitate directly from a low temperature fluid (Worden and Morad, 2003), and authigenic chlorite coatings may be the result of recrystallization of precursor minerals present in original amorphous detrital clay coats (Wooldridge et al., 2017, 2019). The high-energy Paskapoo Formation medium- and coarse-grained sandstone is largely devoid of detrital clay matrix. Infiltration has been invoked as a way of incorporating, shortly after deposition, clay particles into well-sorted and clay-deficient high-energy sand (Walker et al., 1978, Matlack et al., 1989). Surface water carries suspended clays and can percolate through a porous unsaturated (vadose) zone, entraining fine clay sediments within the granular matrix.

According to a compilation of several research studies, chlorite, if not present initially, may have many origins: transformation of detrital Fe-rich berthierine (Longstaffe, 2003), transformation of Mg-rich smectite (Humphreys et al., 1994), reaction of kaolinite with sources of Fe (Burton et al., 1987) and breakdown of volcanic grains (Worden et al., 2020). The global database on authigenic chlorite coatings suggests that those in marine sandstones frequently have a berthierine precursor, whereas chlorite in continental sandstones commonly originates from initial smectite (Worden et al., 2020). Fe-rich clay berthierine is common in soil profiles (Toth and Fritz, 1997). It corresponds to a clay phase that, through several solid-state steps (Xu and Veblen, 1996), transforms into Fe-rich chlorite at temperatures starting at 40°C (Aagaard et al. 2000; Vidal et al., 2012). The transformation of smectite to chlorite follows a stepwise process of dissolution – reprecipitation with evolving smectite-chlorite interstratified assemblages during burial diagenetic processes (Hoffman and Hover, 1979: Humphreys et al., 1994).

Type of interstitial fluid and potential source of HCO_3^- for calcite cement

Oxygen and carbon stable isotope ratios in calcite provide information on two major elements that are essential for understanding the diagenetic events. Water is an infinite oxygen reservoir and $\delta^{18}O_{VPDB}$ values of carbonates are indicative of the nature of the diagenetic fluid (marine, meteoric, burial, and eventual mixing) responsible for the initial precipitation or later alteration/recrystallization of the carbonates. On the other hand, water is a limited carbon reservoir and $\delta^{13}C_{VPDB}$ values of carbonates are indicative of the source of dissolved bicarbonate ions in water and the intensity of eventual interactions (dissolution) with surrounding $CaCO_3$ material prior to precipitation of the carbonate phase. Dissolving large volume of detrital calcite in a saturated porous medium would have no effect on the $\delta^{18}O_{VSMOW}$ value of the diagenetic fluid. However, such dissolution would have a major impact on the $\delta^{13}C_{VPDB}$ value of HCO_3^- in the diagenetic fluid.

For the nature of the fluid present at the time of calcite cementation / alteration in the Paskapoo Formation sandstones, the $\delta^{18}O_{VPDB}$ can provide relative information on the timing of cement precipitation (i.e., either early from Paleocene $\delta^{18}O_{VSMOW}$ depleted meteoric water or later with inputs of isotopically different $\delta^{18}O_{VSMOW}$ from burial fluids in the diagenetic system).

For the source of HCO_3^- leading to the precipitation of calcite cements, the relative significance of two sources can be evaluated: (1) HCO_3^- may be derived from the dissolution of detrital calcite *in situ* in the sediments or at the source of the particles, and (2) HCO_3^- may be derived from soil and atmospheric CO_2.

The Paleocene (66 - 56 Ma) world in western North America

In Early Cenozoic, recent paleogeographic reconstruction locates the general area of Fox Creek under mid / high latitude settings (≈55 – 60°N; van Hinsbergen et al., 2015) at about 1000 km to the east of the Pacific Ocean coastline, the closest oceanic water mass for water vapour source, separated from the latter by the more or less high reliefs of the Rocky Mountains (Scotese, 2014). Atmospheric concentration of CO_2 was high (600 to 1300 ppm; Rae et al., 2021). In Early Cenozoic times, seawater calcite was slightly more negative in $\delta^{18}O_{VPDB}$ (≈ −1‰) compared to modern oceanic ones (≈ 0‰, Veizer et al., 1999; Fig. 8).

From the Paleocene, western North America rotated anticlockwise around 10-15° to reach its actual latitudinal setting. From a geographical perspective, the Fox Creek area was in Paleocene as far away as of today from the Pacific Ocean to the west and separated from it by the high relief paleo-Rocky Mountains. However, there is a major difference between the atmospheric concentrations of CO_2 at that time and today's values (415 ppm, 2021, National Oceanic and Atmospheric (NOAA) Global Monitoring Lab). Because of higher atmospheric concentration of CO_2 during the Paleocene, climate was hotter at higher latitudes (20 – 25°C at 55°N; O'Connor et al., 2023) and modern strong seasonal effects on latitudinal variations for isotopic composition of precipitation are not expected. Based on faunal and floral evidence as well as sedimentary indicators (coals, nature of soil profiles), the climatic conditions were hot and humid for the northernmost locations (e.g., Fox Creek) and semi-arid to very arid southerly (Jerzykiewicz and Sweet, 1988; Koch et al., 1995, Carmichael et al., 2017).

Nature of pore fluids

The baseline paleogeographic parameters compare well with present day conditions, as such, the isotopic fractionation during Rayleigh's distillation from condensation – precipitation events (Dansgaard, 1953, 1964) from the distant original source of water vapor is expected to be in the same general range as modern values. Today's $\delta^{18}O_{VSMOW}$ values of precipitation for the warmest months of the year (June-July-August 2021-2022) in the Fox Creek area are between −16 to −13‰ (D. Kononovs, unpublished preliminary data). This range of values agrees well with results from a 10-year series (1977-1987) for summer months near Edmonton (−17.4 to −13.5‰; average −15.6‰; Maulé et al., 1994). As the values for seawater were slightly more negative than today, it is estimated that the $\delta^{18}O_{VSMOW}$ value of Paleocene freshwater for the Fox Creek area could have ranged between −17 to −14‰.

Urey (1947) first proposed that the isotopic ratio of calcite precipitated from water is temperature dependent. Isotopic fractionation between calcite and water is controlled by kinetic processes, with calcite being enriched to varying degrees in heavy isotopes relative to the parent water. From years of multiple experiments on calcite precipitation at various temperatures, the following empirical equation was proposed by Daëron et al. (2019):

$$10^3 \ln(\alpha_{cc/w}) = 17.57 \times 10^3/T - 29.13$$

where $\alpha_{cc/w}$ is the fractionation coefficient for the calcite/water system and T is temperature in Kelvin.

At 25°C, likely the surface temperature for the Fox Creek area in Paleocene (O'Connor et al., 2023), α would be around 1.03. Hays and Grossman (1991) demonstrated that meteoric calcites from Devonian to modern ones at various paleolatitudes / temperatures are enriched by 4‰ in $\delta^{18}O_{VPDB}$ at 25°C with

respect to the parent water. Therefore, the $\delta^{18}O_{VPDB}$ values of near surface meteoric calcite in the Paleocene of the Fox Creek area could have ranged between −13 to −10‰ (Fig. 8). These values are slightly less depleted than those estimated earlier from modern-day data.

Interpretation of $\delta^{18}O_{VPDB}$ values

The $\delta^{18}O_{VPDB}$ values of calcite (detrital, mud, cement) for sandstone of the Paskapoo Formation are strongly negative. These $\delta^{18}O_{VPDB}$ negative values for the Paskapoo Formation suggest freshwater for calcite cementation and likely isotopic burial resetting of Paleozoic calcite elements prior to erosion in the Paleocene. From isotopic fractionation between calcite and meteoric water ($\delta^{18}O_{SMOW}$ values of −17 to −14‰), the measured $\delta^{18}O_{VPDB}$ data for the Paskapoo Formation calcite of −15.8 to −10.2‰ (Table 5, Fig. 8) agree nicely with the theoretical $\delta^{18}O_{VPDB}$ values of meteoric calcite of −13 to −10‰ at 25°C (Fig. 8). Detrital material from sample MW3E-29 consists of limy mud suggestive of soil profile, the $\delta^{18}O_{VPDB}$ values is consistent with percolation of meteoric water. In the absence of petrographic features indicative of the freshwater vadose zone, it is proposed that calcite cementation precipitated from freshwater in the phreatic zone.

Source of HCO_3^-

The precise age of detrital calcites in the Paskapoo Formation sandstone is unknown. They are most likely derived from sub-aerial erosion of rock units in the adjacent Rocky Mountain Foothills where significant carbonate successions of Cambrian and Devonian-Mississippian ages (Fig. 2) are tectonically stacked (Mossop and Shetsen, 1994). Marine calcites of that time interval in the Paleozoic have $\delta^{13}C_{VPDB}$ values ranging between −2 to +2‰ (Veizer et al., 1999; Fig. 8). From our petrographic work, detrital calcite is largely composed of more or less well preserved micrite clast with local dolomitization. As such, diagenetically altered marine carbonates eroded and resedimented in the fluvial environments of the Paskapoo Formation could have slightly more negative $\delta^{13}C_{VPDB}$ values compared to pristine marine calcite.

The other potential source of HCO_3^- for calcite cementation is *in-situ* soil derived CO_2 to be incorporated in the diagenetic fluid. Soil derived CO_2 originates from plant respiratory processes using atmospheric CO_2. Plant metabolism for photosynthesis follows two distinct patterns, the first one (C3 type) at times of high atmospheric concentration of CO_2 and the second one (C4 type) during times of low atmospheric concentration (Tipple and Pagani, 2007). Prior to the Miocene, all known plants were of the C3 type, plant metabolism evolved to C4 type in response to the significant drawdown of atmospheric CO_2 values from the Miocene to actual values, after the Paleocene-Eocene Thermal Maximum (Quade and Roe, 1999; Tipple and Pagani, 2007). However, C3 type vegetation is still present today. Paleocene vegetation in the Fox Creek area was of C3 type. C3 plants fractionate $\delta^{13}C_{VPDB}$ from atmospheric CO_2 by about −20‰ (Koch et al., 1995), and soil derived HCO_3^- from C3 plants has a wide range of $\delta^{13}C_{VPDB}$ values (−33 to −21‰, Koch et al., 1995; −35 to −20‰, Tipple and Pagani, 2007) with an average of −27‰. Precipitation of calcite from a pool of soil derived HCO_3^- are enriched by 14 to 17‰ in $\delta^{13}C_{VPDB}$ (Koch et al., 1995; Quade and Roe, 1999) and therefore $\delta^{13}C_{VPDB}$ of Paleocene-aged meteoric calcite cement from a source of solely soil-derived HCO_3^- would have ranged between −13 to −10‰ (Fig. 8).

Interpretation of $\delta^{13}C_{VPDB}$ values

Figure 9 presents the $\delta^{13}C_{VPDB}$ values of analysed total CO_2 from individual samples with respect of relative abundance of detrital calcite fragment versus calcite cement from petrographic observation; %Dc of 0 indicates no visible detrital calcite and 100 indicates no visible calcite cement (Table 5). Out of 12 samples submitted for analysis, 10 have thin sections for evaluation of %Dc although 2 samples did not yield sufficient CO_2 for analysis. Therefore, Figure 9 presents $\delta^{13}C_{VPDB}$ results versus %Dc for 8 samples.

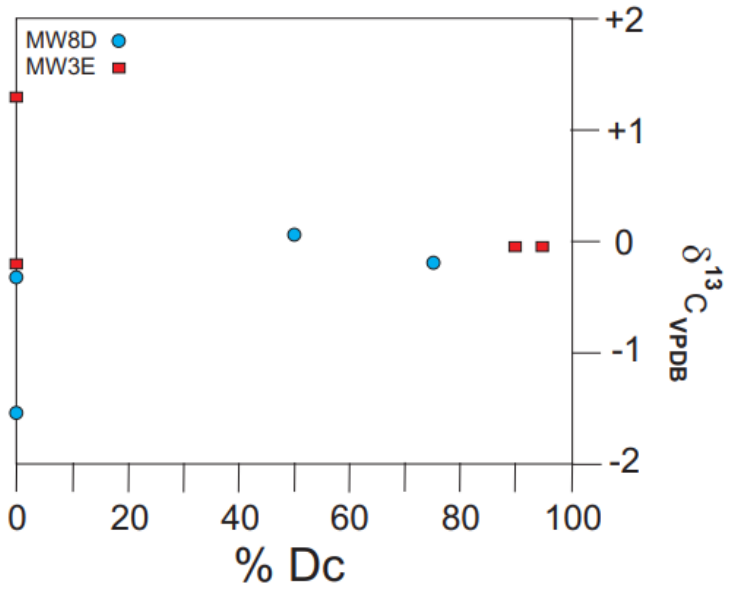

Figure 9. $\delta^{13}C_{VPDB}$ ratios versus relative abundance of detrital calcite over total calcite (% Dc). Data are presented in Table 5.

Despite the limited number of samples available, it seems clear that there is no relationship between the $\delta^{13}C_{VPDB}$ values and the relative abundance of diverse types of calcite component (fragment or cement) (Fig. 9). All values in the dataset agree with the assumed Paleozoic $\delta^{13}C_{VPDB}$ values of marine calcite (Fig. 8), there is thus no isotopic evidence of significant soil-derived HCO_3^- in the diagenetic system. The HCO_3^- clearly originates from the dissolution of Paleozoic calcite fragments that efficiently buffered the $\delta^{13}C_{VPDB}$ values of freshwater.

Paragenesis

The succession of diagenetic elements and events presented here is based on the nomenclature framework of Schmidt and McDonald (1979). Early diagenesis is known as eodiagenesis and encompasses immediate post-sedimentation events and products occurring in the presence of non-modified pore water (in our case, freshwater). Mesodiagenesis follows and covers the burial history with evolved pore fluids, while telodiagenesis, a late diagenetic process, comprises events affecting the sedimentary succession after its eventual return (uplift) to the influence of surface processes. In our case, thermal indicators from *in-situ* organic matter reflectance and apatite fission tracks modelling suggest that the successions went through shallow burial and did not reach temperature over 60°C.

Therefore, the Paskapoo Formation in the Fox Creek area went through a complete cycle of sedimentation, shallow burial and final exhumation to surface conditions.

Eodiagenesis – Early freshwater diagenesis

- Early diagenetic evolution in the presence of freshwater, recorded initially detrital amorphous clay infiltration possibly as chlorite, smectite or berthierine that coated particles, allowing the formation of a "framework" in the vadose zone. Thus, in coarse-grained and most medium-grained sandstones, this early clay coating on quartz particles prevented significant physical compaction that would have led to silica dissolution at point-contact and precipitation of early, pore-filling silica as overgrowth on quartz.
- For some medium-grained sandstones and for all fine-grained sandstones, the presence of detrital argillaceous matrix is observed. That matrix is more or less calcareous.
- Early dissolution of chemically unstable particles such as plagioclase feldspar, chert, volcanic rock and calcite fragments was active in freshwater most likely resulting in an increase in concentration of various ions in groundwater (Ca, Mg, Al, Fe, Si, HCO_3).
- Initial cementation by calcite in the pore space followed and, based on the blocky to equant crystal growth shape and $\delta^{18}O_{VPDB}$ and $\delta^{13}C_{VPDB}$ ratios, precipitation from freshwater in the phreatic zone (aquifer) is suggested from a parent water dominated by a Paleozoic source of bicarbonates (detrital calcite) with no evidence of soil-derived CO_2. The possibility of a late (telodiagenesis) freshwater calcite cementation cannot be entirely ruled out, but a few examples of calcite cement being partly dissolved suggest the presence of the cement prior to late sub-aerial exhumation and dissolution.
- Kaolinite forms at shallow burial depths less than 1,400 m and preferably early, at low temperature, in the presence of freshwater (Khanna et al., 1997; Bjørlykke, 1998). Dissolution of feldspars provides chemicals (Al, Si) needed for precipitation of kaolinite, especially if K is absent in the system (Lønøy et al., 1986; Lanson et al., 2002). No potassic feldspars have been observed in the sediments.

Mesodiagenesis – Burial evolved pore water

- Physical compaction continued and led to a reduction of porosity, especially for pores free of early cements (calcite and/or kaolinite). No post-shallow burial chemical compaction (stylolite) was observed in cement of the calcite-rich samples.
- With increasing depth of burial, formation water flow becomes increasingly limited and is accompanied by a temperature increase. Given the presence of sufficient ionic loads and concentrations, calcite and kaolinite cementation could continue, but at a slower rate. In a relatively closed diagenetic system with a low water/rock ratio, the presence of K in pore water would result in partial dissolution of kaolinite (Lanson et al., 2002).
- Recrystallization of the precursor amorphous clay into well-ordered chlorite appears incomplete. This should have occurred during mesodiagenesis, but the relatively shallow burial and low temperature experienced by the unit prevented complete transformation. For example, detailed TEM/EDS have shown that amorphous Fe-rich clay (berthierine) coating can still be preserved and abundant even at great depths ($>$2.4 km; Aagaard et al. 2000).
- Pore-filling chlorite commonly precipitates in a Fe-rich, closed diagenetic system. Based on previous studies, its usual presence prior to silica cement indicates that the precipitation of

chlorite occurs before 80°C and suggests that it could start at temperature as low as 40°C (Grigsby, 2001). Early formation of chlorite rim on grains is positive for porosity preservation, but late chlorite cement would fill and thus plug much of the pore space. Hence, understanding the timing is critical (Cao et al., 2018).

Telodiagenesis – Late freshwater

- After maximum burial, the Paleocene Paskapoo Formation underwent rapid tectonic exhumation due to post-orogenic isostatic uplift of the foreland basin (Price, 1994) and erosion of up to 1 – 1.5 km of post Paleocene strata (Issler et al., 1990). This resulted in renewed active groundwater circulation in the locally still porous and/or fractured sandstone. This late freshwater circulation led to dissolution of some of the calcite cement and to the creation of new or enhancement of the secondary porosity that could include dissolution of more feldspars, chert and volcanic rock, and calcite detrital fragments.
- Outcrop and well studies have shown that regional stress-fractures (NE-SW; Bell and Bachu, 2003) are correlated with higher aquifer transmissivity (Chen et al., 2007; Grasby et al., 2008). Fracture measurements in outcrops of the Paskapoo Formation in central Alberta documented a principal fracture system with a N55° trend and its N140° conjugate (Babcock, 1974). Near surface open fractures in the Paskapoo Formation would have served as important pathways for freshwater infiltration in the porous sandstone.

The stepwise evolution of the total porosity of the system is shown on Figure 10 and summarized below (steps 1 to 5) using a hypothetical highly porous, coarse-grained, high-energy sandstone as the starting sediment.

(1) The original high primary porosity is partially reduced by early grain rearrangement and compaction. Thin rims of early clay coating, while important for later preservation of the pore space, have an insignificant absolute impact on the volume of the preserved primary pore space, although their potential for clogging small pore throats and slightly reducing permeability should not be ignored.

(2) Dissolution of feldspars, chert, volcanic rock and calcite fragments generated initial secondary porosity in the freshwater vadose zone.

(3) Calcite and kaolinite started to precipitate in the freshwater phreatic aquifer, resulting in a net overall porosity reduction, although dissolution of metastable components was still in progress.

(4) In the mesodiagenetic domain, physical compaction was reduced from the presence of calcite and kaolinite pore filling cements, whereas limited chlorite cementation diminished the overall pore space.

(5) Late exhumation of the succession resulted in freshwater circulation in newly formed surface-connected fractures and preserved pore space. Most of this stage resulted in significant dissolution of pore-filling calcite cement and likely dissolution of more detrital carbonate, feldspars, chert and volcanic rock fragments. Late dissolution resulted in a significant increase in the overall total porosity and crumbliness of some porous and permeable sandstones, eventually resulting in poorly and even unconsolidated sandstone intervals.

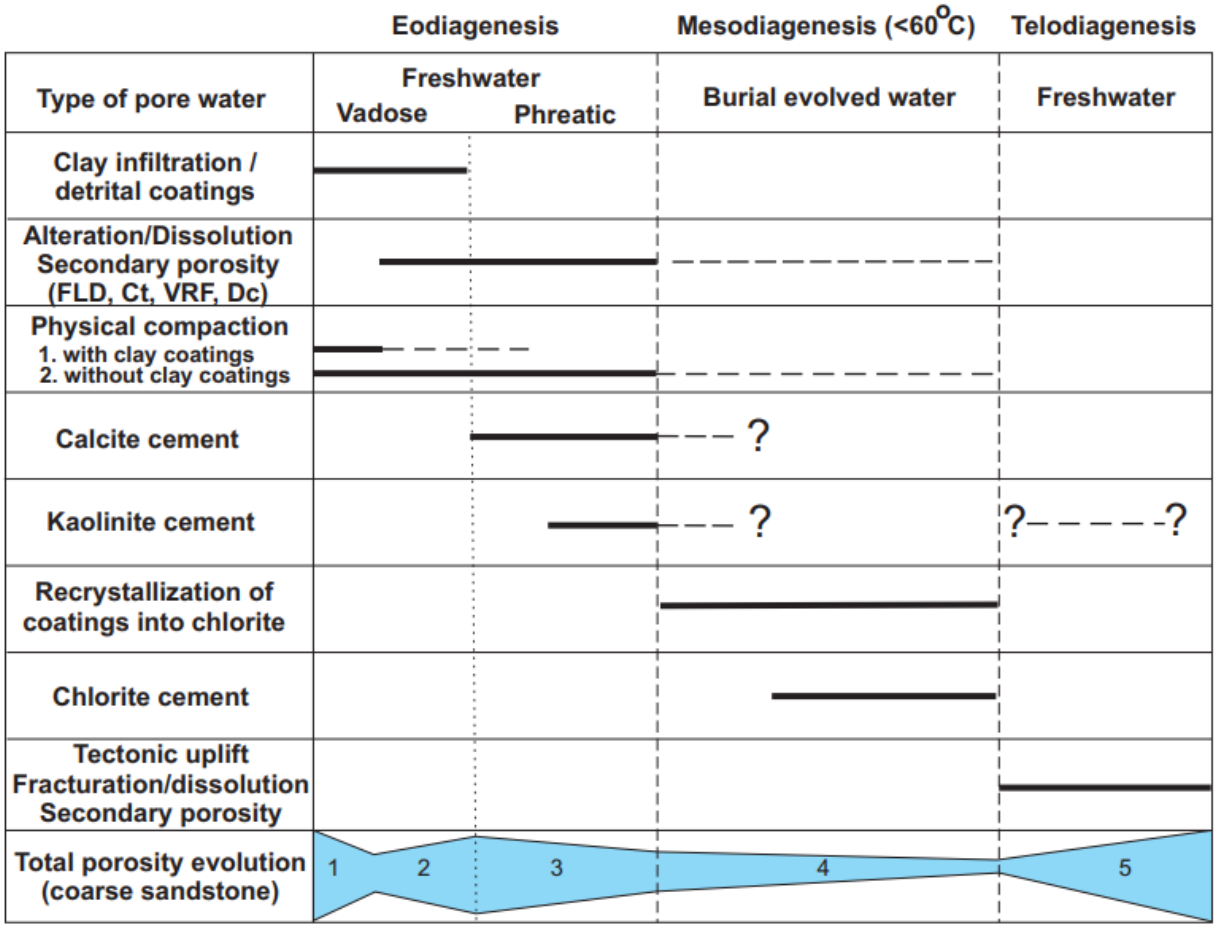

Figure 10. Paragenetic succession of diagenetic events and products in the sandstone of the Paskapoo Formation in the Fox Creek area. FLD is feldspar, Ct is chert, VRF is volcanic rock fragment, Dc is detrital calcite, ? is for uncertain presence. 1 to 5 are porosity evolution steps discussed in the text. The increasing or reducing blue envelope expresses the variation of relative total porosity during the different steps, no absolute values is implied. Based on Schmidt and McDonald (1979) diagenetic framework.

Hydraulic conductivity, a function of diagenesis and fractures

Significance of cementation and fracturing for aquifer high transmissivity

In early hydrogeological studies in Alberta, pioneer hydrogeologists documented the critical importance of high porosity and low degree of cementation relative to grain size for the overall capacity and yield of Paleocene sandstone aquifers. Farvolden (1961) recognized that aquifer capacity is associated with a low degree of cementation in the sandstone. Ozoray (1972), in the Wabamum Lake area, quantified the yield of various aquifer types based on the degree of cementation and/or fracturing of the carrier bed. The highest yields (up to 2,250 L/min) are reported for highly friable sandstones, whereas the less friable sandstone and siltstone of the Paskapoo Formation would yield between 100 – 450 L/min. A similar trend of decreasing yield with increasing cementation is documented by Tokarsky (1971).

Chen et al. (2007), using transmissivity values from over a thousand (1,309) short pumping tests

(during well development) that lasted more than 2 hours in the Paskapoo Formation, identified a dominant NE-SW transmissivity trend with a subordinate perpendicular (NW-SE) one. Structural mapping of Haynes Member outcrops along the Bow and Red Deer rivers identifies a strong NE-SW trend in fracture orientation (Grasby et al., 2008), in line with Bell and Bachu (2003) maximum horizontal stress (S_{Hmax}) field for the basin. Babcock (1974) measured 3,677 joint orientations (29 stations) mostly in the Paskapoo Formation of Central Alberta; the overwhelmingly dominant system (N55° and conjugate N140°) is very similar to his results in Southern Alberta (Babcock, 1973) and with the field data of Grasby et al. (2008). These suggest that syn- to post-burial fracturing of the Paskapoo Formation sandstone is a major aspect not only in promoting shallow groundwater circulation, but it may have also played an important role in setting up the stage by allowing a large volume of freshwater to access porous carrier beds with a still significant percentage of chemically metastable elements for late dissolution resulting in enhanced hydraulic conductivity.

Combining channel orientation and fracturing

Regionally, the best hydraulic conductivities in the Paskapoo Formation are associated with medium- to coarse-grained, high energy sandstone channel fills. However, predicting the lateral extension and orientation of buried channels without the benefit of high-resolution shallow 3D seismic data, is a challenging task as multiple more or less easily quantifiable parameters must be considered with sinuosity and meandering being the more important ones. In a significant synthesis of over 1,500 ancient and Quaternary fluvial channel systems, Gibling (2006) introduces a new classification model for fluvial sandstone: (1) low-sinuosity mobile channel belt such as braided systems, (2) high-sinuosity mobile channel belt such as meandering systems, and (3) fixed channel belt which includes anastomosing systems. The Paskapoo Formation aquifer system in the vicinity of Calgary (Haynes Aquifer) is interpreted to belong to the fixed channel belt system (Hamblin, 2004; Burns et al., 2010). These fixed channel belt systems are characterized by low-gradient, multiple, laterally stable interconnected channels, with low width / depth ratios (Gibling, 2006). No such interpretation is available for the Sunchild Aquifer in the Fox Creek area.

Burns et al. (2010) attempted geostatistical modeling of the Paskapoo Formation channels for an area just north of Calgary. This work was refined through more stochastic modeling of the same geological data (Matthews, 2011). These two studies document the complexity in modeling these fluvial systems over some distance.

In this contribution, we preliminary discuss of a potential link, if any, between the main channel orientations and the regional fracture network. Measuring paleocurrent indicators in a well exposed field section is a relatively common task although the representativity of single measurements can be misleading. To generate meaningful data, numerous measurements from many field sections at various sites and orientations are needed to reach an average regional trend free of local noises created by high number of meanders and/or changing sinuosity. Jerzykiewicz and Labonté (1991) recognized a strongly dominated northeastward channel trend for the Paskapoo Formation in southern and central Alberta. East-northeast and north-east orientations have been documented by Hamblin (2007a, b, c) for the area between Calgary up to the north of Red Deer, for channels in both the Haynes and Lacombe members. In a detailed survey, Hamblin (2007a) recognized a main N80° (ENE) orientation for high-energy channels compared to a N50° (NE) trend for thin splays. The average of N60° (NE) agrees with other regional surveys.

As discussed above, from detailed field fracture measurements, the regional fracture pattern has a strong and dominant northeast component, therefore in the same overall direction as the general orientation of channels in the Paskapoo Formation.

Conclusions

The Paleocene Paskapoo Formation is the most important shallow groundwater aquifer in Alberta. A 700 km^2 watershed west of the locality of Fox Creek (west-central Alberta) was selected to study amongst other aspects, the hydrogeological context and characteristics of the groundwater aquifer.

In the study area, the shallow aquifer corresponds to the Sunchild Aquifer equivalent to the Dalehurst Member of the Paskapoo Formation. Three shallow boreholes were drilled (32, 32 and 100 meters) and cored in 2022. Alternating intervals of shale, mudstone, siltstone, and sandstone forming fine- and coarse-grained clastic lithofacies assemblages are recognized. The Paskapoo Formation consists of sedimentary facies belonging to a fluvial depositional system with various scales channel-fill sandstone and associated fine-grained overbank deposits. The sandstone is fine- to coarse-grained, more or less calcareous and locally contains decimeter- to meter-thick friable to unconsolidated intervals intercalated in the compacted sandstone. These enigmatic intervals are potential “highways” for groundwater circulation with potential very high yields; explaining the cause for these enigmatic accumulations is the subject of this study.

The petrographic observation of 20 sandstone samples revealed that they are litharenites and composed predominantly of quartz and rock fragments (volcanic, sedimentary, chert and metamorphic) with subordinate poorly preserved feldspars, coal fragments and rare heavy minerals. Generally, the coarser-grained sandstone is more porous than the finer-grained one. Visible porosity can reach up to 25% and the coarse sediment is totally devoid of fine-grained detrital matrix.

The porosity is dominated by primary intergranular porosity with subordinate volume of secondary dissolution porosity at various scales. The nature of the pore-filling material has been identified, although time relationships between various fills are locally ambiguous. For medium- and coarse-grained sandstones, a first post-sedimentation event coeval with the onset of compaction consists of significant micrometer-thick rims of amorphous clay material coating the margin of detrital particles (quartz and rock fragments). Such rims may also cover entirely the walls of primary pore space; some sandstones do not have these rims. The exact nature of the clay material is unknown; from the study of a similar fluvial sedimentary succession in southern Alberta, smectite is documented under SEM as the original coating clay which later recrystallized into chlorite. The first phases of the diagenetic evolution of the sandstone took place in the presence of freshwater in the pore system. The circulating freshwater resulted in locally significant early dissolution of metastable minerals such as feldspars, chert, volcanic and carbonate rock fragments.

Inputs of silica, aluminum, iron and bicarbonates in groundwater from dissolution of metastable phases created the favorable chemical conditions for the relatively rapid and low temperature precipitation of diverse cement phases. In the shallow freshwater phreatic diagenetic system, precipitation of kaolinite was initiated rapidly. The increase saturation of groundwater in bicarbonates from the early dissolution of detrital carbonates with no detected input of plant-derived soil CO_2, resulted in the precipitation of freshwater phreatic zone calcite cement in primary and some early secondary dissolution pore space. The transition of the sediment in the freshwater diagenetic

environment resulted in locally significant dissolution but more importantly, in precipitation of early pore-filling cements leading in a net reduction of pore space in the sandstone.

The foreland basin succession was progressively buried under a less than 2 kilometers thick sedimentary pile, freshwater circulation was stopped and from an open water-dominated diagenetic environment, the conditions evolved into a closed rock-dominated system. The precursor amorphous clay coating likely started to recrystallize into chlorite in the deeper burial environment. The increase in surrounding temperature from burial resulted in the precipitation of a small volume of pore-filling chlorite, and the possible continuation of calcite cementation. The transition of the succession in the burial diagenetic environment led to more cement precipitation in the pores. However, the presence of clay coatings on detrital particles significantly limited the available surfaces for pore-filling cements to precipitate.

In the Fox Creek area, the sandstones of the upper part of the Paskapoo Formation never experienced burial temperatures over 60°C. This limit is an important element for the aquifer performance in the Paskapoo Formation, at these relatively low temperature, extensive pore-filling chlorite and quartz cementation did not take place. At the end of the Laramide Orogeny (Eocene), the succession of the Paskapoo Formation was rapidly tectonically brought back to near surface conditions during post-orogenic isostatic rebound of the foreland basin. Newly created late fractures and still preserved porosity/permeability in the sandstone were the loci of renewed freshwater circulation and significant dissolution of detrital carbonates, pore-filling calcite cements and metastable minerals. In more permeable carrier beds, major dissolution resulted in the collapse of the porous friable sandstone into the unconsolidated accumulation.

High energy, coarse-grained channel-fill sandstones represent the optimal initial material for high capacity and yield for a clastic aquifer. The regional sediment transport in Paskapoo channels is oriented northeast, roughly perpendicular to the Rocky Mountains. The fact that the regional fracture pattern also coincides with the main channel elongation is an important consideration since this combination creates ideal conditions for a high capacity, high yield aquifer.

Acknowledgements

Dr. Omid Haeri Ardakani is thanked for his efficient review of the initial manuscript that improved the final product. Thanks are extended to Dr. Josué Jautzy, lab head and the staff of the stable isotope Delta-Lab (GSC-Quebec) for the preparation and analysis of the Fox Creek calcite samples. This project is part of the Geological Survey of Canada Environmental Geoscience and Groundwater Geoscience programs.

References

Aagaard, P., Jahren, J.S., Harstad, A.O., Nilsen, O. and Ramm, M. 2000. Formation of grain coating chlorite in sandstones. Laboratory synthesized vs. natural occurrences. Clay Minerals, v. 35, p. 261–269. https://doi.org/10.1180/000985500546639

Alberta Geological Survey, 2019. Alberta Table of Formations. Alberta Energy Regulator, https://ags.aer.ca/publications/Table_of_Formations_2019.html

Allan, J.A. and Sanderson, J.O.G. 1945. Geology of Red Deer and Rosebud sheets, Alberta. Research Council of Alberta, Report 3, 109 p. https://ags.aer.ca/publication/rep-13

Ardakani, O.H. 2022. Organic petrography and thermal maturity of the Paskapoo Formation in the Fox Creek area, west-central Alberta; Geological Survey of Canada, Open File 8903, 20 p. https://doi.org/10.4095/330296

Babcock, E.A. 1973. Regional jointing in southern Alberta. Canadian Journal of Earth sciences, v. 10, p. 1769-1781. https://doi.org/10.1139/e73-173

Babcock, E.A. 1974. Jointing in Central Alberta. Canadian Journal of Earth Sciences, v. 11, p. 1181-1186. https://doi.org/10.1139/e74-111

Bachu, S. and Cao, S. 1992. Present and past geothermal regimes and source-rock maturation, Peace River Arch area, Canada. Bulletin of the American Association of Petroleum Geologists, v. 76, p. 1533-1549. https://doi.org/10.1306/BDFF8A38-1718-11D7-8645000102C1865D

Bell, J.S. and Bachu, S. 2003. In situ stress magnitude and orientation estimates for Cretaceous coal-bearing strata beneath the plains area of central and southern Alberta. Bulletin of Canadian Petroleum Geologist, v. 51, p. 1–28. https://doi.org/10.2113/gscpgbull.51.1.1

Bernasconi, S.M., Daëron, M., Bergmann, K.D. and 57 others. 2021. InterCarb: A Community Effort to Improve Interlaboratory Standardization of the Carbonate Clumped Isotope Thermometer Using Carbonate Standards. Geochemistry, Geophysics, Geosystems, v. 22, Article number e2020GC009588. https://doi.org/10.1029/2020GC009588.

Bjørlykke, K. 1998. Clay mineral diagenesis in sedimentary basins – a key to the prediction of rock properties. Example from the North Sea Basin. Clay Minerals, v. 33, p. 15–34. https://doi.org/10.1180/000985598545390

Burns, E. B., Bentley, L. R., Hayashi, M., Grasby, S. E. and Hamblin, A. R. 2010. Hydrogeological Implications of Paleo-Fluvial Architecture of Complex Aquifer Systems: Numerical Modeling Results and Sensitivity Analysis for the Paskapoo Formation, SW Alberta Canada. Hydrogeology Journal, v. 18, p. 1375-1390. https://doi.org/10.1007/s10040-010-0608-y

Burton, J.H., Krinsley, D.H. and Pye, K. 1987. Authigenesis of kaolinite and chlorite in Texas Gulf Coast sediments. Clay and Clay Minerals, v. 35, p. 291-296. https://doi.org/10.1346/CCMN.1987.0350406

Cao, Z., Liu, G., Meng, W., Wang, P. and Yang, C. 2018. Origin of different chlorite occurrences and their effects on tight clastic reservoir porosity. Journal of Petroleum Science and Engineering, v. 160, p. 384-392. https://doi.org/10.1016/j.petrol.2017.10.080

Carmichael, M.J., Inglis, G.N., Marcus P.S. Badger, M.P.S., Naafs, B.D.A., Behrooz, L., Remmelzwaal, S., Monteiro, F.M., Rohrssen, M., Farnsworth, A., Buss, H.L., Dickson, A.J., Valdes, P.J., Lunt, D.J. and Pancost, R.D. 2017. Hydrological and associated biogeochemical consequences of rapid global warming during the Paleocene-Eocene Thermal Maximum. Global and Planetary Change, v. 157, p. 114-138. https://doi.org/10.1016/j.gloplacha.2017.07.014

Carrigy, M.A. 1970. Proposed revisions of the boundaries of the Paskapoo Formation in the Alberta Plains. Bulletin of Canadian Petroleum Geology, v. 18, p. 156-165. https://doi.org/10.35767/gscpgbull.18.2.156

Carrigy, M.A. 1971. Lithostratigraphy of the uppermost Cretaceous (Lance) and Paleocene strata of the Alberta Plains. Research Council of Alberta, Bulletin 27, 161 p. https://ags.aer.ca/publication/bul-027

Charlaftis, D., Jones, S.J., Dobson, K.J., Crouch, J. and Acikalin, S. 2021. Experimental study of chlorite authigenesis and influence on porosity maintenance in sandstones. Journal of Sedimentary Research, v. 91, p. 197-212. https://doi.org/10.2110/jsr.2020.122

Chen, Z., Grasby, S.E. and Wozniak, P.R.J. 2007. Paskapoo Groundwater Study Part VI: Aquifer transmissivity estimation and a preliminary data analysis of the Paskapoo Formation, Alberta, Geological Survey of Canada, Open File 5444, 31 p. https://doi.org/10.4095/224035

Corlett, H., Schultz, R., Branscombe, P., Hauck, T., Haug, K., MacCormack, K. and Shipman, T. 2018. Subsurface faults inferred from reflection seismic, earthquakes, and sedimentological relationships: Implications for induced seismicity in Alberta, Canada. Marine and Petroleum Geology, v. 93, p. 135-144. https://doi.org/10.1016/j.marpetgeo.2018.03.008

Daëron, M., Drysdale, R.N., Peral, M., Huyghe, D., Blamart, D., Coplen, T.B., Lartaud, F. and Zanchetta, G. 2019. Most Earth-surface calcites precipitate out of isotopic equilibrium. Nature Communications, v. 10, article 429. https://doi.org/10.1038/s41467-019-08336-5

Dansgaard, W. 1953, The abundance of 0^{18} in atmospheric water and water vapour. Tellus, v. 5, p. 461-469. https://doi.org/10.3402/tellusa.v5i4.8697

Dansgaard, W. 1964. Stable isotopes in precipitation. Tellus, v. 16, p. 436-468. https://doi.org/10.3402/tellusa.v16i4.8993

Demchuk, T.D. and Hills, L.V. 1991. A re-examination of the Paskapoo Formation in the central Alberta Plains: the designation of three new members. Bulletin of Canadian Petroleum Geology, v. 39, p. 270–282. https://doi.org/10.35767/cspgbull.39.3.270

Dowey, P.J., Hodgson, D.M. and Worden, R.H. 2012. Pre-requisites, processes, and prediction of chlorite grain coatings in petroleum reservoirs: a review of subsurface examples. Marine and Petroleum Geology, v. 32, p. 63–75. https://doi.org/10.1016/j.marpetgeo.2011.11.007

Farvolden, R.N. 1961. Groundwater resources, Pembina area, Alberta. Research Council of Alberta, Edmonton, Alberta, Report 61-4, 26 p. https://ags.aer.ca/publication/esr-1961-04

Folk, R.L. 1980. Petrology of sedimentary rocks; Hemphill's Publishing Company, Austin Texas, 170 p.

Gibling, M.R. 2006. Width and thickness of fluvial channel bodies and valley fills in the geological record: a literature compilation and classification. Journal of Sedimentary Research, v.76, p. 731–770. https://doi.org/10.2110/jsr.2006.060

Grasby, S., Tan, W., Chen, Z. and Hamblin, A.P. 2007. Paskapoo groundwater study. Part I: Hydrogeological properties of the Paskapoo Formation determined from six continuous cores; Geological Survey of Canada, Open File 5392, 6 p. https://doi.org/10.4095/223756

Grasby, S. E., Chen, Z., Hamblin, A. P., Wozniak, P. R. J. and Sweet, A. R. 2008. Regional characterization of the Paskapoo bedrock aquifer system, southern Alberta. Geological Survey of Canada Contribution 2008-0479. Canadian Journal of Earth Sciences, v. 45, p. 1501–1516. https://doi.org/10.1139/E08-069

Griffiths, J., Worden, R.H., Wooldridge, L.J., Utley, J.E.P. and Duller, R.A. 2018. Detrital Clay Coats, Clay Minerals, and Pyrite: A Modern Shallow-Core Analogue For Ancient and Deeply Buried Estuarine Sandstones. Journal of Sedimentary Research, v. 88, p. 1205-1237. https://doi.org/10.2110/jsr.2018.56

Griffiths, J., Worden, R.H., Utley, J.E.P., Brostrøm, C., Martinius, A.W., Lawan, A.Y. and Al-Hajri, A.I. 2021. Origin and distribution of grain-coating and pore-filling chlorite in deltaic sandstones for reservoir quality assessment. Marine and Petroleum Geology, v. 134, 105326. https://doi.org/10.1016/j.marpetgeo.2021.105326

Grigsby, J.D. 2001. Origin and growth mechanism of authigenic chlorite in sandstones of the lower Vicksburg Formation, south Texas. Journal of Sedimentary Research, v. 71, p. 27-36. https://doi.org/10.1306/060100710027

Hamblin, A.P. 2004. Paskapoo-Porcupine Hills formations in western Alberta: synthesis of regional geology and resource potential. Geological Survey of Canada, Open File 4679, 30 pages, https://doi.org/10.4095/215631

Hamblin, A.P. 2007a. Paskapoo Groundwater Study, Part IV: Detailed outcrop measured sections of the Paskapoo Formation in the Red Deer region, Alberta. Geological Survey of Canada, Open File 5535, 20 p., 1 CD. https://doi.org/10.4095/223774

Hamblin, A.P. 2007b. Paskapoo Groundwater Study, Part V: Detailed outcrop measured sections of the Scollard, Porcupine Hills and Paskapoo formations in the Calgary region, Alberta. Geological Survey of Canada, Open File 5536, 16 p., 1 CD. https://doi.org/10.4095/223775

Hamblin, A.P. 2007c. Paskapoo Groundwater Study Part III: Detailed core measured sections of the Paskapoo Formation in central Alberta; Geological Survey of Canada, Open File 5537, 13 p., 1 CD. https://doi.org/10.4095/223894

Hays, P.D. and Grossman, E.L. 1991. Oxygen isotopes in meteoric calcite cements as indicators of continental paleoclimate. Geology, v. 19, p. 441-444. https://doi.org/10.1130/0091-7613(1991)019<0441:OIIMCC>2.3.CO;2

Heald, M.T. and Anderegg, R.C. 1960. Differential cementation in the Tuscarora sandstones. Journal of Sedimentary Petrology, v. 30, p. 568–577. https://doi.org/10.1306/74D70AA1-2B21-11D7-8648000102C1865D

Heald, M.T. and Larese, R.E. 1974. Influence of coatings on quartz cementation. Journal of Sedimentary Petrology, v. 44, p. 1269–1274. https://doi.org/10.1306/212F6C94-2B24-11D7-8648000102C1865D

Hoffman, J. and Hower, J. 1979. Clay mineral assemblages as low grade metamorphic geothermometers: Application to the thrust faulted disturbed belt of Montana, USA. In: Scholle P.A., Schluger P.R. (eds.) Aspects of diagenesis. Society of Economic Paleontologist and Mineralogist, Special Publication 26, p. 55-79. https://doi.org/10.2110/pec.79.26.0055

Hornybrook, E. and Longstaffe, F.J. 1996. Berthierine from the Lower Cretaceous Clearwater Formation, Alberta, Canada. Clay and Clay Minerals, v. 44, p. 1-21. https://doi.org/10.1346/CCMN.1996.0440101

Hughes, A.T., Smerdon, B.D. and Alessi, D.S. 2017a. Hydraulic properties of the Paskapoo Formation in west-central Alberta. Canadian Journal of Earth Sciences, v. 54, p. 883–892. https://doi.org/10.1139/cjes-2016-0164

Hughes, A.T., Smerdon, B.D. and Alessi, D.S. 2017b. A summary of hydraulic conductivity values for the Paskapoo Formation in West-Central Alberta. Alberta Energy Regulator, AER/AGS Open File Report 2016-03, 25 p. http://ags.aer.ca/publications/OFR_2016_03.html

Humphreys, B., Kemp, S.J., Lott, G.K., Bermanto, Dharmayanti, D.A. and Samsori, I. 1994. Origin of grain-coating chlorite by smectite transformation: an example from Miocene sandstones, North Sumatra back-arc basin, Indonesia. Clays and Clay Minerals, v. 29, p. 681-692. https://doi.org/10.1180/claymin.1994.029.4.21

Issler, D.R., Beaumont, C., Willett, S.D., Donelick, R.A., Mooers, J. and Grist, A. 1990. Preliminary evidence from apatite fission-track data concerning the thermal history of the Peace River Arch region, Western Canada Sedimentary Basin. Bulletin of Canadian Petroleum Geology, v. 38A, p. 250-269. https://doi.org/10.35767/gscpgbull.38a.1.250

Jerzykiewicz, T. 1997. Stratigraphic framework of the uppermost Cretaceous to Paleocene strata of the Alberta Basin. Geological Survey of Canada, Bulletin 510, 121 p. https://doi.org/10.4095/208902

Jerzykiewicz, T. and Labonté, M. 1991. Representation and statistical analysis of directional sedimentary structures in the uppermost Cretaceous-Paleocene of the Alberta Foreland Basin. Geological Survey of Canada. Geological Survey of Canada, Paper no. 91-1B, p. 47-49. https://doi.org/10.4095/132539

Jerzykiewicz, T. and Sweet, A.R. 1988. Sedimentology and palynological evidence of regional climatic changes in the Campanian to Paleocene sediments of the Rocky Mountains Foothill, Canada. Sedimentary Geology, v. 59, p. 29-76. https://doi.org/10.1016/0037-0738(88)90099-1

Khanna, M., Saigal, G.C. and Bjorlykke, K. 1997. Kaolinitization of Upper Triassic-Lower Jurassic Sandstones of the Tampen Spur Area, North Sea: Implications for Early Diagenesis and Fluid Flow. In Montanez, I.P., Gregg, J.M. and Shelton, K.L. (eds.). Basin-Wide Diagenetic Patterns: Integrated Petrologic, Geochemical, and Hydrologic Considerations. SEPM Special Publication 57, p. 253-268. https://doi.org/10.2110/pec.97.57

Khidir, A. and Catuneanu, O. 2010. Diagenesis of the Cretaceous-Tertiary Willow Creek sandstones, southwestern region of Alberta. Bulletin of Canadian Petroleum Geology, v. 58, p. 342-360. https://doi.org/10.2113/gscpgbull.58.4.342

Koch, P.L., Zachos, J.C. and Dettman, D.L. 1995. Stable isotope stratigraphy and paleoclimatology of the Paleogene Bighorn Basin (Wyoming, USA). Palaeogeograhy, Palaeoclimatology, Palaeoecology, v. 115, p. 61-89. https://doi.org/10.1016/0031-0182(94)00107-J

Lanson, B., Beaufort, D., Berger, G., Bauer, A., A. Cassagnabère, A. and Meunier, A. 2002. Authigenic kaolin and illitic minerals during burial diagenesis of sandstones: a review. Clay Minerals, v. 37, p. 1-22. https://doi.org/10.1180/0009855023710014

Lawton, T.F. 2019. Chapter 13 – Laramide Sedimentary Basins and Sediment-Dispersal Systems. In Miall, A.D. (ed.). The Sedimentary Basins of the United States and Canada, Second Edition, p. 529-557. https://doi.org/10.1016/B978-0-444-63895-3.00013-9

Lennox, D.H. 1993. Groundwater In the Interior Plains Region. (Chapter 6: Economic Geology). In Sedimentary Cover of the Craton in Canada, D.F. Stott and J.D. Aitken (eds.) Geology of Canada, v. 5, p. 616-642. https://doi.org/10.4095/192376

Lerbekmo, J.F. and Sweet, A.R. 2000. Magnetostratigraphy and biostratigraphy of the continental Paleocene in the Calgary area, southwestern Alberta; Bulletin of Canadian Petroleum Geology, v. 48, p. 285–306. https://doi.org/10.2113/48.4.285

Longman, M.W. 1980. Carbonate diagenetic textures from nearsurface diagenetic environments. AAPG Bulletin, v. 64, p. 416-487. https://doi.org/10.1306/2F918A63-16CE-11D7-8645000102C1865D

Longstaffe, F.J. 2003. Berthierine. In: Middleton, G.V., Church, M.J., Coniglio, M., Hardie, L.A. and Longstaffe, F.J. (eds) Encyclopedia of Sediments and Sedimentary Rocks. Encyclopedia of Earth Sciences Series. Springer, Dordrecht. https://doi.org/10.1007/978-1-4020-3609-5_26

Lønøy, A., Akelsen, J. and Rønning, K. 1986. Diagenesis of a deeply buried sandstone reservoir: Hield Field, northern North Sea. Clay Minerals, v. 21, p. 497-511. https://doi.org/10.1180/claymin.1986.021.4.06

Lyster, S. and Andriashek, L.D. 2012. Geostatistical rendering of the architecture of hydrostratigraphic units within the Paskapoo Formation, central Alberta. Energy Resources Conservation Board, ERCB/AGS Bulletin 66, 103 p. http://ags.aer.ca/publications/BUL_066.html.

Mack, G.H. and Jerzykiewicz, T. 1989. Provenance of post-Wapiabi sandstones and its implications for Campanian to Paleocene tectonic history of the southern Canadian Cordillera. Canadian Journal of earth Sciences, v. 26, p. 665-676. https://doi.org/10.1139/e89-057

Matlack, K.S., Houseknecht, D.W. and Applin, K.R. 1989. Emplacement of clay into sand by infiltration. Journal of Sedimentary Petrology, v. 59, p. 77–87. https://doi.org/10.1306/212F8F21-2B24-11D7-8648000102C1865D

Matthews, V. A. 2011. Stochastic Modeling of the Paskapoo Formation (Unpublished master's thesis). University of Calgary, Calgary, AB. https://doi.org/10.11575/PRISM/22504

Maulé, C.P., Chanasyk, D.S. and Muehlenbachs, K. 1994. Isotopic determination of snow-water contribution to soil water and groundwater. Journal of Hydrology, v. 155, p. 73–91. https://doi.org/10.1016/0022-1694(94)90159-7

Meyboom, P. 1961. Groundwater resources of the city of Calgary and vicinity. Research Council of Alberta, Bulletin 8, 72 p. https://ags.aer.ca/publication/bul-008

Mossop, G.D. and Shetsen, I. 1994. Chapter 1 – Introduction to the Geological Atlas of the Western Canada Sedimentary Basin. In Mossop, G.D. and Shetsen, I. (comps). Geological atlas of the Western Canada Sedimentary Basin; Canadian Society of Petroleum Geologists and Alberta Research Council. https://ags.aer.ca/atlas-the-western-canada-sedimentary-basin/chapter-1-introduction

O'Connor, L.K., Crampton-Flood, E.D., Jerrett, R.M., Price, G.D., Naafs, B.D.A., Pancost, R.D., McCormack, P., Lempotesis-Davies, A., van Dongen, B.E. and Lengger, S.K. 2023. Steady decline in mean annual air temperatures in the first 30 k.y. after the Cretaceous-Paleogene boundary. Geology, https://doi.org/10.1130/G50588.1

Ozoray, J.F. 1972. Hydrogeology of the Wabamum Lake area, Alberta. Research Council of Alberta, Report 72-8, 19 p. https://ags.aer.ca/publication/esr-1972-08

Price, R.A. 1994. Chapter 2 – Cordilleran Tectonics and the Evolution of the Western Canada Sedimentary Basin. In: G.D. Mossop and I. Shetsen (comps.). Geological Atlas of the Western Canada Sedimentary Basin. Canadian Society of Petroleum Geologists and Alberta Research Council. https://ags.aer.ca/atlas-the-western-canada-sedimentary-basin/chapter-2-cordilleran-tectonics.

Prior, G.J., Hathway, B., Glombick, P.M., Pana, D.I., Banks, C.J., Hay, D.C., Schneider, C.L., Grobe, M., Elgr, R. and Weiss, J.A. 2013. Bedrock geology of Alberta. Alberta Energy Regulator, AER/AGS Map 600, scale 1:1,000,000. http://ags.aer.ca/publications/MAP_600.html

Quade, J. and Roe, L.J. 1999. The stable-isotope composition of early ground-water cements from sandstone in paleoecological reconstruction. Journal of Sedimentary Research, v. 69, p. 667–674. https://doi.org/10.2110/jsr.69.667

Rae, J.W.B., Zhang, Y.G., Liu, X., Foster, G.L., Stoll, H.M. and Whiteford, R.D.M. 2021. Atmospheric CO2 over the Past 66 Million Years from Marine Archives. Annual Reviews of Earth and Planetary Sciences, v. 49, p. 609–641. https://doi.org/10.1146/annurev-earth-082420-063026

Riddell, J.T.F., Andriashek, L.D., Jean, G. and Slattery, S.R. 2009. Preliminary results of sediment and bedrock coring in the Edmonton–Calgary Corridor, central Alberta. Energy Resources Conservation Board, ERCB/AGS Open File Report 2009-17, 81 p. https://ags.aer.ca/publication/ofr-2009-17

Rivard C. 2022. Assessment of potential impacts of oil and gas development activities on shallow aquifers in the Fox Creek area (AB). *In* Aubut Bernard, J., Outridge, P.M., Kao, H., Rivard, C., Desbarats, A.J., Jautzy, J., Galloway, J.M. and Larmagnat, S. Public presentations (126th) of May 10th, 2022: Environmental Geoscience Program, current status of research projects for the 2019-2024 program cycle; Geological Survey of Canada, Scientific Presentation 144, 1 pdf file. https://doi.org/10.4095/330891

Schmidt, V. and McDonald, D. A. 1979. The role of secondary porosity generation in the course of sandstone diagenesis. In: P. A. Scholle and P. R. Schluger (eds.). Aspects of Diagenesis. SEPM Special Publication 26, p. 175–207. https://doi.org/10.2110/pec.79.26.0209

Scotese, C.R. 2014. Atlas of Paleogene Paleogeographic Maps (Mollweide Projection), Maps 8-15, Volume 1, The Cenozoic, PALEOMAP Atlas for ArcGIS, PALEOMAP Project, Evanston, IL. https://10.13140/2.1.3417.6961

Smerdon, B.D., Atkinson, L.A., Hartman, G.M.D., Playter, T.L. and Andriashek, L.D. 2016. Field evidence of nested groundwater flow along the Little Smoky River, west-central Alberta; Alberta Energy Regulator, AER/AGS Open File Report 2016-02, 34 p. https://ags.aer.ca/publication/ofr-2016-02

Tipple, B.J. and Pagani, M. 2007. The Early Origins of Terrestrial C4 Photosynthesis. Annual Reviews of Earth and Planetary Sciences, v. 35, p. 435–461. https://doi.org/10.1146/annurev.earth.35.031306.140150

Tokarsky, O. 1971. Hydrogeology of the Rocky Mountain House area, Alberta. Research Council of Alberta, Report 71-3, 15 p. https://ags.aer.ca/publication/esr-1971-03

Toth, J. 1966. Groundwater geology, Movement, Chemistry, and Resources Near Olds, Alberta. Research Council of Alberta, Bulletin 17, 126 p. https://ags.aer.ca/publication/bul-017

Toth, T.A. and Fritz, S.J., 1997. An Fe-berthierine from a Cretaceous laterite. 1. Characterization. Clay and Clay Minerals, v. 45, p. 564–579. https://doi.org/10.1346/CCMN.1997.0450408

Urey, H. C. 1947. The thermodynamic properties of isotopic substances. Journal of the Chemical Society p. 562–581. https://doi.org/10.1039/jr9470000562

van Hinsbergen, D.J., De Groot, L.V., van Schaik, S.J., Spakman, W., Bijl, P.K., Sluijs, A., Langereis, C.G. and Brinkhuis, H. 2015. A paleolatitude calculator for paleoclimate studies. PLoS One, v. 10. https://doi.org/10.1371/journal.pone.0126946

Veizer, J., Ala, D., Azmy, K., Bruckschen, P., Buhl, D., Bruhn, F., Carden, G.A.F., Diener, A., Ebneth, S., Godderis, Y., Jasper, T., Korte, C., Pawellek, F., Podlaha, O.G. and Strauss, H. 1999. $^{87}Sr/^{86}Sr$, $\delta^{13}C$ and $\delta^{18}O$ evolution of Phanerozoic seawater. Chemical Geology, v. 161, p. 59-88. https://doi.org/10.1016/S0009-2541(99)00081-9

Velde, B. 1985. Clay minerals, a physico-chemical explanation of their occurrence. Developments in Sedimentology, v. 4, Elsevier, New York, 427 p.

Vidal, O., Baldeyrou, A., Beaufort, D., Fritz, B., Geoffroy, N. and Lanson, B. 2012. Experimental study of the stability and phase relations of clays at high temperature in a thermal gradient. Clays and Clay Minerals, v. 60, p. 200-225. https://doi.org/10.1346/CCMN.2012.0600209

Walker, T.R., Waugh, B. and Grone, A.J. 1978. Diagenesis in first-cycle desert alluvium of Cenozoic age, southwestern United States and northwestern Mexico. Geological Society of America Bulletin, v. 89, p. 19-32. https://doi.org/10.1130/0016-7606(1978)89<19:DIFDAO>2.0.CO;2.

Wooldridge, L.J., Worden, R.H., Griffiths, J. and Utley, J.E.P. 2017. Clay-coated sand grains in petroleum reservoirs: understanding their distribution via a modern analogue. Journal of Sedimentary Research, v. 87, p. 338–352. https://doi.org/10.2110/jsr.2017.20

Wooldridge, L.J., Worden, R.H., Griffiths, J. and Utley, J.E.P. 2019. Clay coat diversity in marginal marine sediments. Sedimentology, v. 66, p. 1118–1138. https://doi.org/10.1111/sed.12538

Worden, R.H. and Morad, S. 2003. Clay minerals in sandstones: controls on formation distribution and evolution. International Association of Sedimentologists, Special Publication 34, p. 3-41. https://doi.org/10.1002/9781444304336.ch1

Worden, R.H., Griffiths, J., Wooldridge L.J., Utley, J.E.P., Lawan, A.Y., Muhammed, D.D., Simon, N. and Armitage, P.J. 2020. Chlorite in sandstones. Earth-Science Reviews, v. 204, 103105. https://doi.org/10.1016/j.earscirev.2020.103105

Xu, H. and Veblen, D.R. 1996. Interstratification and other reaction microstructures in the chlorite-berthierine series. Contribution to Mineralogy and Petrology, v. 124, p. 291-301. https://doi.org/10.1007/s004100050192

ANNEX 1 – DETAILED DESCRIPTION OF WELL MW9B

Well	Sample	From (m)	To (m)	Description
MW9B		1.98	2.84	Till
MW9B		2.84	5.99	Fine brown sand
MW9B		5.99	6.2	Medium to coarse grey sand
MW9B		6.2	7.92	Fine brown sand
MW9B		7.92	11.58	Fine to medium brown sand
MW9B		11.58	12.07	Very fine to fine brown sand
MW9B		12.07	13.72	Fine to medium brown sand
MW9B		13.72	14.55	Brown siltstone, soft
MW9B		14.55	16	Grey-brownish mudstone, very friable
MW9B		16	16.08	Grey-brownish mudstone, very friable and fractured
MW9B		16.08	16.76	Grey-brownish mudstone, very friable
MW9B		16.76	18.44	Brown mudstone with millimetric oxidized beds, very friable
MW9B		18.44	18.47	Siltstone
MW9B		18.47	19.81	Grey-brownish siltstone, very friable
MW9B		19.81	21.26	Brown mudstone, unconsolidated
MW9B		21.26	21.72	Very fine grained brown sandstone, friable
MW9B	9B-3	21.72	22.86	Fine grained brown calcareous sandstone
MW9B	9B-4	22.86	23.67	Fine grained grey non calcareous sandstone, unconsolidated (sand)
MW9B	9B-5	23.67	24.38	Fine grained brown non calcareous sandstone, unconsolidated (sand)
MW9B		24.38	25.6	Fine to medium grained brown non calcareous sandstone, poorly consolidated and very friable
MW9B		25.6	25.91	Fine to medium grained brown non calcareous sandstone, unconsolidated (sand)
MW9B		25.91	26.97	Very fine grained brown non-calcareous sandstone, unconsolidated and very friable
MW9B		26.97	27.43	Very fine to fine grained brown non calareous sandstone, unconsolidated and very friable (sand)
MW9B	9B-6	27.43	30.48	Fine to medium grained brown to dark brown non calcareous sandstone, poorly consolidated
MW9B		30.48	32	Grey siltstone with some black and oxidized beds, well consolidated

ANNEX 2 – DETAILED DESCRIPTION OF WELL MW8D

Well	Sample	From (m)	To (m)	Description
MW8D		1.98	2.64	Brown clay
MW8D		2.64	6.6	Till
MW8D		6.6	8.84	Very fine to fine brown sand, with traces of silt and alternating oxidized beds
MW8D		8.84	9.45	Brown clayish silt with grey mudstone chunks
MW8D		9.45	9.88	Very fine to fine grey non calcareous sandstone, unconsolidated with darker millimetric interbeds
MW8D		9.88	12.5	Grey-blueish mudstone, friable
MW8D		12.5	12.9	Grey siltstone, slightly fractured
MW8D		12.9	13.61	Coarse grained grey sandstone
MW8D		13.61	13.72	Grey mudstone, friable
MW8D		13.72	14.3	Coarse to very coarse grained grey sandstone, with centimetric inclusions of mudstone/mudstone
MW8D		14.3	14.4	Sandstone with coal clasts
MW8D	8D-7	14.4	14.66	Coarse to very coarse grained grey slighty calcareous sandstone
MW8D		14.66	14.76	Coarse grained sandstone with coal clasts
MW8D	8D-2	14.76	15.16	Coarse to very coarse grained calcareous sandstone
MW8D	8D-3; 8D-8	15.16	18.87	Coarse grained grey calcareous sandstone with finer millimetric beds
MW8D		18.87	19.41	Fine grained slightly calcareous sandstone, with centimetric round mudstone clasts
MW8D		19.41	19.86	Grey-blueish mudstone, with millimetric coal laminae
MW8D		19.86	19.91	Grey-blueish calcareous mudstone, friable, fractured
MW8D		19.91	21.34	Grey-blueish slightly calcareous mudstone, with some millimetric coal laminae
MW8D		21.34	21.41	Grey and blue-grey pluricentrimetric mudstone beds
MW8D		21.41	21.77	Grey mudstone, with some millimetric coal laminae
MW8D	8D-9	21.77	23.01	Fine grained grey calcareous sandstone
MW8D		23.01	23.16	Grey mudstone
MW8D		23.16	24.74	Very fine grained slightly calcareous sandstone, with some millimetric darker interbeds
MW8D		24.74	26.31	Grey slightly calcareous mudstone
MW8D		26.31	26.39	Coal, fractured
MW8D		26.39	27.43	Grey mudstone to very fine grained sandstone
MW8D		27.43	28.78	Grey mudstone
MW8D		28.78	28.88	Coal, friable
MW8D		28.88	30.3	Grey-blue-greenish mudstone
MW8D		30.3	31.45	Grey mudstone, friable and fractured
MW8D		31.45	31.8	Grey siltstone, friable and very fractured
MW8D	8D-10; 8D-11	31.8	32	Fine grained grey calcareous sandstone

ANNEX 3 – DETAILED DESCRIPTION OF WELL MW3E

Well	Sample	From (m)	To (m)	Description
MW3E		2.59	6.1	Till
MW3E		6.1	6.71	Till
MW3E		6.71	8.84	Till
MW3E		8.84	10.67	Grey mudstone
MW3E		10.67	11.15	Grey mudstone, with some darker beds
MW3E		11.15	11.23	Grey mudstone, very fractured, with some darker beds
MW3E		11.23	11.94	Grey mudstone, with some darker beds
MW3E	3E-27	11.94	12.65	Grey argillaceous non calcareous siltstone, oxidized in some places
MW3E		12.65	13.72	Very fine grained grey non calcareous sandstone, homogeneous
MW3E		13.72	14.45	Very fine to fine grey non calcareous sandstone, with finer interbeds and some oxidized beds
MW3E		14.45	14.91	Grey mudstone, locally oxidized
MW3E		14.91	15.77	Alternating centimetric beds of very fine grained grey sandstone and grey siltstone
MW3E		15.77	16.21	Grey argillaceous siltstone
MW3E		16.21	16.76	Very fine grained grey non calcareous sandstone, with some oxidized interbeds
MW3E		16.76	17.45	Very fine grained grey non calcareous sandstone, with some darker beds
MW3E		17.45	17.81	Fine grained grey-brownish sandstone, homogeneous
MW3E		17.81	18.19	Very fine to fine grained grey sandstone, homogeneous
MW3E		18.19	18.49	Fine grained grey-brownish sandstone, homogeneous
MW3E		18.49	19.81	Very fine grained pale grey sandstone, homogeneous
MW3E	3E-28	19.81	20.7	Very fine grained grey calcareous sandstone, homogeneous
MW3E		20.7	20.93	Fine grained pale grey calcareous sandstone
MW3E		20.93	22.25	Very fine to fine grained grey calcareous sandstone, alternating with pluricentimetric siltstone beds
MW3E		22.25	22.86	Grey mudstone, well consolidated
MW3E		22.86	24.59	Very fine to fine grained grey slightly calcareous sandstone, with centimetric siltstone beds
MW3E		24.59	25.53	Very fine to fine grained grey sandstone, homogeneous
MW3E	3E-2;	25.53	25.86	Medium grained grey sandstone, with fossils (gastropods)

MW3E		25.86	25.91	Dark mudstone (gas smell), friable
MW3E		25.91	26.31	Grey mudstone (gas smell), with fossil shells
MW3E		26.31	26.52	bentonite (silty clay)
MW3E	3E-29	26.52	28.96	Grey calcareous mudstone (gas smell), fractured but well consolidated, with fossil shells
MW3E		28.96	29.62	Alternating very fine to fine grained grey sandstone beds and grey siltstone beds
MW3E		29.62	30.18	Alternating grey mudstone, grey mudstone and grey siltstone
MW3E		30.18	31.17	Alternating very fine to medium grey sandstone beds and grey mudstone, locally oxidized
MW3E		31.17	31.27	Grey mudstone
MW3E		31.27	32	Centimetric interbeds of very fine grained grey sandstone and grey siltstone, locally oxidized
MW3E		32	34.49	Alternating grey mudstone and grey siltstone
MW3E		34.49	34.52	Millimetric beds of coal, black
MW3E		34.52	34.67	Alternating grey mudstone and grey siltstone
MW3E		34.67	34.75	Grey fine grained slightly calcareous sandstone
MW3E		34.75	35.66	Grey mudstone, homogeneous
MW3E		35.66	36.91	Grey mudstone to siltstone, homogeneous
MW3E		36.91	37.97	Alternating centimetric beds of fine grained grey sandstone and grey siltstone
MW3E		37.97	38.1	Grey-greenish mudstone (gas smell)
MW3E		38.1	38.2	Grey-greenish mudstone
MW3E		38.2	38.33	Very fine grained grey sandstone, with millimetric coal beds
MW3E		38.33	38.4	Black millimetric coal beds
MW3E		38.4	38.53	Fine grained grey sandstone, with millimetric coal beds
MW3E		38.53	39.52	Fine to medium grained sandstone, with siltstone interbeds
MW3E		39.52	39.93	Medium to coarse grained grey sandstone, with fossils (shells) and some millimetric coal beds
MW3E		39.93	39.98	Coal
MW3E		39.98	40.26	Fine grained grey sandstone
MW3E		40.26	40.49	Medium to coarse grained sandstone, with millimetric coal beds, and some fossils (shells)
MW3E		40.49	41.15	Fine grained grey sandstone, with millimetric coal beds
MW3E	3E-30	41.15	42.21	Medium grained grey slightly calcareous sandstone, with some millimetric coal beds
MW3E		42.21	42.47	Medium grained grey sandstone, unconsolidated, with some millimetric coal beds
MW3E		42.47	42.98	Medium grained brown sandstone, unconsolidated
MW3E		42.98	43.87	Medium grained brown calcareous sandstone

MW3E		43.87	44.2	Medium grained grey calcareous sandstone
MW3E	3E-31	44.2	47.24	Medium grained brown calcareous sandstone, unconsolidated and homogeneous
MW3E		47.24	48.46	Fine to medium grained brown calcareous sandstone, friable
MW3E		48.46	51.21	Fine to medium grained brown calcareous sandstone, unconsolidated and friable
MW3E		51.21	53.34	Fine to medium grained brown calcareous sandstone, unconsolidated
MW3E	3E-12	53.34	55.78	Fine grained grey-brownish calcareous sandstone, homogeneous
MW3E		55.78	56.39	Fine to medium grained grey calcareous sandstone, homogeneous
MW3E	3E-14	56.39	59.44	Fine to medium grained grey calcareous sandstone, homogeneous and well consolidated
MW3E		59.44	59.59	Fine to medium grained grey calcareous sandstone, and unconsolidated
MW3E		59.59	62.48	Fine to medium grained grey calcareous sandstone, consolidated
MW3E		62.48	63.55	Fine to medium grained grey calcareous sandstone, unconsolidated
MW3E		63.55	64.31	Fine to medium grained grey calcareous sandstone
MW3E	3E-16, -18	64.31	65.99	Fine to medium grained grey calcareous sandstone, with pluricentimetric siltstone or mudstone clasts
MW3E		65.99	66.22	Very fine grained grey calcareous sandstone
MW3E		66.22	66.29	Medium grained grey calcareous sandstone, with some siltstone interbeds
MW3E		66.29	66.75	Coarse grained grey calcareous sandstone, not sorted, with some finer interbeds
MW3E	3E-32	66.75	67.51	Medium to coarse grained grey calcareous sandstone
MW3E		67.51	68.58	Coarse grained grey calcareous sandstone, friable and unconsolidated
MW3E		68.58	70.03	Medium to coarse grained grey calcareous sandstone, friable
MW3E	3E-19	70.03	71.63	Fine to medium grained grey calcareous sandstone, well consolidated
MW3E	3E-20	71.63	75.44	Medium to coarse grained grey-blackish calcareous sandstone, with darker millimetric interbeds
MW3E	3E-33	75.44	76.5	Alternating medium grained sandstone and fine to medium grained sandstone
MW3E		76.5	76.94	Medium to coarse grained dark grey calcareous sandstone
MW3E		76.94	77.57	Coal, slightly fractured
MW3E		77.57	77.72	Mudstone with some millimetric coal fragments
MW3E		77.72	80.77	Alternating grey siltstone, with some coal fragments, and very fine grained grey sandstone

MW3E		80.77	80.85	Siltstone
MW3E		80.85	80.87	Coal
MW3E		80.87	80.95	Grey mudstone, with siltstone clasts
MW3E		80.95	81.99	Grey siltstone
MW3E		81.99	82.07	Coal, friable
MW3E		82.07	82.75	Grey mudstone, with coal fragments
MW3E		82.75	82.78	Coal
MW3E		82.78	82.96	Grey mudstone or siltstone
MW3E		82.96	83.13	Coal, well consolidated
MW3E		83.13	84.12	Grey siltstone, with some mudstone fragments
MW3E		84.12	85.14	Grey mudstone
MW3E		85.14	85.22	Coal
MW3E		85.22	85.52	Grey mudstone
MW3E		85.52	85.55	Coal
MW3E		85.55	86.13	Grey mudstone, with coal fragments
MW3E		86.13	86.16	Bentonite
MW3E		86.16	86.31	Grey mudstone
MW3E		86.31	87.17	Coal, well consolidated
MW3E		87.17	87.55	Grey-black mudstone, friable
MW3E		87.55	87.88	Coal
MW3E	3E-34	87.88	89.41	Alternating grey fine grained calcareous sandstone and grey mudstone
MW3E		89.41	90.47	Coal
MW3E		90.47	90.78	Grey mudstone friable
MW3E		90.78	91.52	Coal, well consolidated
MW3E		91.52	94.84	Grey mudstone friable
MW3E		94.84	95.25	Coal
MW3E		95.25	96.01	Grey mudstone friable
MW3E	3E-25, -26	96.01	98.81	Alternating fine grained grey calcareous sandstone and medium grained grey sandstone beds
MW3E		98.81	98.91	Coal
MW3E		98.91	99.16	Alternating siltstone and mudstone, with millimetric coal beds
MW3E		99.16	100.43	Alternating grey siltstone and grey mudstone

ANNEX 4: PHOTOGRAPHS OF CORE MW9B

Photo at 15.8 m. Soil slickensides (arrows).

Photo at 19.8 m. Vertisol in mudstone.

Photo at 27.4 m. Unconsolidated sand.

Photo at 29 m. Friable sandstone.

ANNEX 5: PHOTOGRAPHS OF CORE MW8D

Photo at 13.4 m. Calcareous coarse-grained sandstone.

Photo at 15.2 m. Friable calcareous sandstone.

Photo at 20.6 m. Fine-grained sandstone.

Photo at 30 m. Burrowed mudstone.

Photo at 23 m. Medium-grained calcareous sandstone.

Photo at 31.5 m. Fine-grained friable calcareous sandstone.

ANNEX 6: PHOTOGRAPHS OF CORE MW3E

Photo at 25.3 m. Shale with clay shrinkage.

Photo at 26.5 m. Mudstone with coal laminae.

Photo at 28.8 m. Fine-grained sandstone with bivalves and gastropods.

Photo at 31.4 m. Cross-laminated fine grained sandstone.

Photo at 39 m. Small channel filled sandstone in mudstone.

Photo at 42.7 m. Very friable calcareous coarse sandstone.

Photo at 55.8 m. Calcareous fine-grained sandstone.

Photo at 62.1 m. Calcareous coarse-grained sand.

Photo at 65.2 m. Coarse-grained sandstone with mudstone clasts.

Photo at 65.8 m. Self-supported, well-rounded mudstone clasts in coarse grained sandstone, a gravel lag.

Photo at 66.2 m. Compaction-driven injection of sandstone in mudstone.

Photo at 73.1 m. Coarse-grained sandstone (left box) passing into fine-grained sandstone (right box).

Photo at 79.2 m. Cross-laminated calcareous sandstone.

Photo at 83 m. Coal layer with siltstone interbeds.

ANNEX 7: PHOTOMICROGRAPHS OF SAMPLES FROM WELL MW9B

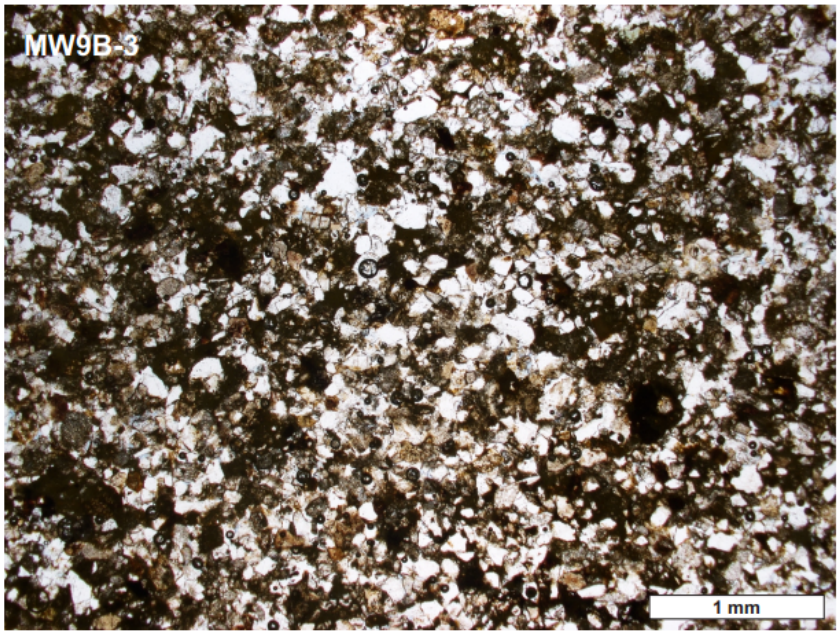

MW9B-3. Tightly compacted fine-grained sandstone, rich in quartz and clay matrix.

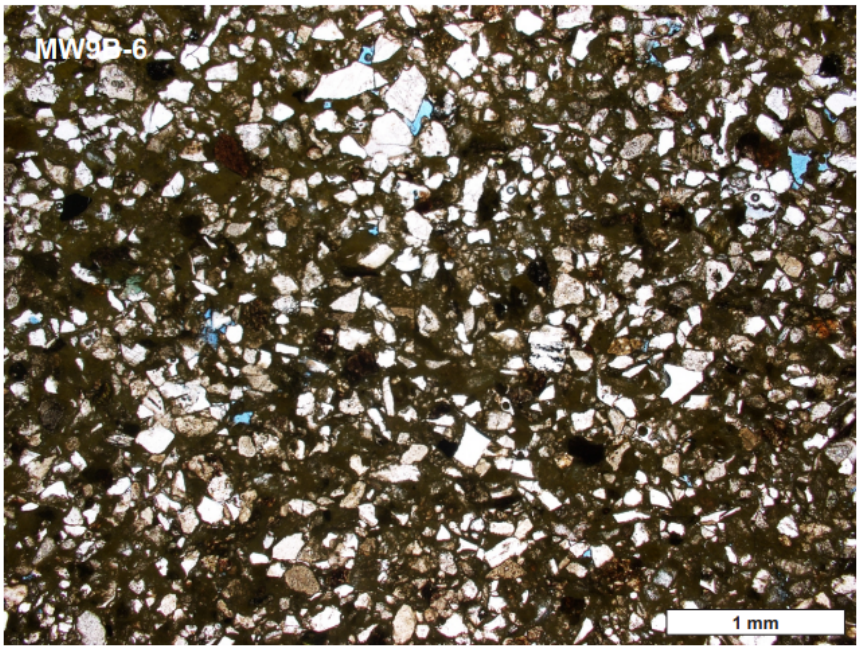

MW9B-6. Tightly compacted fine-grained sandstone with abundant angular quartz and 5% porosity (in blue).

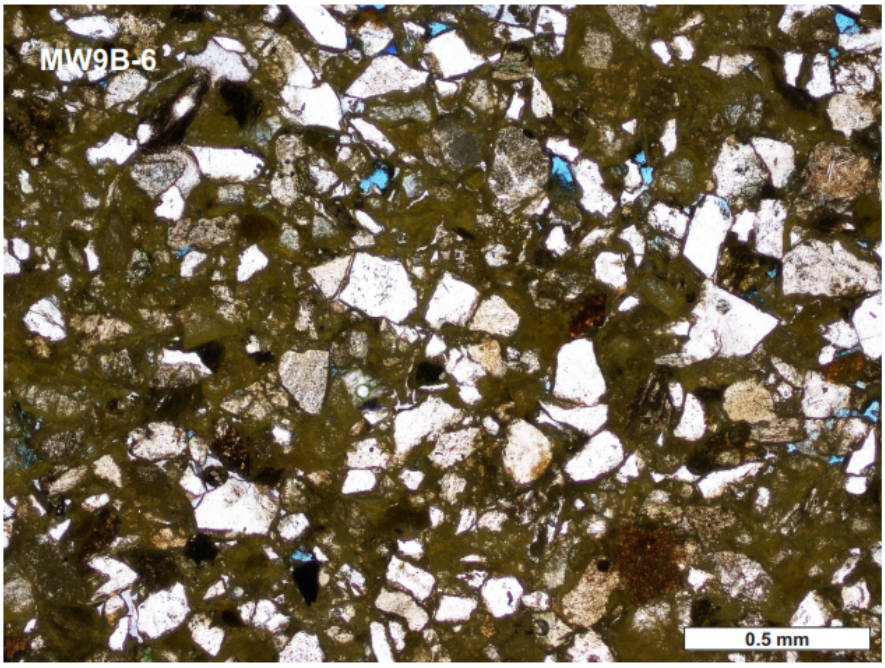

MW9B-6. Fine-grained sandstone with abundant clay matrix and 5% porosity in blue.

ANNEX 8: PHOTOMICROGRAPHS OF SAMPLES FROM WELL MW8D

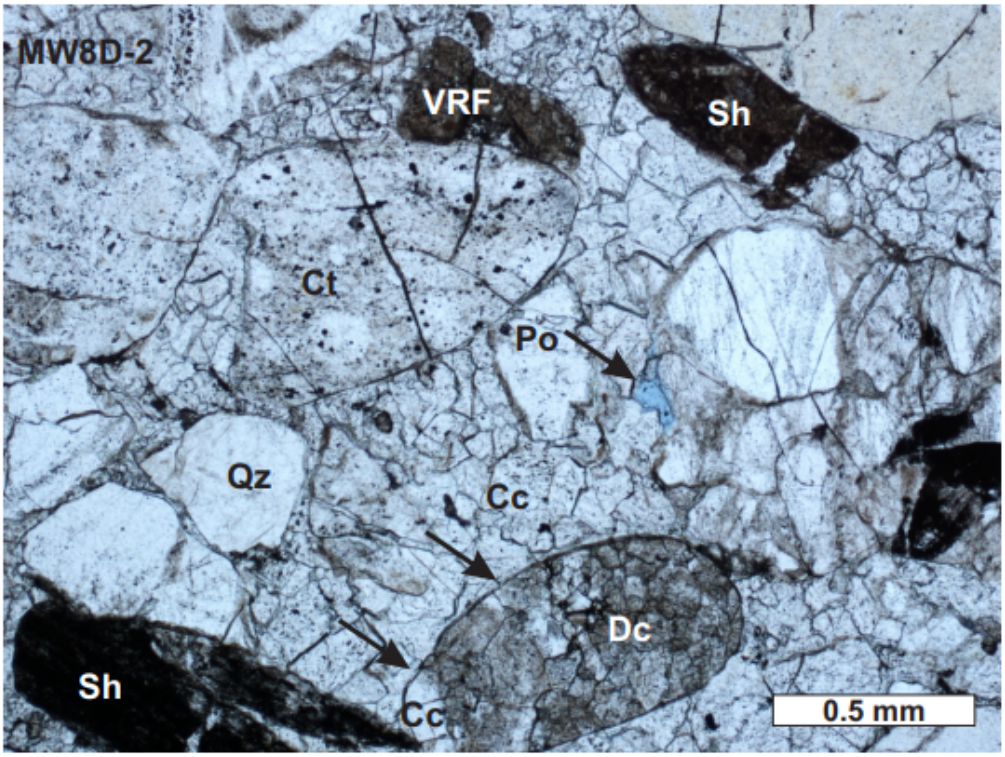

MW8D-2. Pore-filling calcite cement (Cc), the calcite cement fills a mold in a fragment of calcite (Dc). The border of the fragment is shown by arrows. Qz; Quartz, VRF: Volcanic rock fragment, Sh: Shale. Pore space (Po) is shown below.

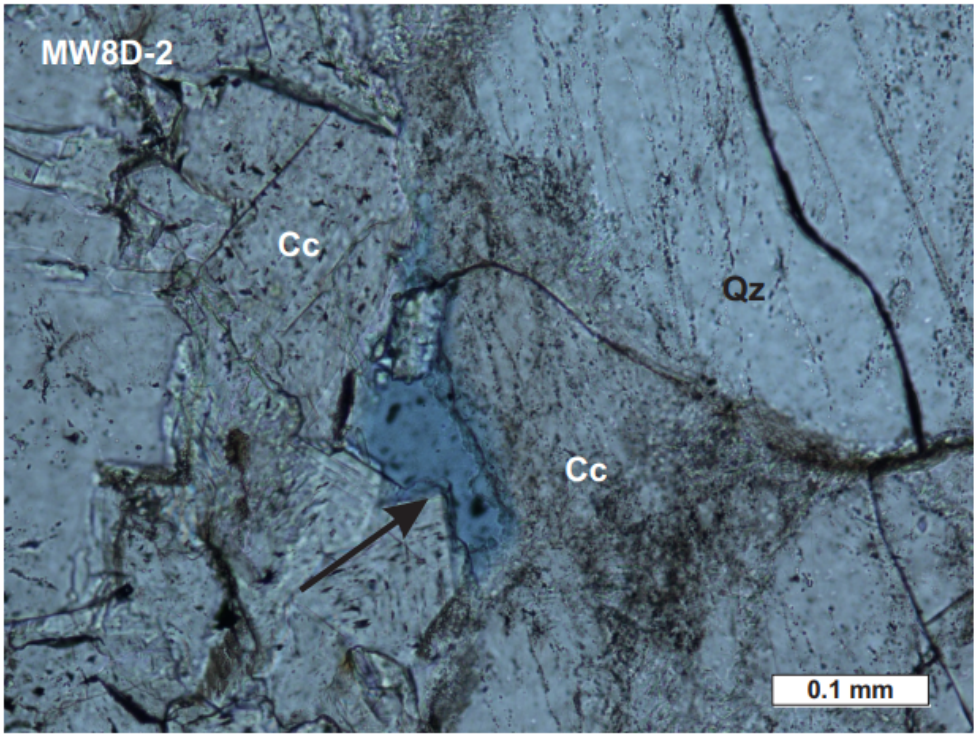

MW8D-2. Pore space preserved between calcite cement (Cc). The well-preserved crystal tip (arrow) indicate that calcite grew in open pore space, indicating that the pore space is primary. Qz: Quartz

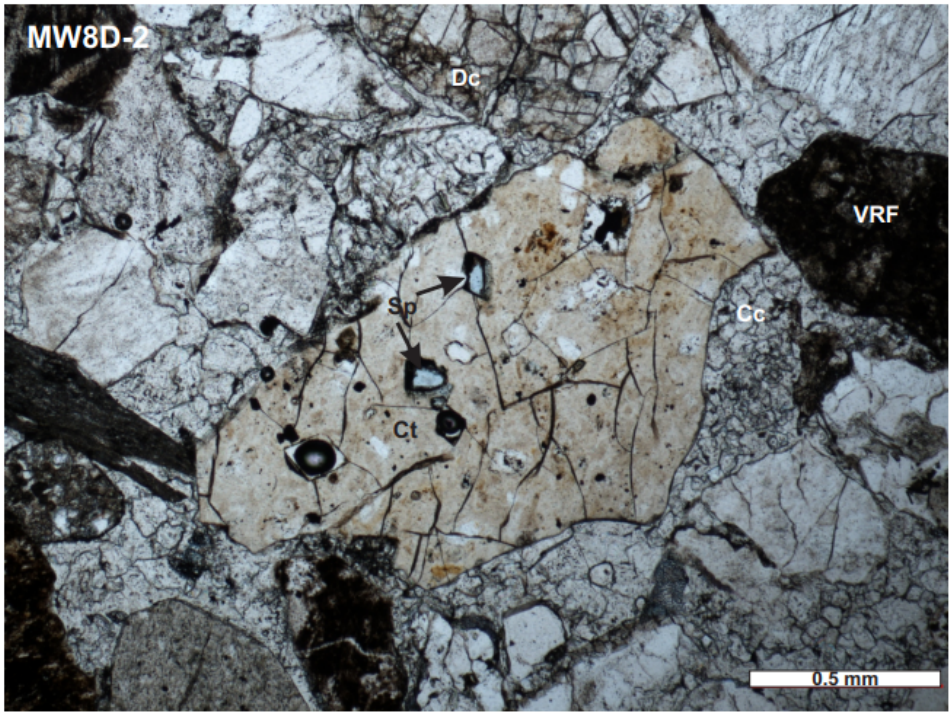

MW8D-2. Chert (Ct) with small dissolution secondary porosity (Sp). Dc: Detrital calcite, Cc: Calcite cement, VRF: Volcanic rock fragment.

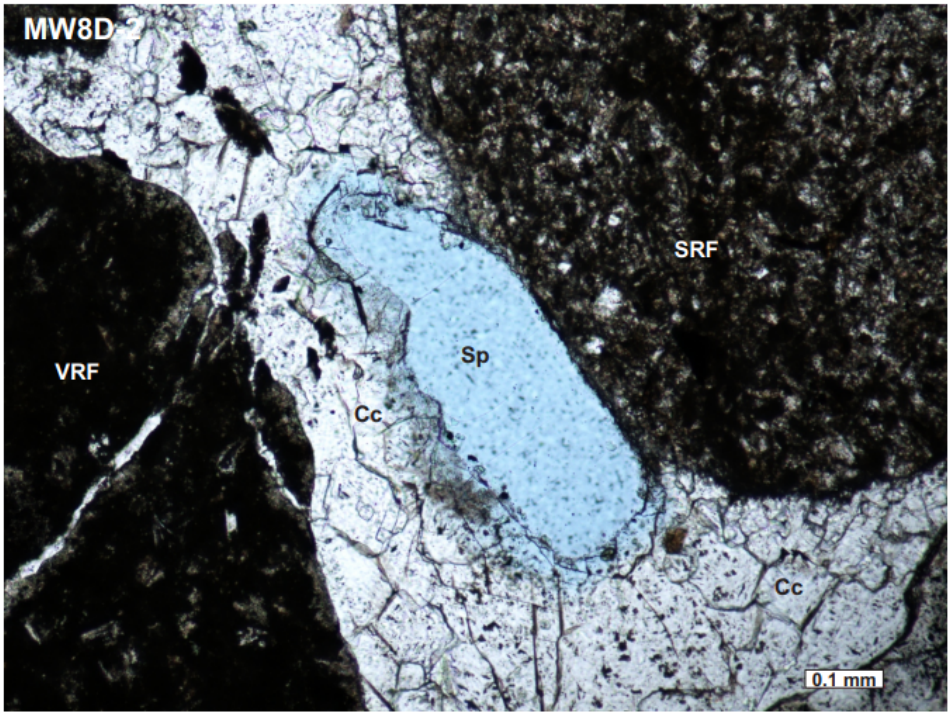

MW8D-2. Secondary dissolution porosity (Sp) in blocky calcite cement (Cc). SRF: Sedimentary rock fragment, VRF: Volcanic rock fragment.

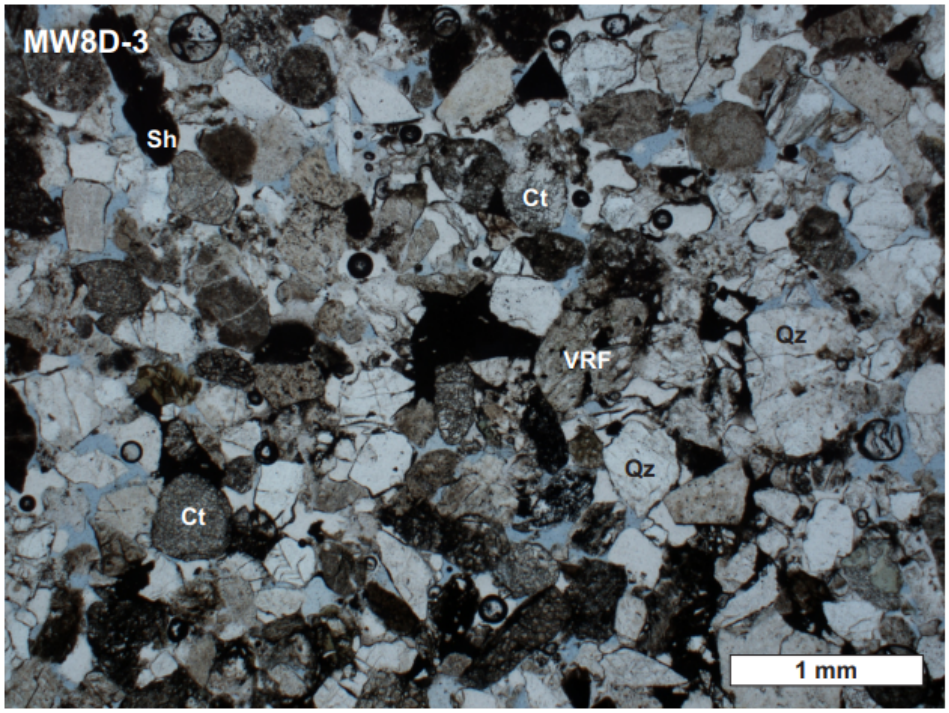

MW8D-3. General view of medium coarse-grained sandstone. 5% of pore space in blue. Qz: Quartz, VRF: Volcanic rock fragment, Ct: Chert, Sh: Shale.

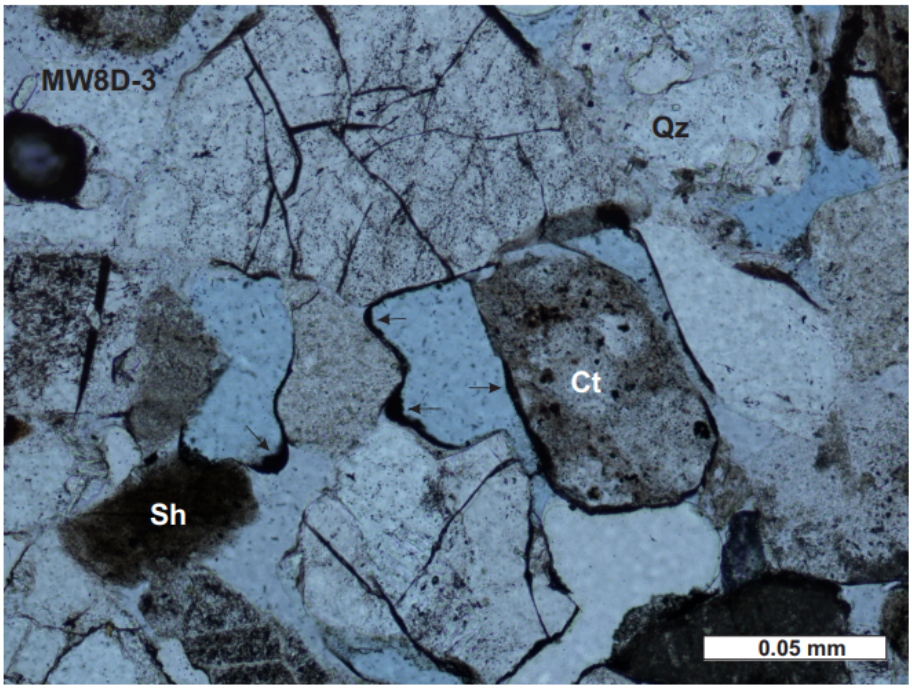

MW8D-3. Close-up of pore space (blue), surrounding crystals have isopachous rims of clay coatings (arrows). The clay lining to the left (arrow) seems to float in porosity suggesting that a now dissolved metastable mineral was present. The chert grain (Ct) is partly dissolved. Qz: Quartz, Sh: Shale.

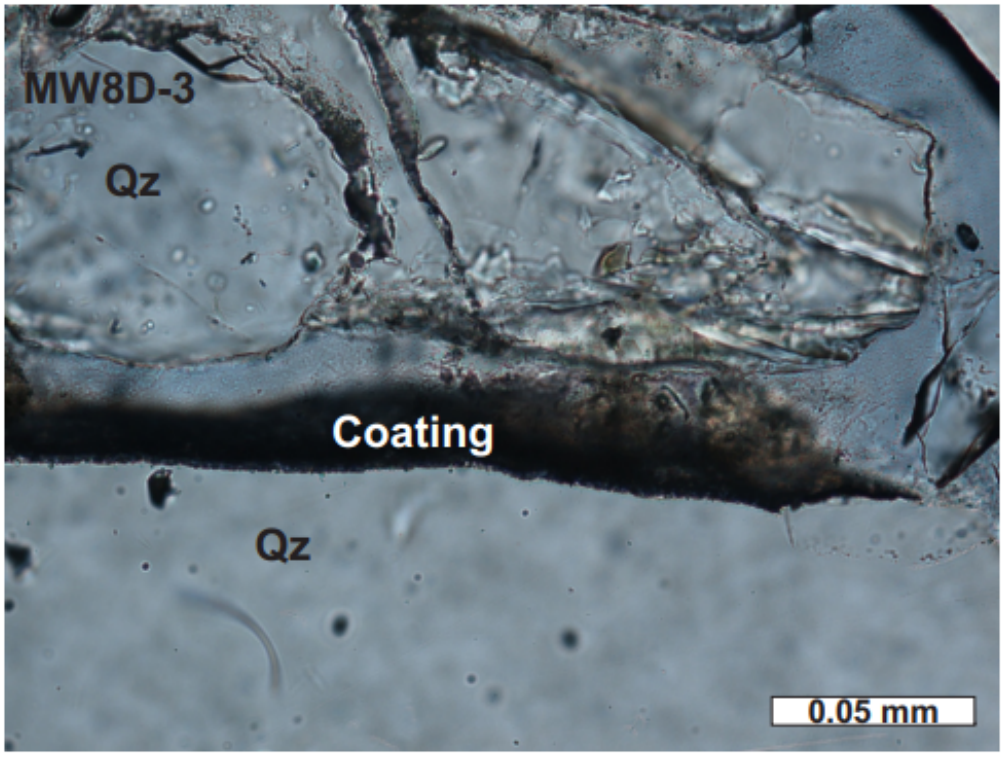

MW8D-3. Close-up view of clay coating on quartz crystals. Qz: Quartz.

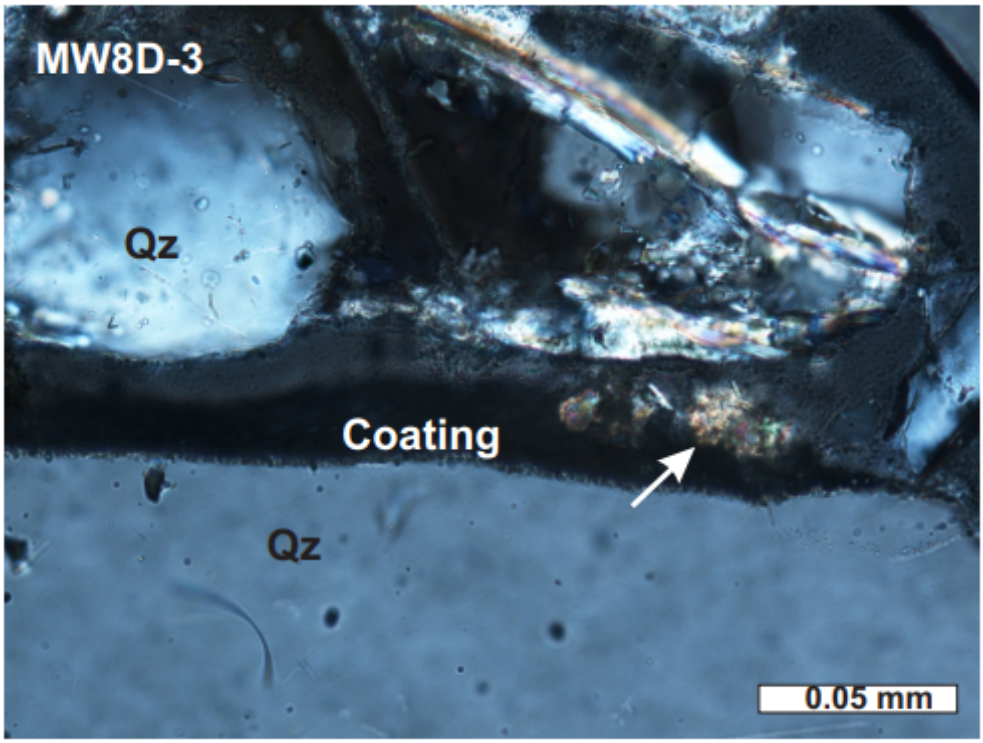

MW8D-3. Same as above but under cross-polarized light. Initial recrystallization of amorphous clay is visible at right end of coating (arrow), the greenish small crystals are likely chlorite.

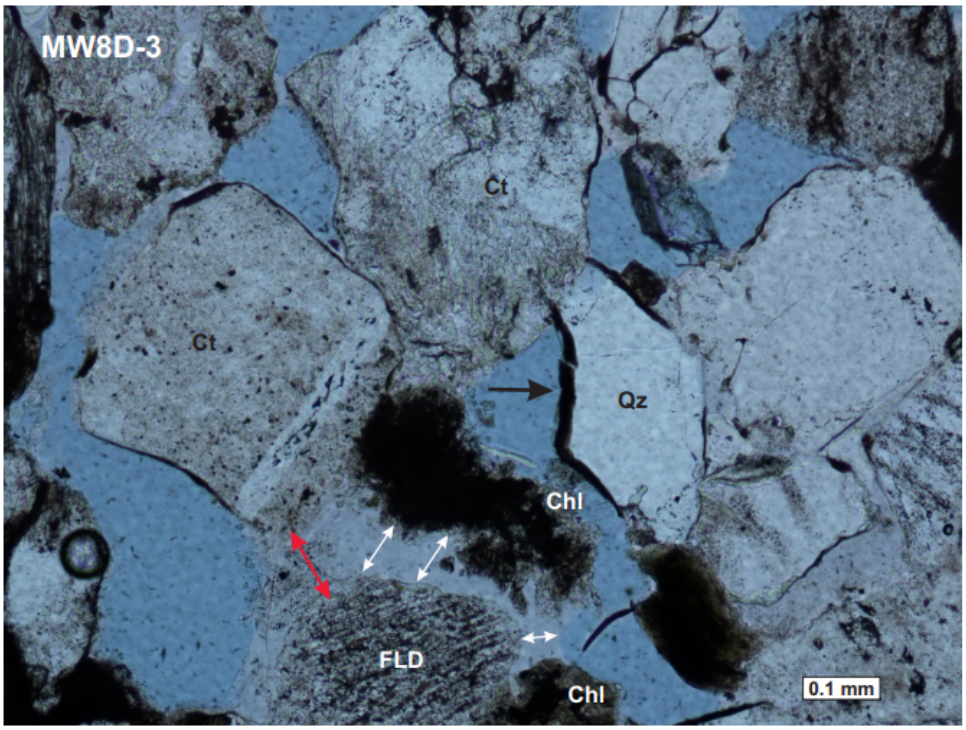

MW8D-3. Pore-filling chlorite (Chl) cement. Clay coating (black arrow) on a quartz (Qz) crystal. The white arrows indicate areas where a precursor mineral phase (feldspar, FLD) has been dissolved. The red arrow indicates an area with partial dissolution of feldspar. Ct: Chert.

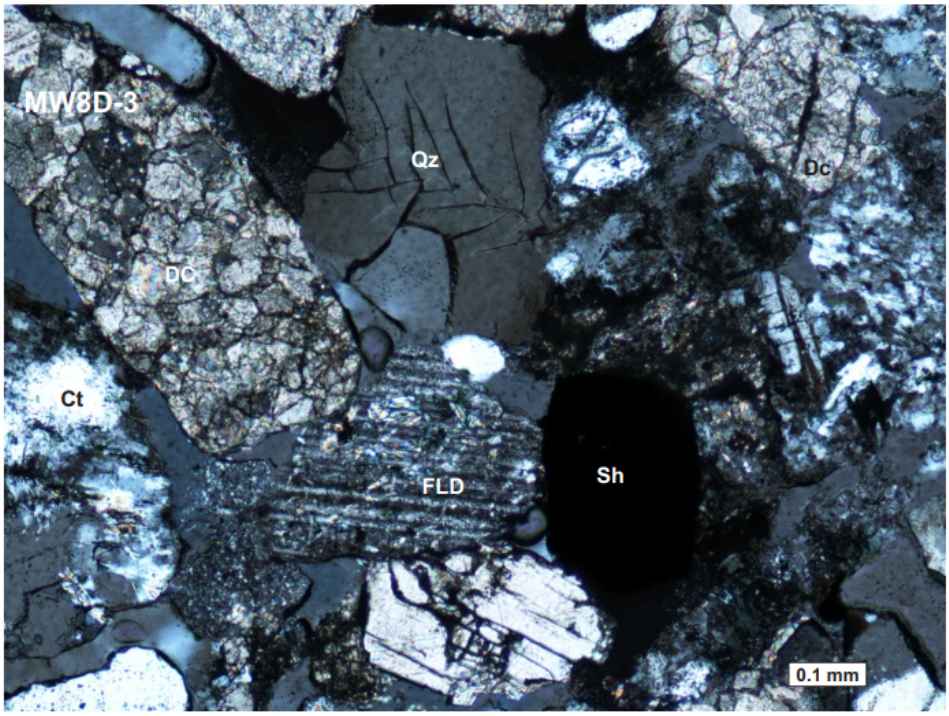

MW8D-3. Under cross-polarized light, heavily sericitized feldspar (FLD). Dc: Detrital calcite, Qz: Quartz, Ct: Chert, Sh: Shale.

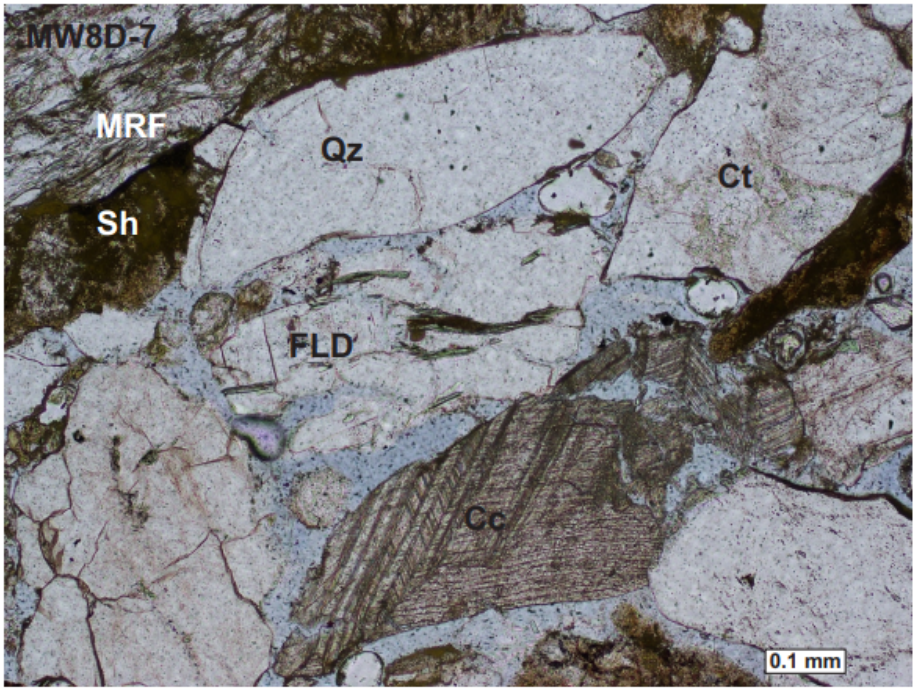

MW8D-7. Broken up poikilitic calcite cement (Cc). Feldspar (FLD) is partly dissolved. MRF: Metamorphic rock fragment, Sh: Shale, Qz: Quartz, Ct: Chert.

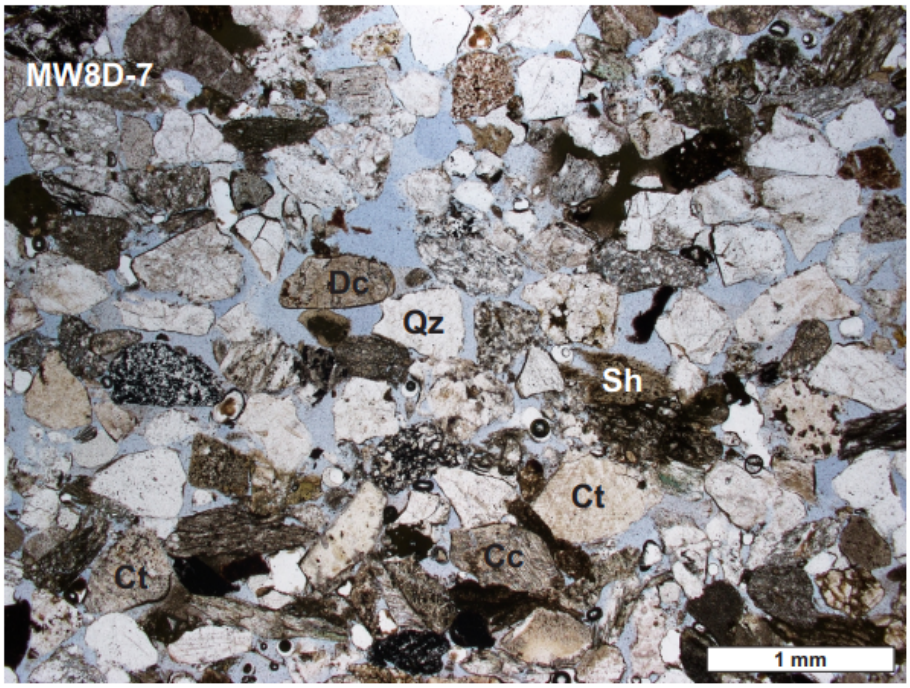

MW8D-7. Porous medium-grained sandstone with 15% porosity. Cc: Calcite cement, Dc: Detrital calcite, Ct: Chert, Sh : Shale, Qz: Quartz.

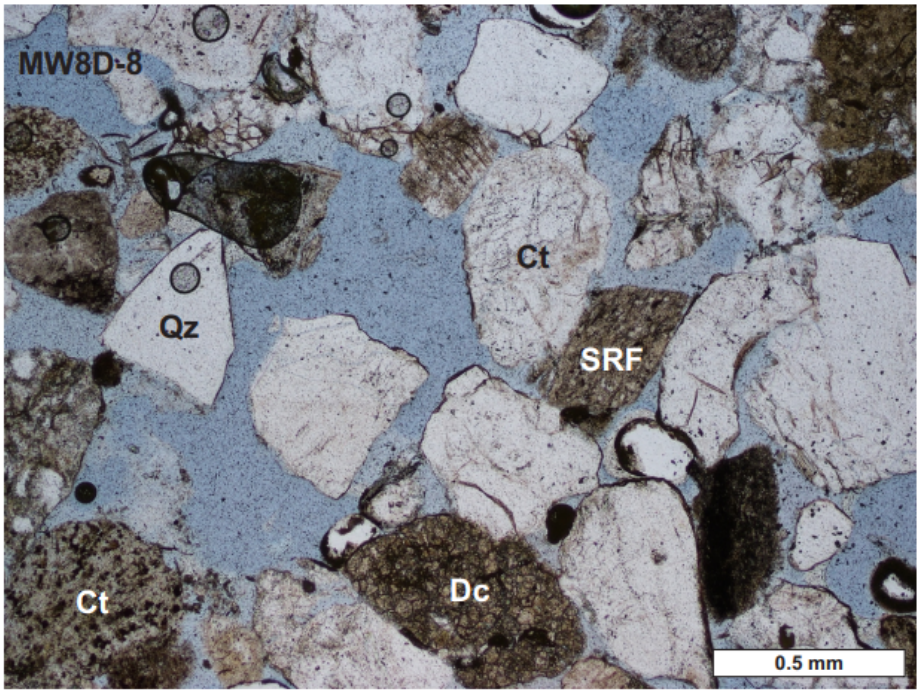

MW8D-8. Very porous medium-grained sandstone with thin clay coatings on detrital particles. Ct: Chert, Dc: Detrital calcite, SRF: Sedimentary rock fragment, Qz: Quartz.

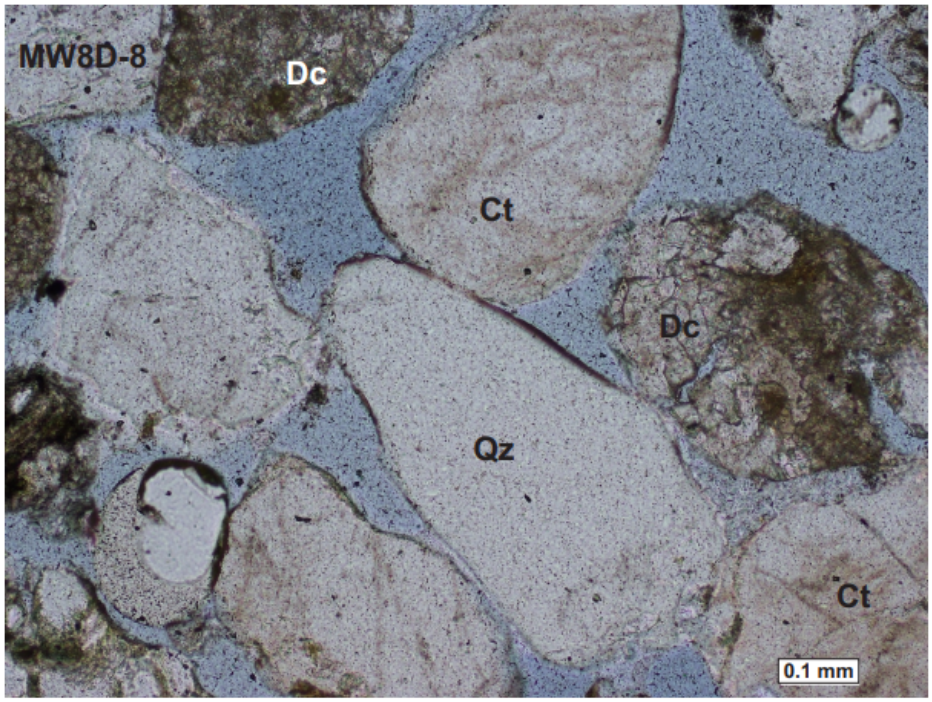

MW8D-8. Thin clay coating partly surrounding detrital particle. The clay coating was present before the compacted contact between the quartz (Qz) and chert (Ct) fragments. Dc: Detrital calcite.

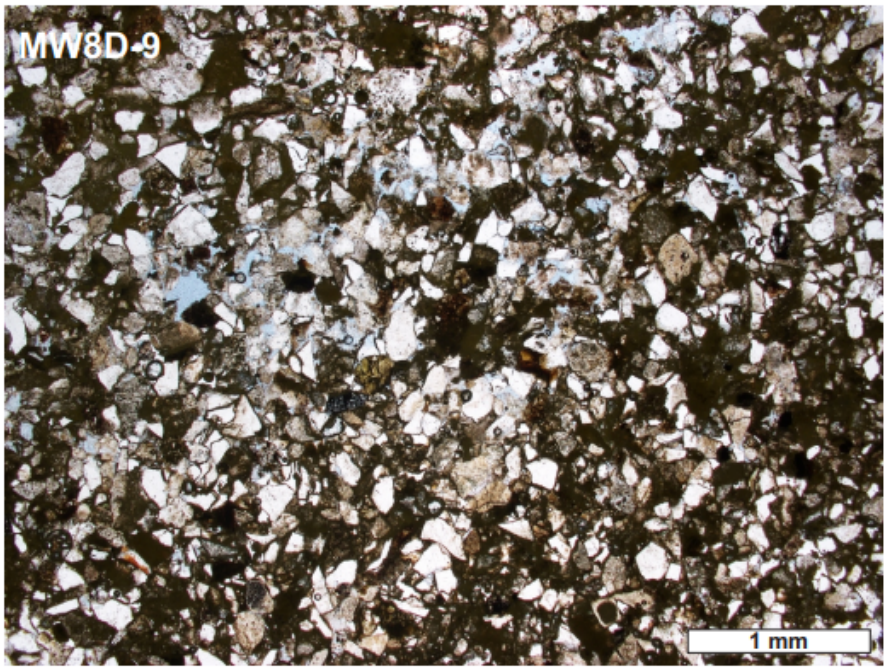

MW8D-9. Fine-grained sandstone with abundant angular quartz and clay matrix. 2% porosity in blue.

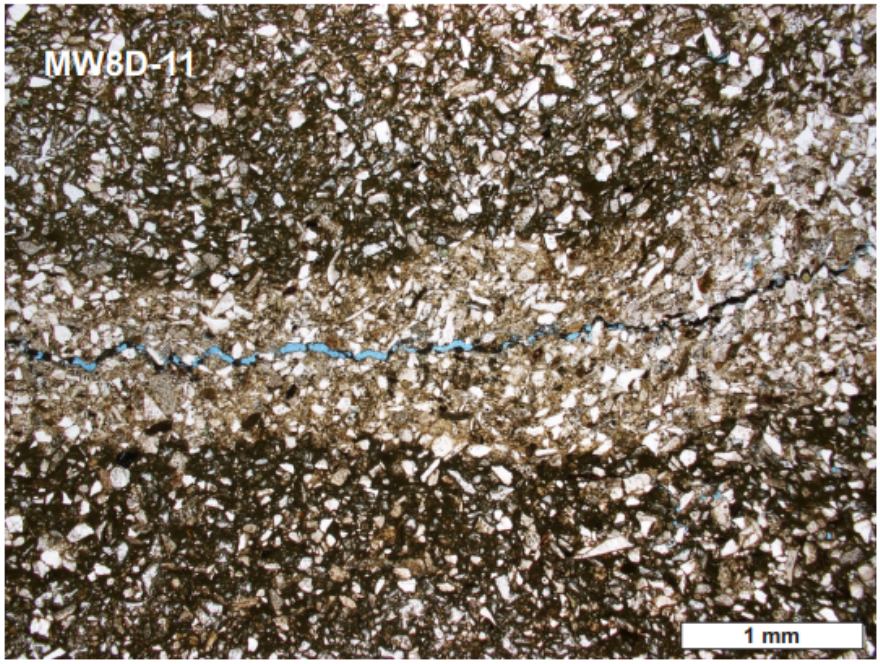

MW8D-11. Very-fine grained burrowed sandstone. Physical properties of the sediment in the burrowed zone (lighter shade) have been modified compared to the non-borrowed domain (darker shade).

ANNEX 9: PHOTOMICROGRAPHS OF SAMPLES FROM WELL MW3E

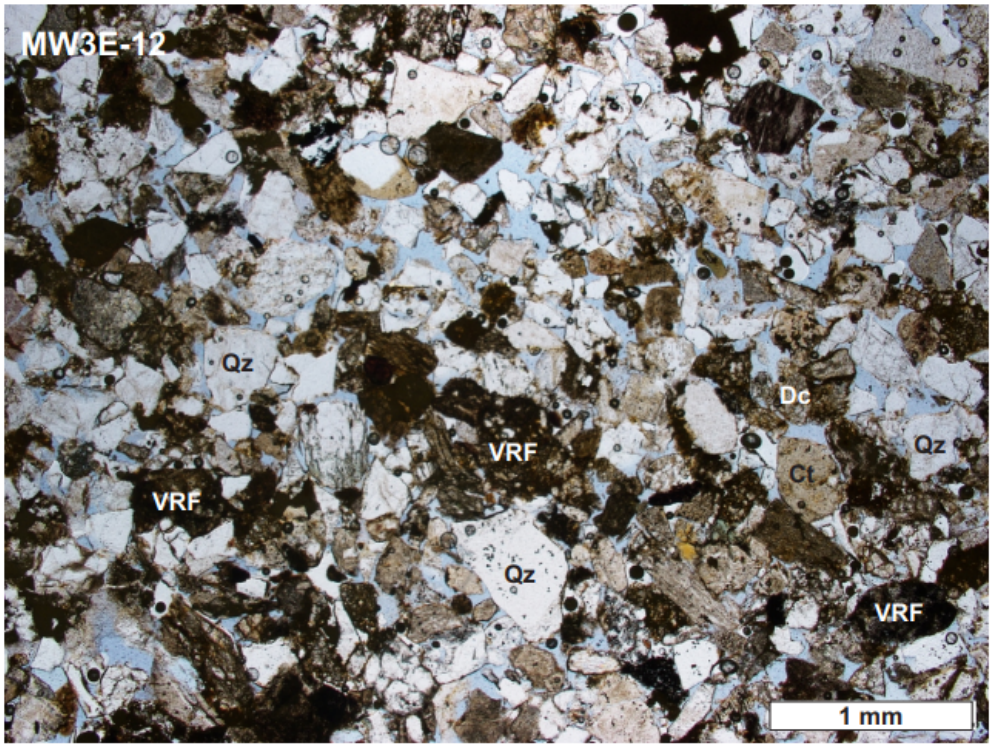

MW3E-12. Well-compacted, medium-grained sandstone with 10% pore space. Qz: Quartz, VRF: Volcanic rock fragment, Dc: Detrital calcite, Ct: Chert.

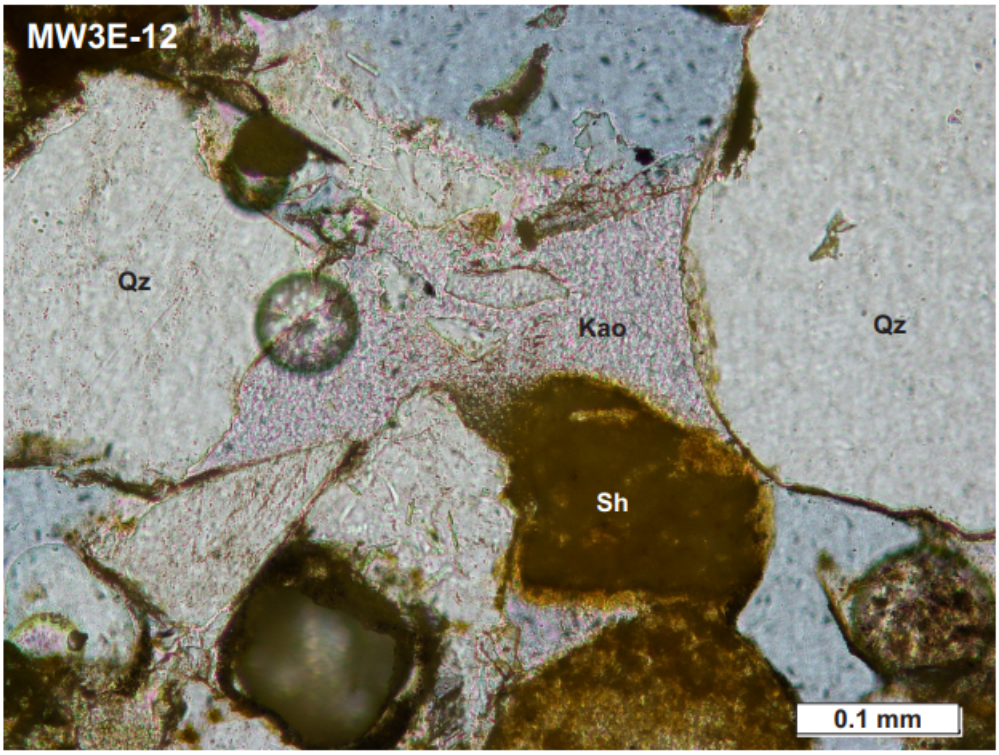

MW3E-12. Pore-filling kaolinite (Kao) cement. Qz: Quartz, Sh: Shale.

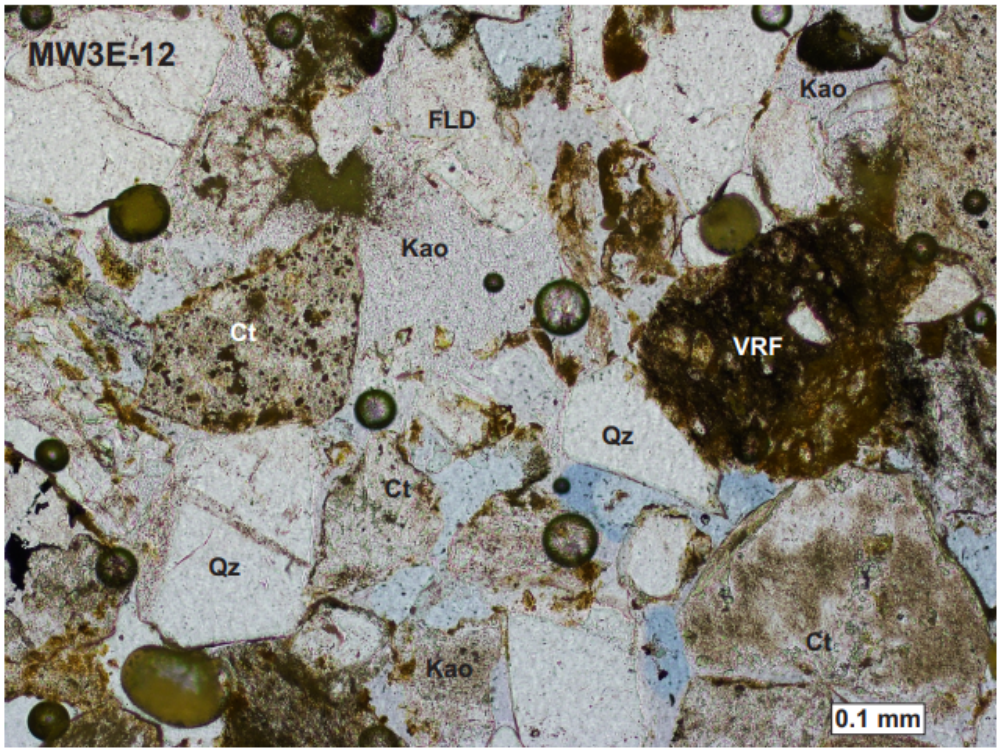

MW3E-12. Abundant pore-filling kaolinite (Kao) cement. The feldspar (top center, FLD) is partly dissolved and engulfed in the kaolinite. Qz: Quartz, VRF: Volcanic rock fragment, CT: Chert.

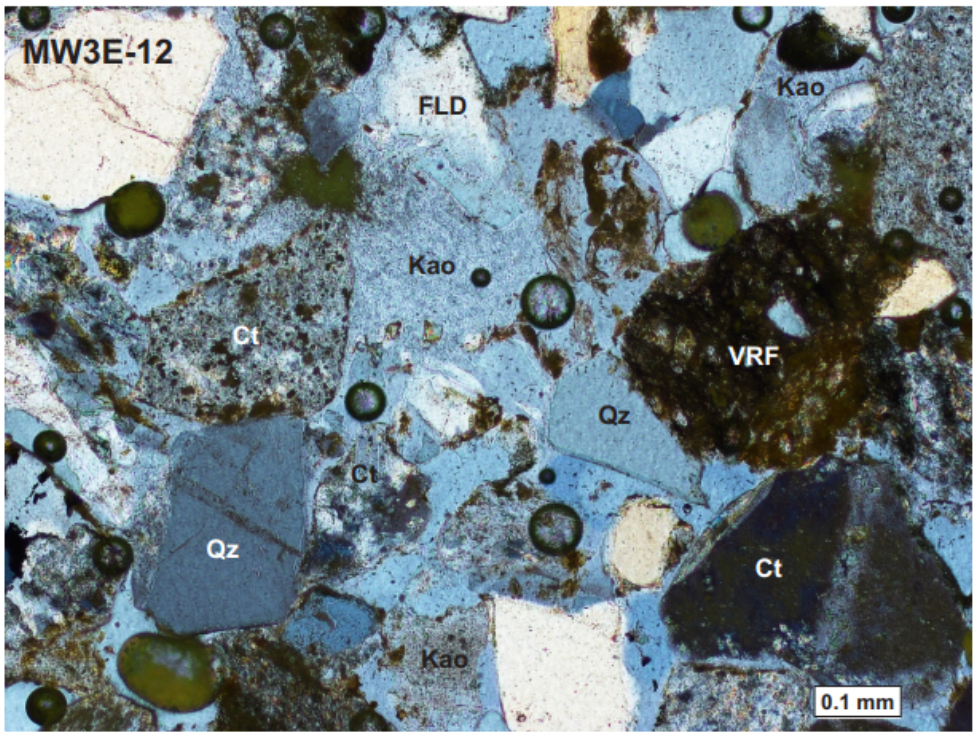

MW3E-12. Same as above under cross-polarized light. The dissolution of feldspar (FLD) is more visible.

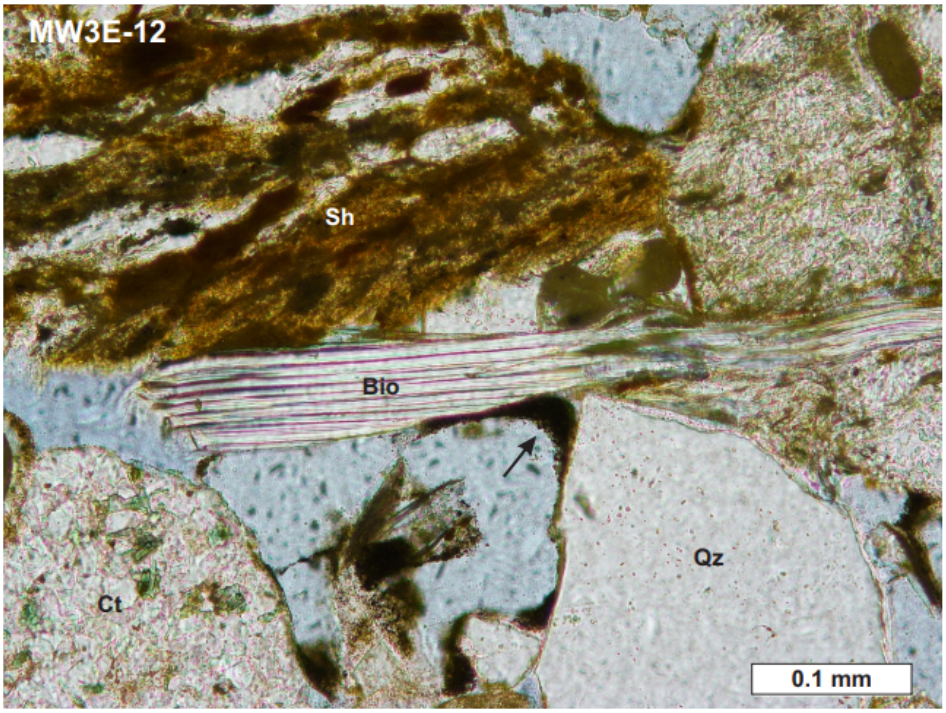

MW3E-12. Medium-grained sandstone with a biotite (Bio) fragment partly coated with a clay rim (arrow). Qz: Quartz, Sh: Shale, Ct: Chert.

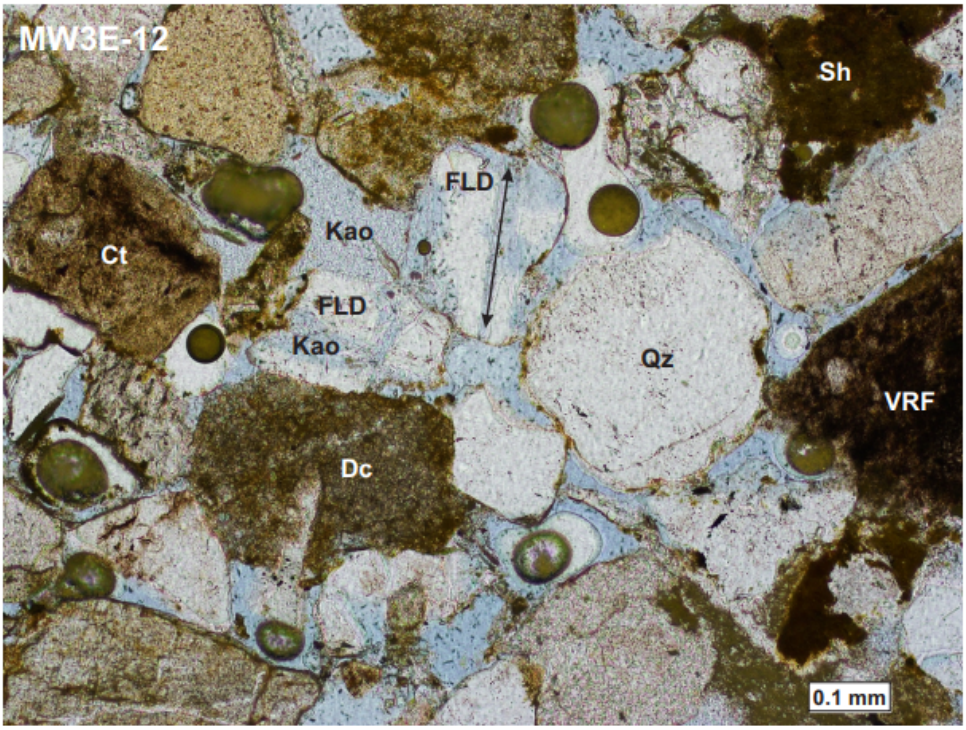

MW3E-12. Feldspar (FLD) partial dissolution, the top crystal shows dissolution along twinning plane (arrow). To the left, feldspar is irregularly dissolved and engulfed in kaolinite (Kao) cement. Qz: Quartz, VRF: Volcanic rock fragment, Dc: Detrital calcite, Sh: Shale, Ct: Chert.

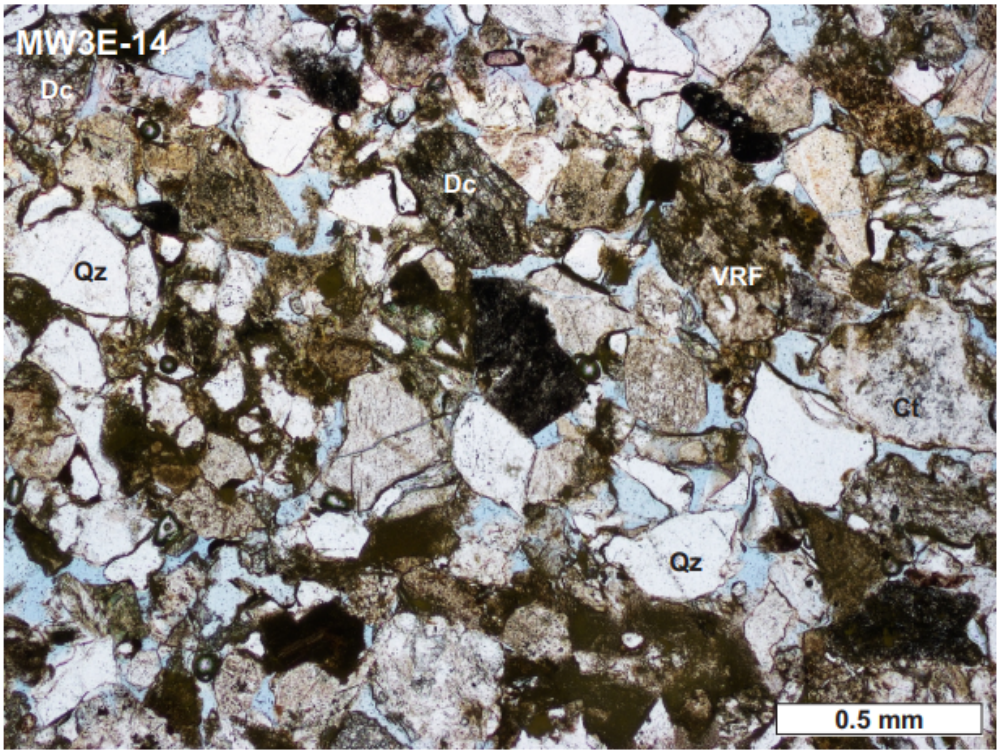

MW3E-14. Medium-grained sandstone, with strong compaction and 10% open pore space. Qz: Quartz, VRF: Volcanic rock fragment, Dc: Detrital calcite, Ct: Chert.

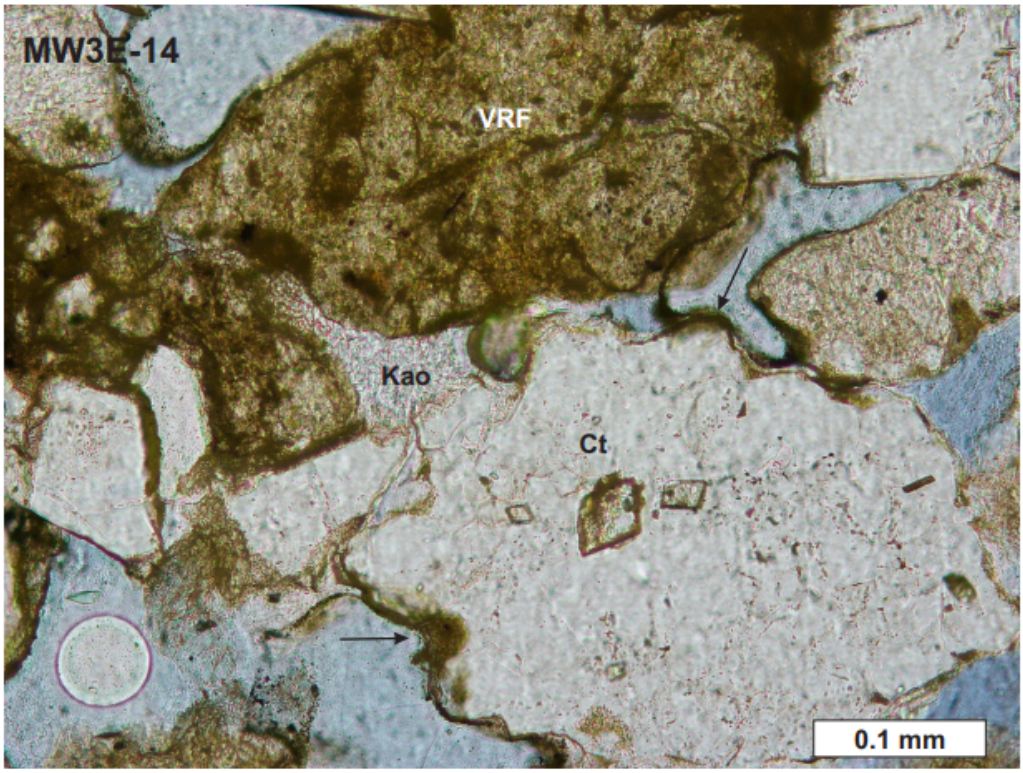

MW3E-14. Pore-filling kaolinite (Kao) cement between Chert (Ct) and a volcanic rock fragment (VRF). Clay coatings on clasts (arrows). Note the dissolved scalloped surface of the chert grain.

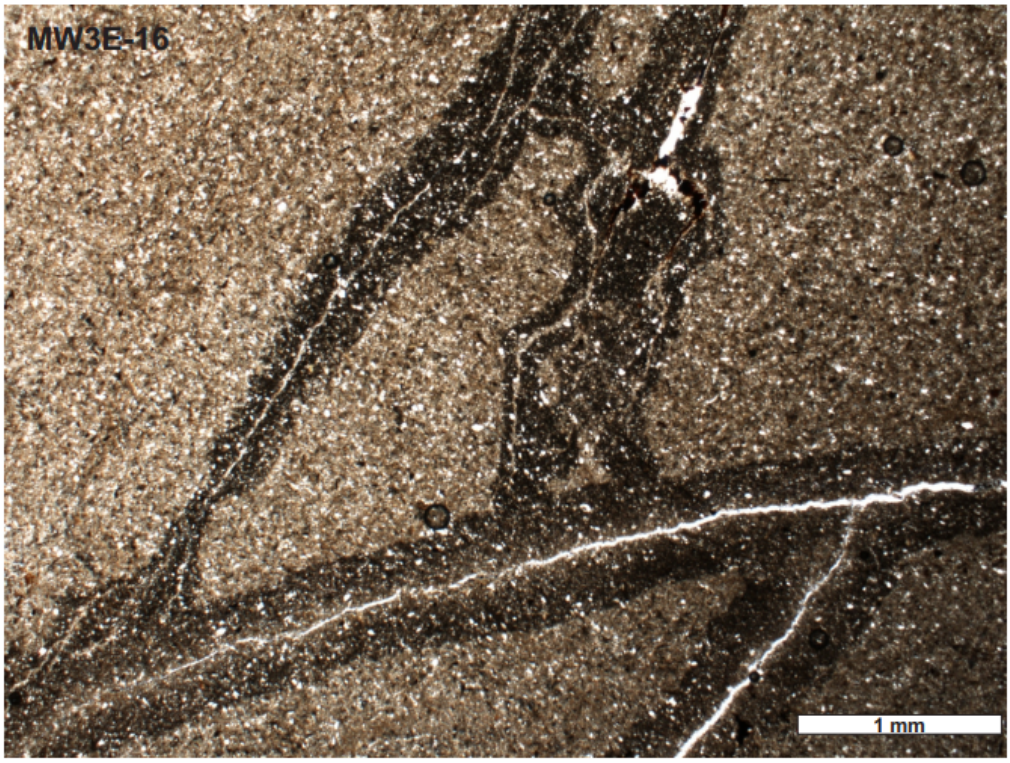

MW3E-16. Oxidized plant roots in a mudstone clast within a non-porous sandstone.

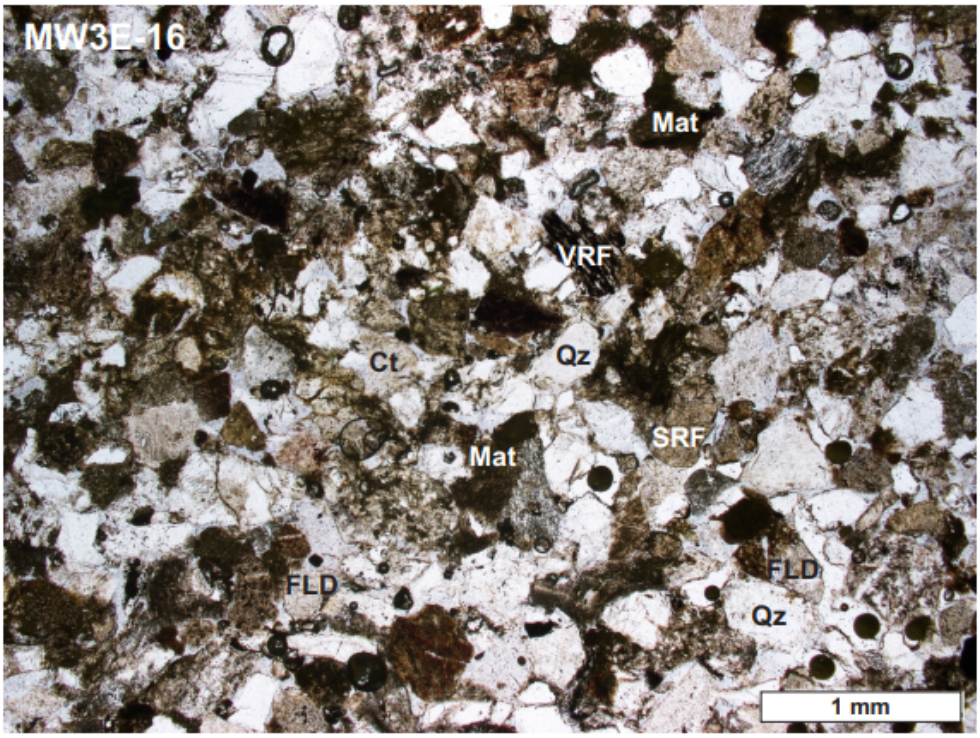

MW3E-16. Non-porous, medium-grained, strongly compacted sandstone. 2% of detrital matrix (Mat). Qz: Quartz, Ct: Chert, SRF: Sedimentary rock fragment, VRF: Volcanic rock fragment.

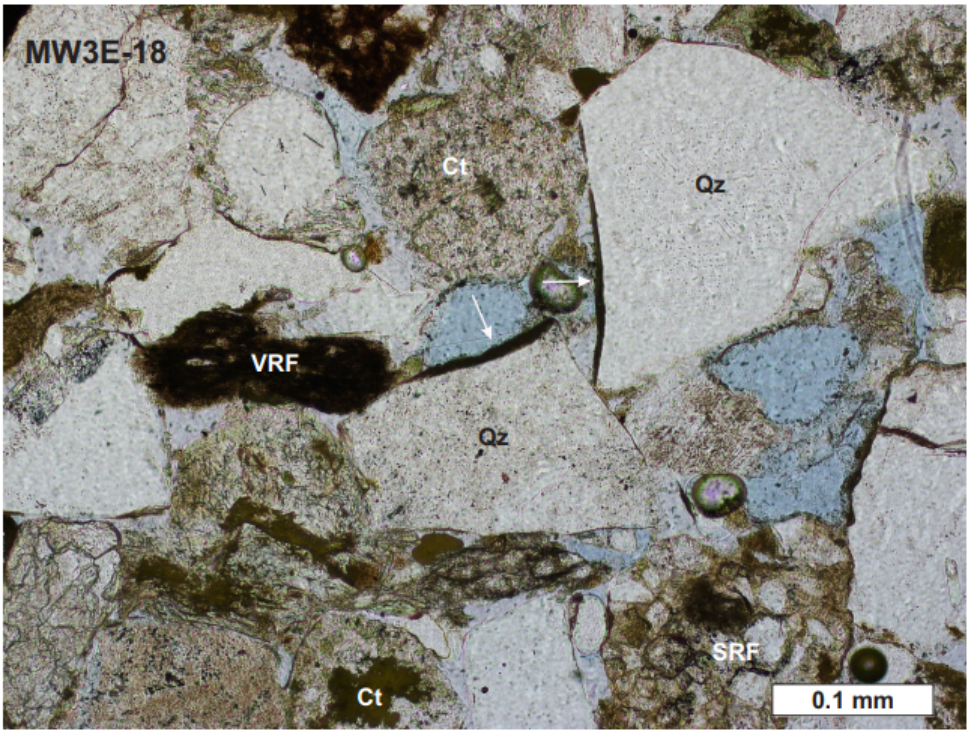

MW3E-18. Incomplete clay coating (arrows) on quartz (Qz) particles. VRF: Volcanic rock fragment, SRF: Sedimentary rock fragment, Ct: Chert.

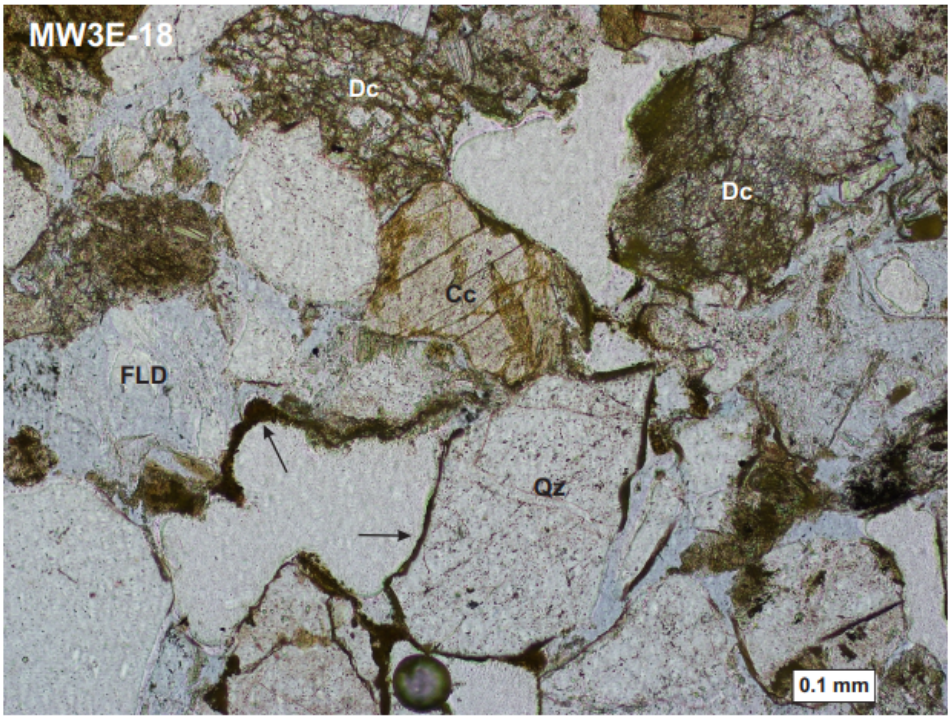

MW3E-18. Medium-grained sandstone with detrital calcite (Dc), quartz (Qz) and feldspar (FLD). The feldspar (FLD) is intensely dissolved with ghost crystal remains. Poikilotopic calcite cement (Cc) in pore space is partly dissolved at outer surface. Clay coatings (arrows) lining some pore space.

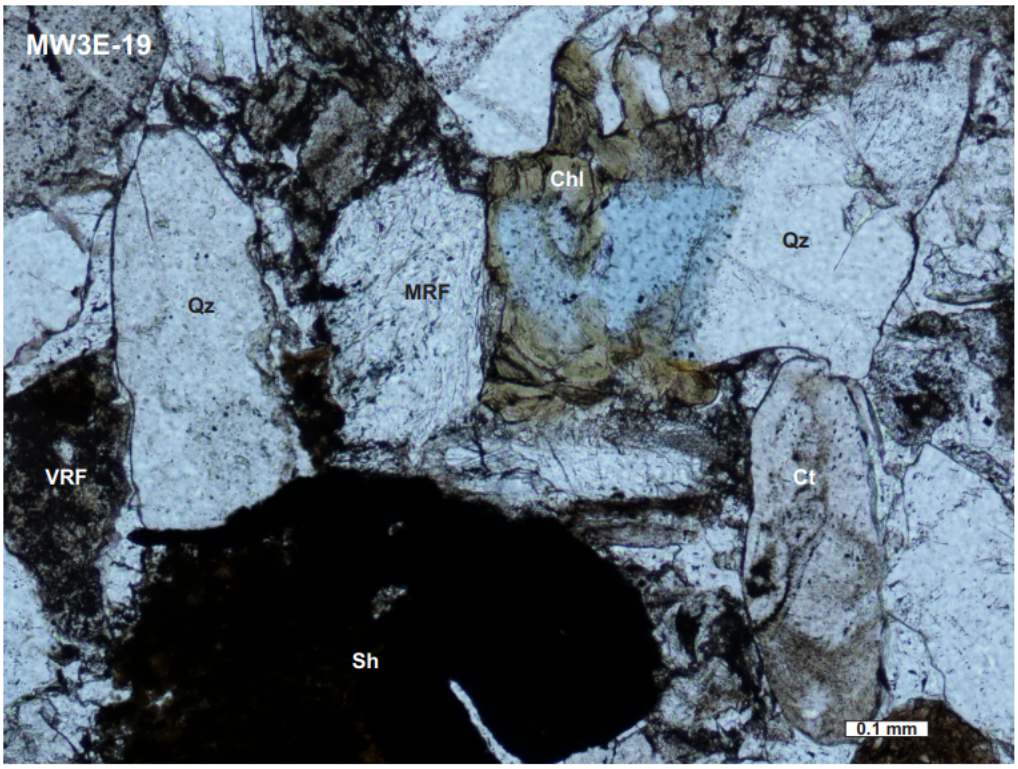

MW3E-19. Medium-grained sandstone with chlorite (Chl) cement imperfectly coating pore wall. Qz: Quartz, VRF: Volcanic rock fragment, MRF: Metamorphic rock fragment, Sh: Shale, Ct: Chert.

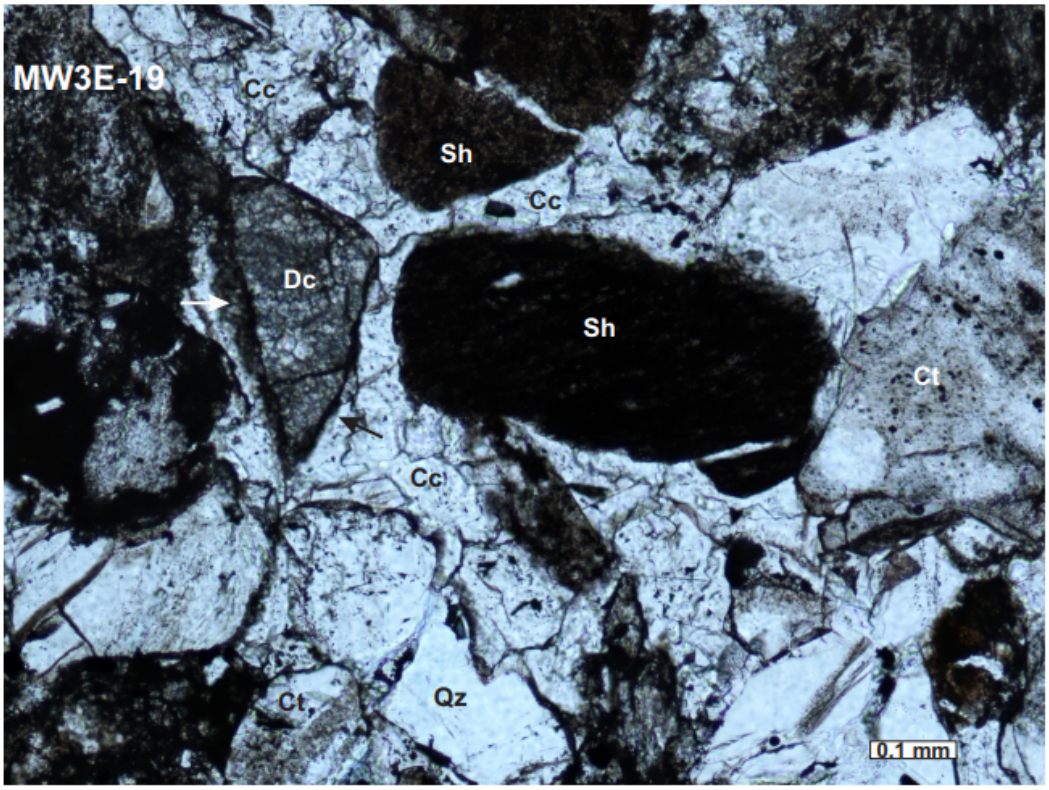

MW3E-19. Calcite cement (Cc) filling pore space. A detrital calcite (Dc) particle is coated by clay rim (arrows). Qz: Quartz, Sh: Shale, Ct: Chert.

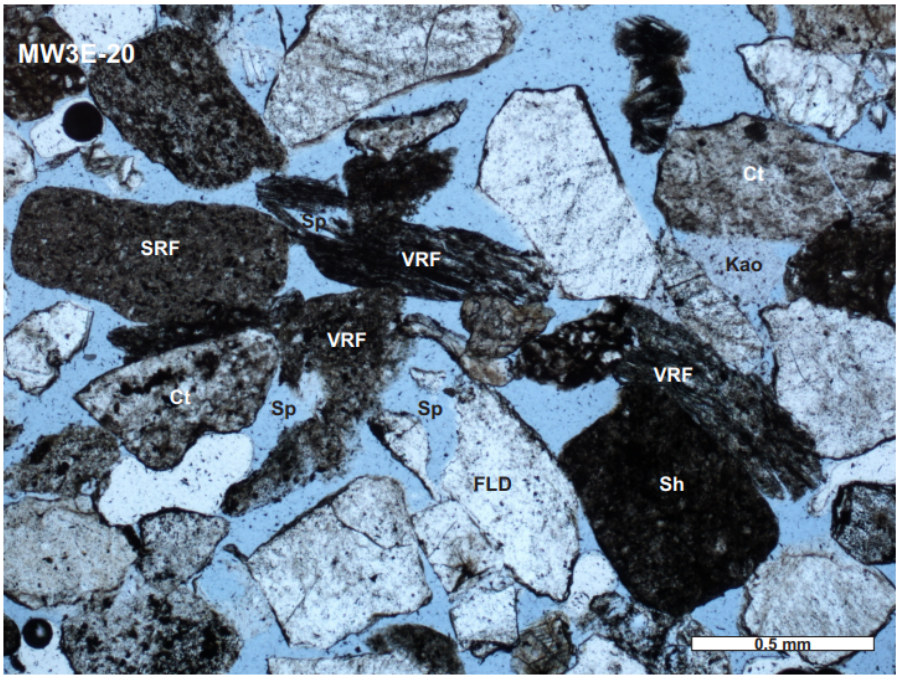

MW3E-20. Secondary porosity (Sp) developed in volcanic rock fragments (VRF) and feldspar (FLD). Kaolinite (Kao) cement. Abundant clay coatings. SRF: Sedimentary rock fragment, Sh: Shale, Ct: Chert.

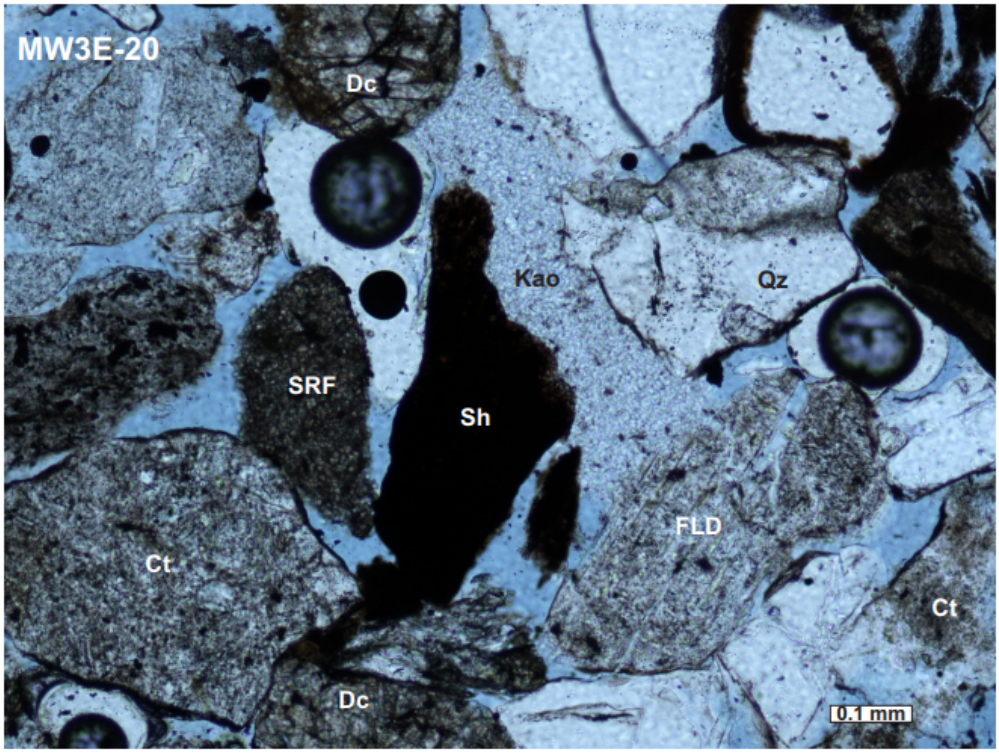

MW3E-20. Pore-filling kaolinite (Kao) cement. Dc: Detrital calcite, FLD: Feldspar, Qz: Quartz, SRF: Sedimentary rock fragment, Sh: Shale, Ct: Chert.

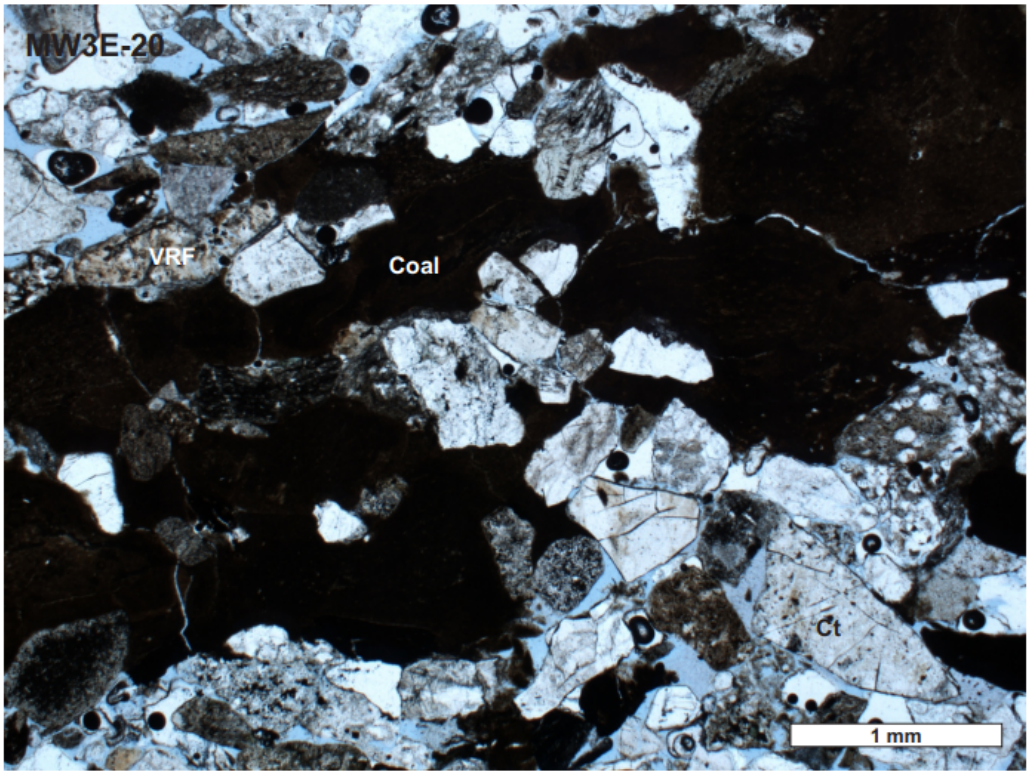

MW3E-20. Broken pieces of coal in a lamination with detrital material. VRF: Volcanic rock fragment, Ct: Chert.

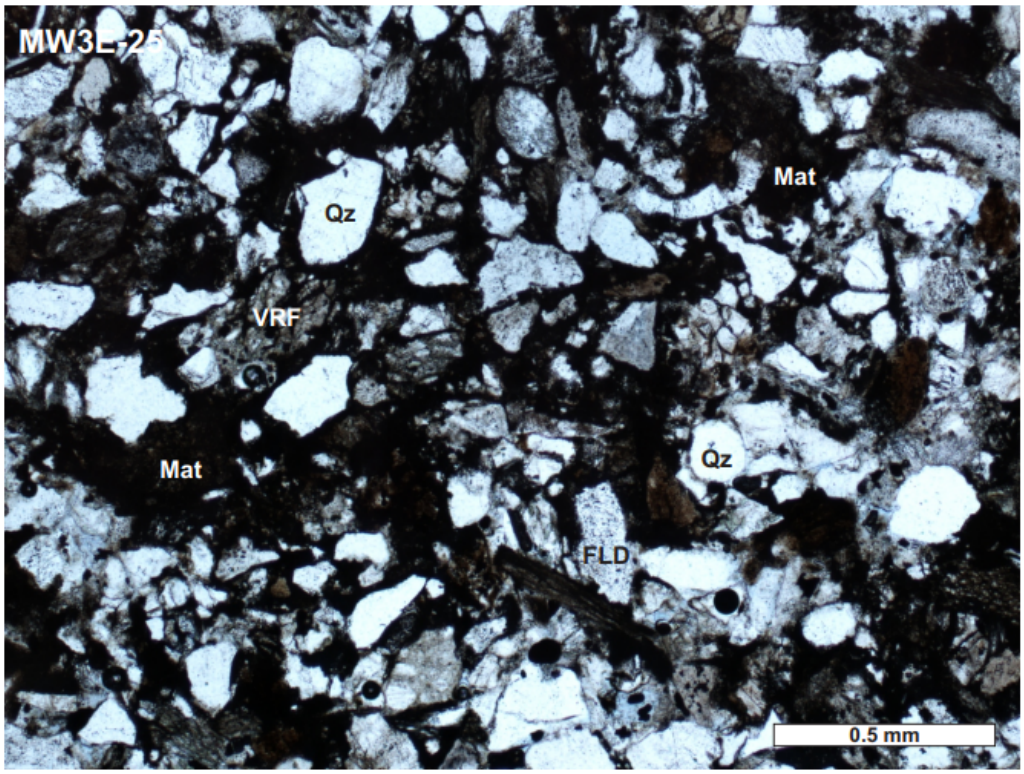

MW3E-25. Fine-grained sandstone with abundant detrital matrix (Mat). Less than 2% pore space. Qz: Quartz, VRF: Volcanic rock fragment, FLD: Feldspar.

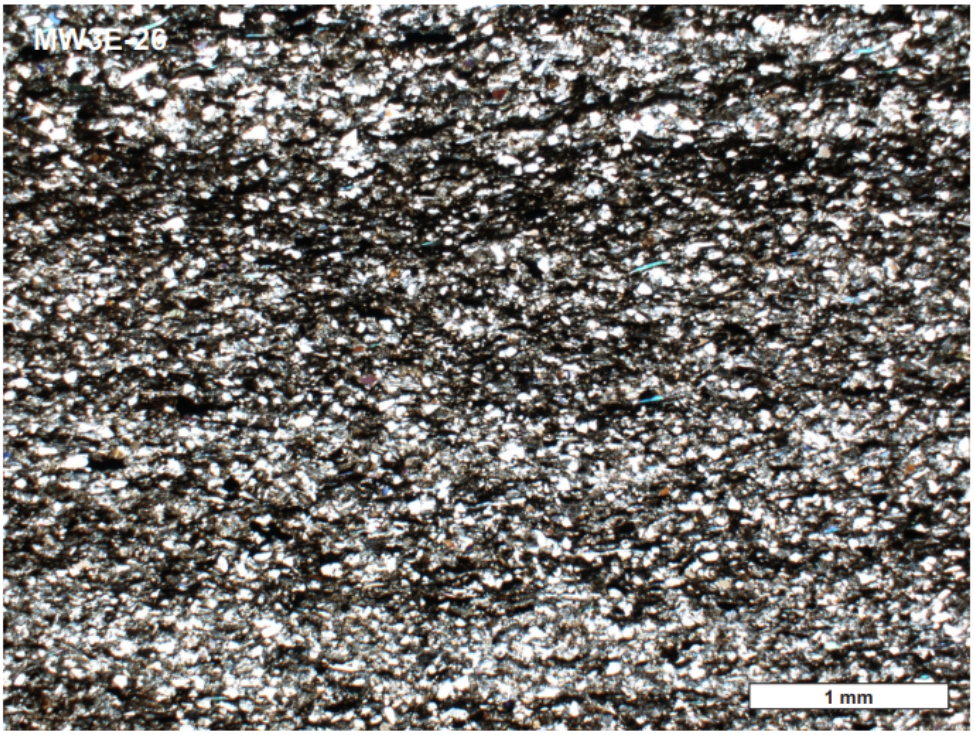

MW3E-26. Fine-grained sandstone made up of alternating mud-rich and mud-poor laminations.

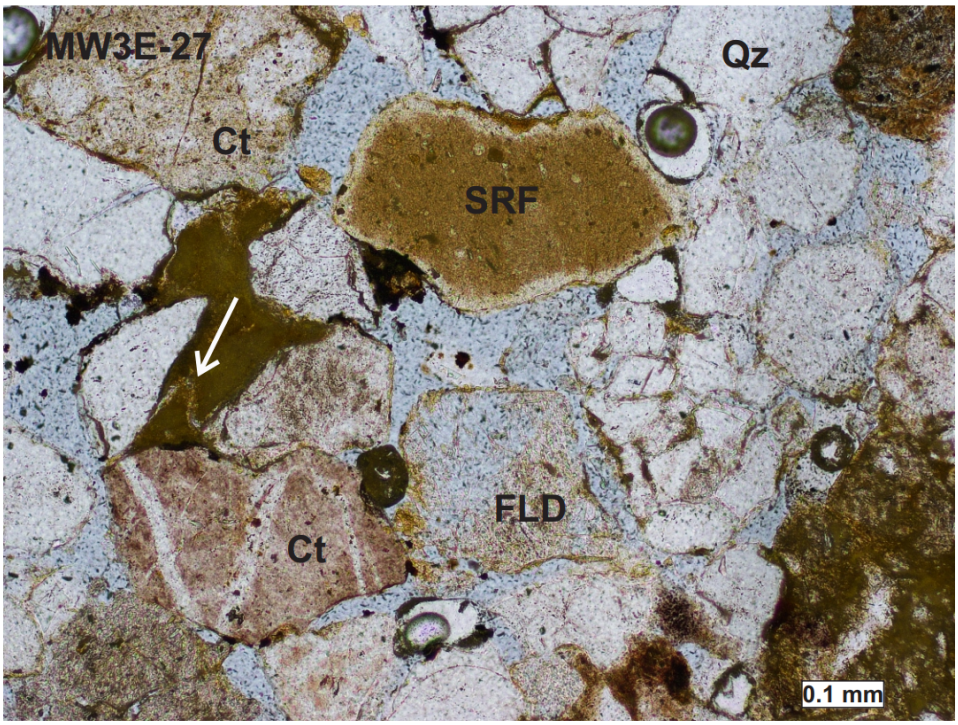

MW3E-27. Medium-grained porous sandstone with strongly dissolved feldspar (FLD). A mud infill is visible, the mud has been plastically deformed during compaction (arrow points to a deformed internal lamination in the mud). Ct: Chert, SRF: Sedimentary rock fragment, Qz: Quartz.

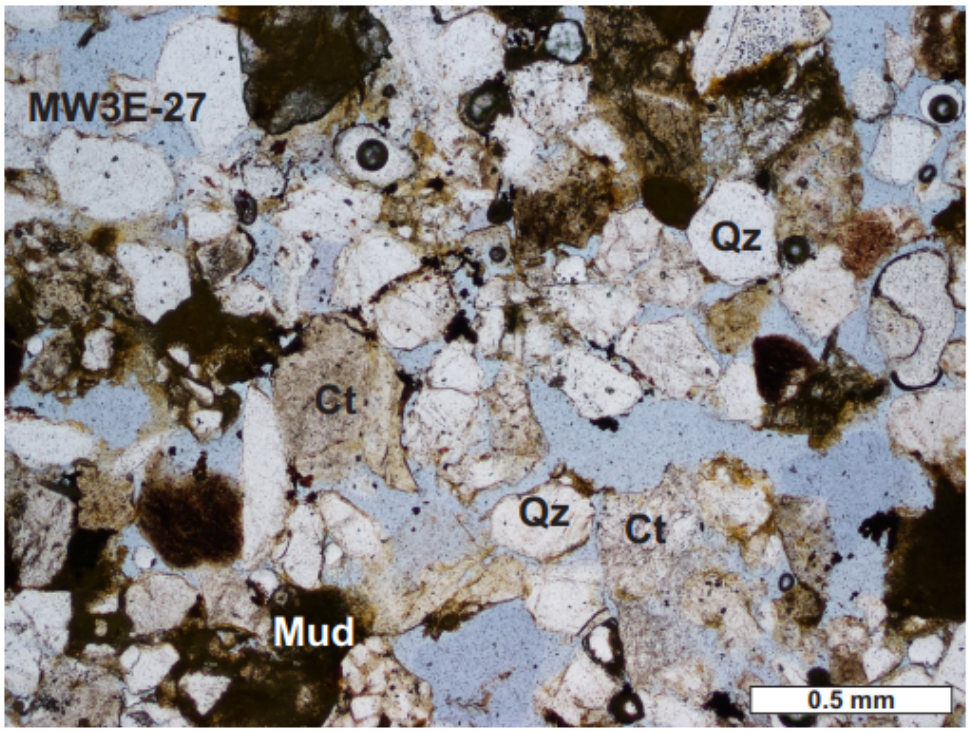

MW3E-27. Very porous medium-grained sandstone with local mud infill. A chert (Ct) fragment is partly leached. Qz: Quartz.

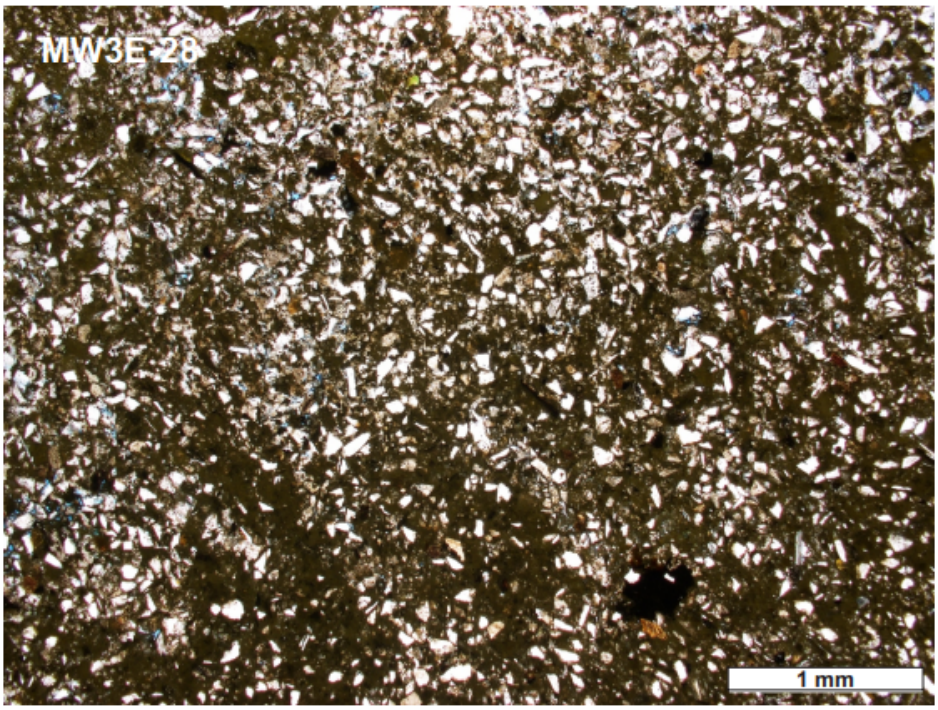

MW3E-28. Fine-grained sandstone with abundant angular quartz and detrital mud matrix.

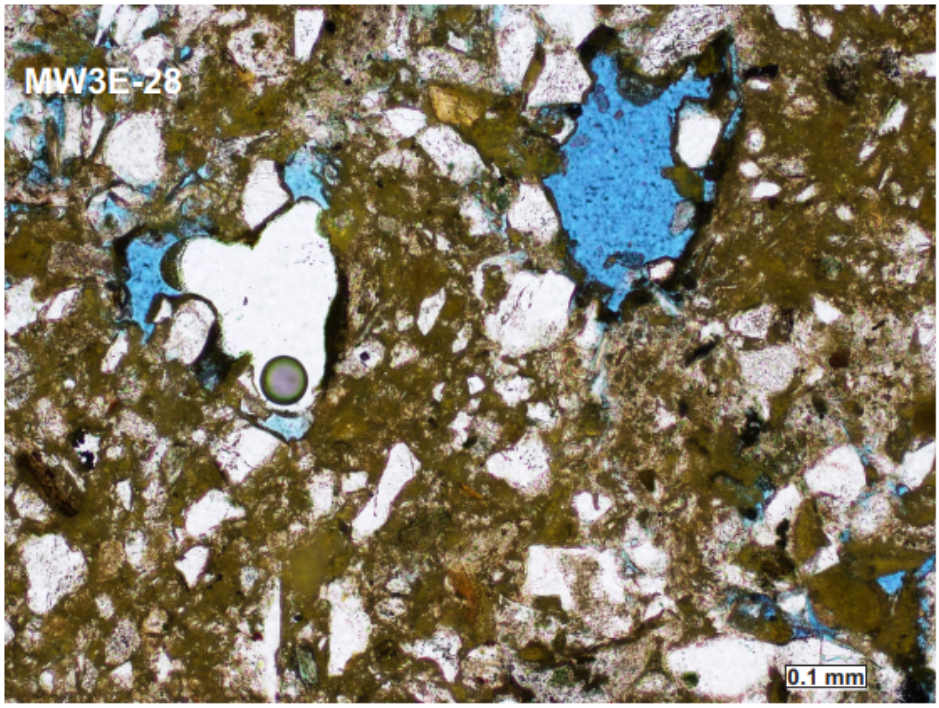

MW3E-28. Small pore space (in blue) in fine-grained sandstone. Dark clay coating rims preserved the porosity.

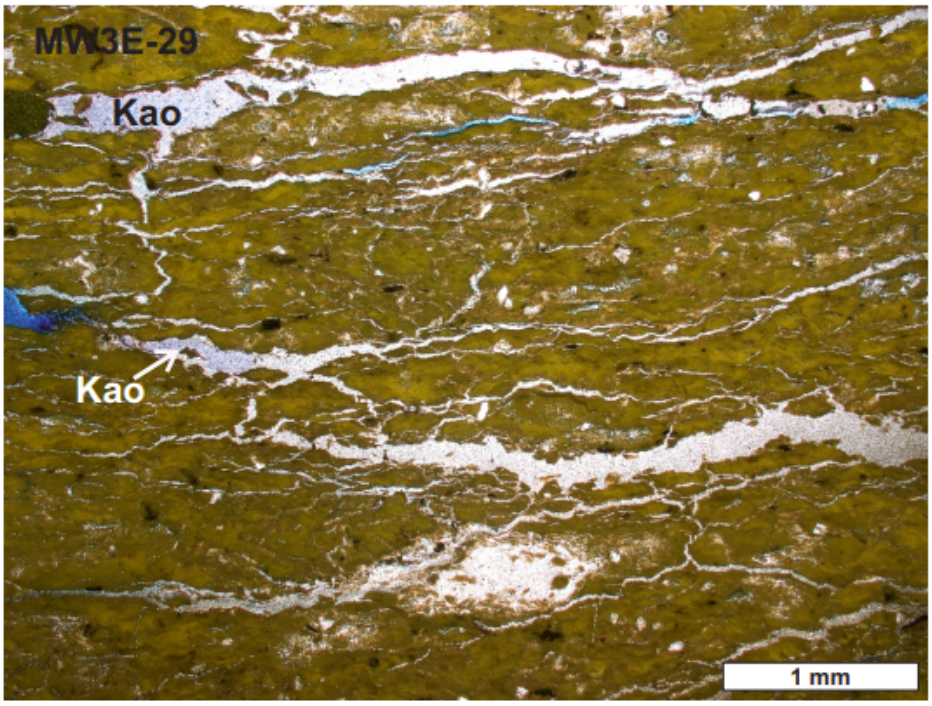

MW3E-29. Well compacted calcareous mud with abundant open horizontal shrinkage fissures. The horizontal fissures are connected by small vertical ones. Kao is kaolinite. Soil profile.

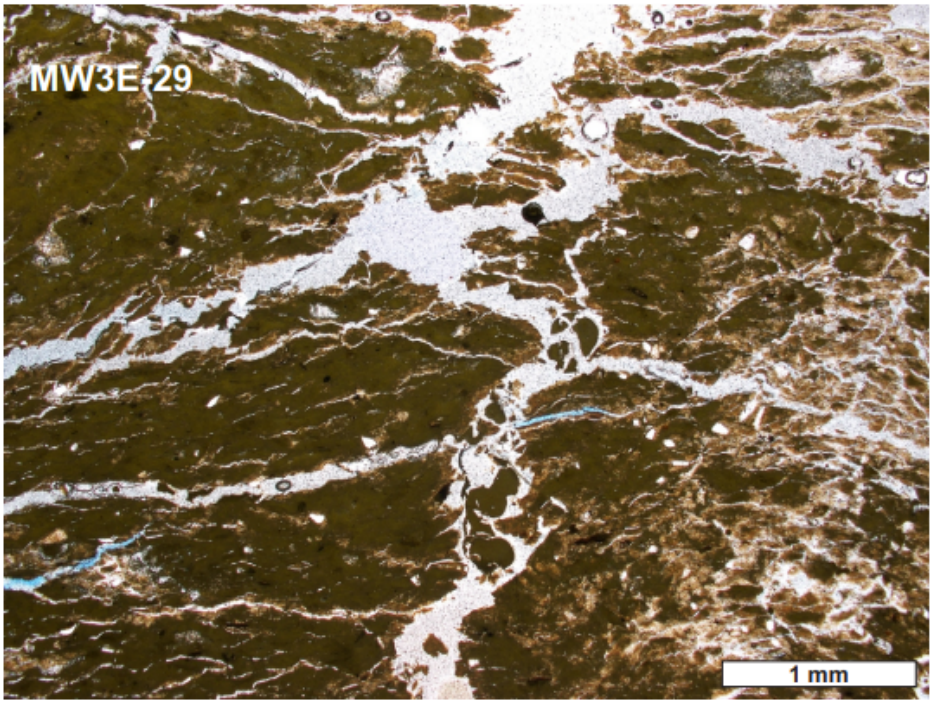

MW3E-29. Calcareous mudstone with abundant open horizontal and vertical shrinkage fissures resulting in development of micro-brecciated zones. Soil profile.

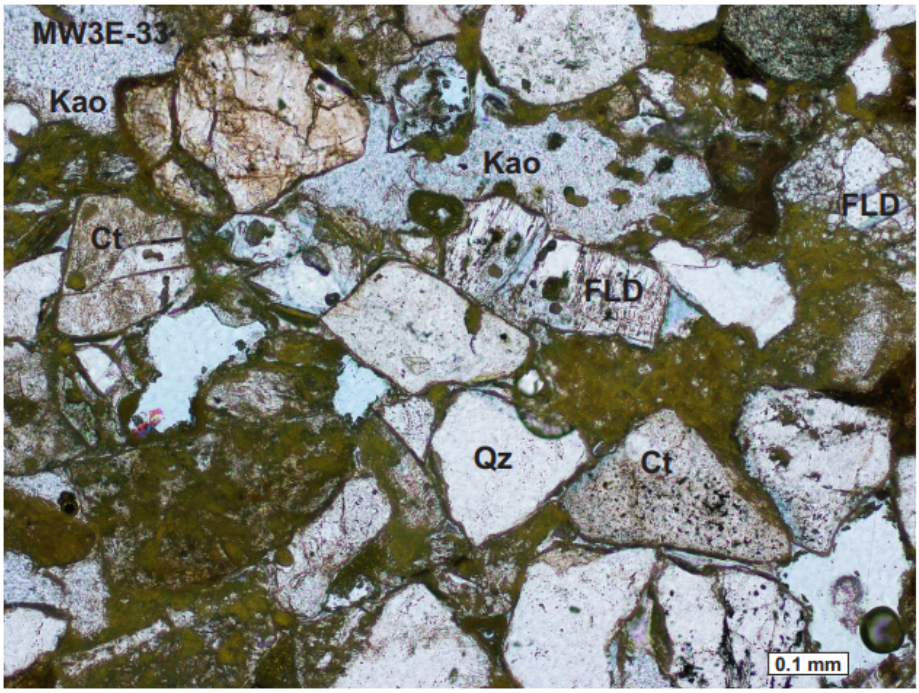

MW3E-33. Pore-filling kaolinite (Kao) in medium-grained muddy sandstone. Feldspar (FLD) is partly dissolved. Ct: Chert, Qz: Quartz.

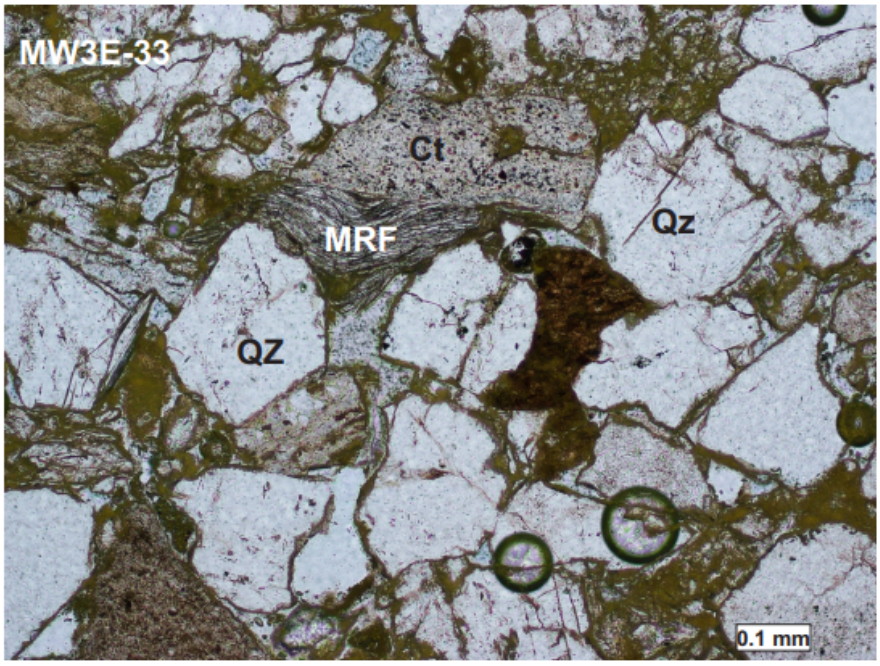

MW3E-33. Medium-grained sandstone with a deformed slaty metamorphic rock fragment (MRF) compacted between quartz (Qz) and chert (Ct).

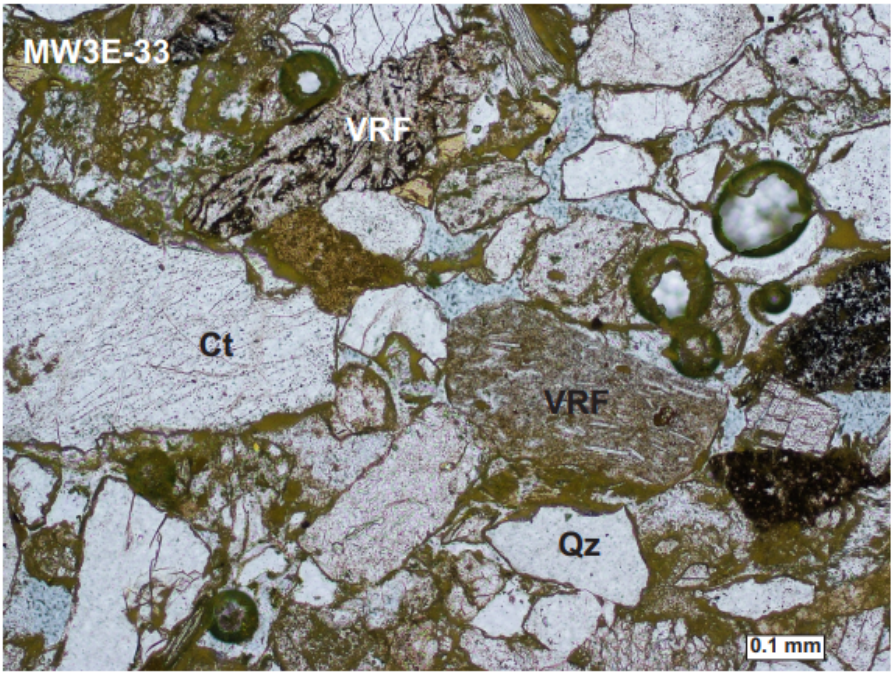

MW3E-33. Medium-grained sandstone with 5% porosity. VRF: Volcanic rock fragment, Qz: Quartz, Ct : Chert.

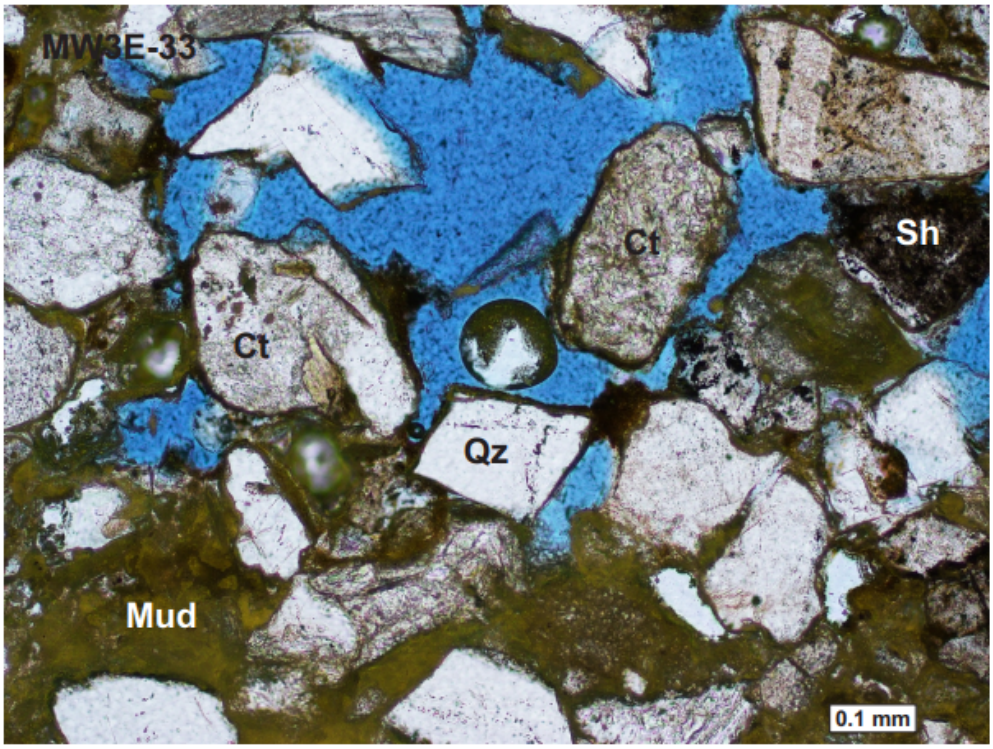

MW3E-33. Medium-grained sandstone with a porous zone overlying a mud-rich domain. Detrital particles surrounding the pore space are coated with rims of clay. Qz: Quartz, Ct: Chert, Sh: Shale.

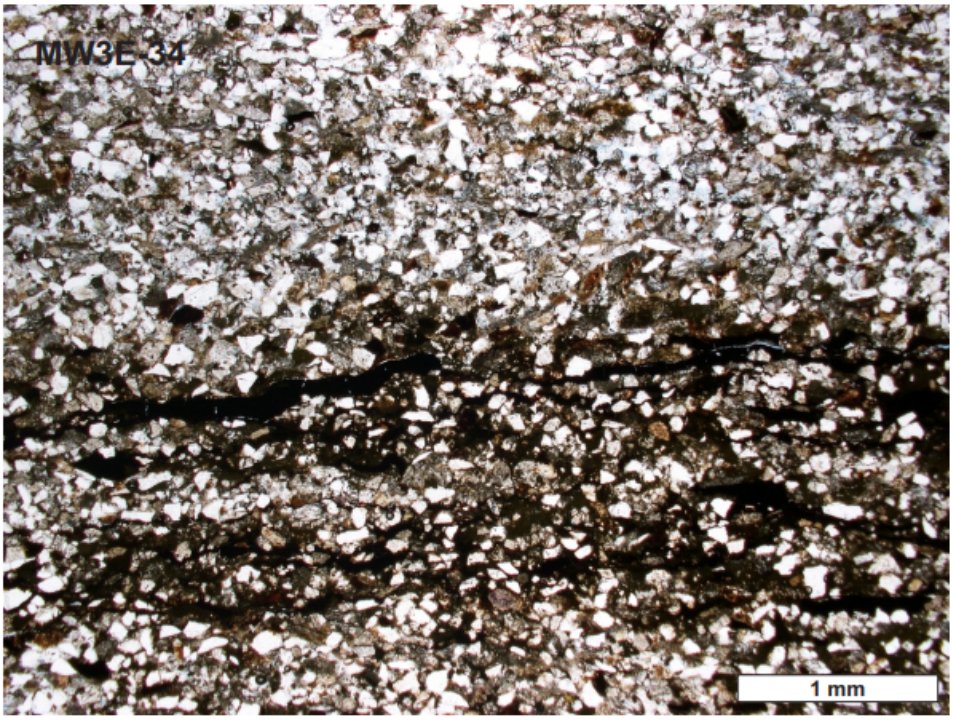

MW3E-34. Fine-grained quartz-rich sandstone with dark coaly laminations.